THE UNIVERSITY OF OKLAHOMA

GRADUATE COLLEGE

DECOMPOSITION OF FORMIC ACID ON CLEAN NICKEL (100) SURFACE

A DISSERTATION

SUBMITTED TO THE GRADUATE FACULTY

in partial fulfillment of the requirements for the

degree of

DOCTOR OF PHILOSOPHY

BY

CHANG-OU LEE

Norman, Oklahoma

1975

DECOMPOSITION OF FORMIC ACID ON

CLEAN NICKEL (100) SURFACE

APPROVED BY

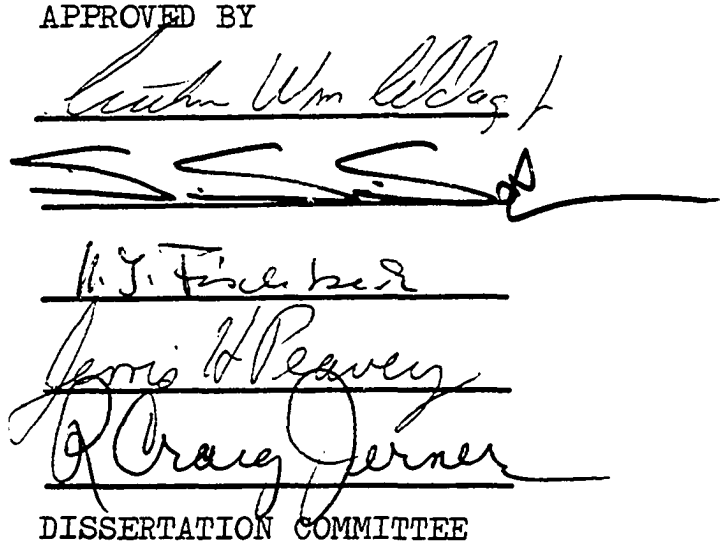

DISSERTATION COMMITTEE

ABSTRACT

The decomposition of formic acid on clean Ni (100) surface has been studied using flash desorption mass spectrometry. The experiments were performed in a controlled ultra-high vacuum environment (10^{-9} torr). Both faces of the substrate were electron bombardment and sputter ion cleaned and the subsequent composition of each face monitored using Auger Electron Spectroscopy.

The coverage, activation energy and order of reaction of the decomposition products (H_2, CO and CO_2) has been determined from the flash desorption spectra. These values are compared to those obtained from the individual adsorption characteristics of H_2, CO and CO_2 on the same crystal. In conclusion, the interaction of formic acid on clean Ni (100) surface consists of both a second order dehydrogenation reaction of formic acid to yield the products H_2 and CO_2 and a first order dissociation reaction of CO_2 liberating CO and leaving oxygen on the surface.

ACKNOWLEDGEMENT

This author wishes to thank Dr. A. W. Aldag for his guidance and thoughtful suggestions through the course of this work.

Thanks are also extended to Dr. J. H. Peavey for his countless assistance and continuous encouragement.

Both thanks and apology are due to my family for their patience and sacrifice.

TABLE OF CONTENTS

TABLE OF CONTENTS (CONT'D)

LIST OF TABLES

LIST OF TABLES (CONT'D)

LIST OF ILLUSTRATIONS

LIST OF ILLUSTRATIOS (CONT'D)

LIST OF ILLUSTRATIONS (CONT'D)

LIST OF ILLUSTRATIONS (CONT'D)

DECOMPOSITION OF FORMIC ACID ON CLEAN NICKEL (100) SURFACE

CHAPTER I

INTRODUCTION

1-1 Examination of Decomposition of Formic Acid

The decomposition of formic acid on metals, metal oxides, or metal alloys has been the interest of many experimental investigators for a number years. Excellent and comprehensive reviews have been given by Bond (1) and by Mars, et al (2). Generally this decomposition reaction is shown to behave in one of the three following manners:

$$HCOOH \longrightarrow H_2 + CO_2 \qquad (1\text{-}1)$$

$$HCOOH \longrightarrow H_2O + CO \qquad (1\text{-}2)$$

$$2HCOOH \longrightarrow H_2O + CO_2 + CH_2O. \qquad (1\text{-}3)$$

On metals the dehydrogenation reaction (1-1) is the only reaction. The dehydration reaction (1-2) may occur on metals or metal oxides. Reaction (1-3) has not been observed on metals (2). One of the main reasons for choosing this reaction is the simplicity of the reacting system (A$\longrightarrow$B+C). Also the analytical determination of these reaction products is easily performed.

Futhermore, on almost all metals it proceeds at a measureable rate, and is in easily accessible regions of temperature. Finally, this reaction has often been studied for the activity of catalysts. The mechanism of the catalytic dehydrogenation of formic acid is not fully understood at this time. Two possible mechanisms have been proposed for this reaction (1). The first assumes that a formate ion is formed on catalysts between 70-100°C. Above and below this temperature range, the ion may become less important and the formic acid is adsorbed as a radical. The processes may be written as:

$$HCOOH + 2^* \xrightarrow{slow} O{=}C(H){-}O^- + H \xrightarrow[+2^*]{fast} O{=}C{-}O + 2H \qquad (1\text{-}4)$$

or

$$HCOOH + 2^* \xrightarrow{slow} O{=}C(H){-}O + H \xrightarrow{fast} O{=}C{-}O + 2H. \qquad (1\text{-}5)$$

The hydrogen atoms will recombine rapidly. The second proposed mechanism of the catalytic decomposition of formic acid is either

$$HCOOH + 2^* \xrightarrow{slow} HCOO + H \xrightarrow{fast} CO_2 + 2H \qquad (1\text{-}6)$$

or

$$HCOOH + 2^* \xrightarrow{fast} H{-}C(OH){-}O \xrightarrow[+2^*]{slow} O{-}C(H){-}O + H \xrightarrow{fast} O{-}C{=}O + 2H. \qquad (1\text{-}7)$$

It is difficult to judge which mechanism is right because each appears to agree equally well with most of the previous observations.

In this study, the interaction of formic acid is specified on a clean single crystal Ni (100) surface. The techniques of the traditional catalytic studies of this reaction have been to investigate it in a batch or flow reactor under relatively high pressure (10^{-5}-100 torr). Also the experimental studies have been done using infra-red spectroscopy, volumetric measurements or studies of the change of resistance of evaporated films following adsorption. Usually, the surface used is not well defined in terms of the composition and surface structure. Many authors (3-9) have reported that the dehydrogenation of formic acid on nickel is the predominant reaction. The extent of the dehydration reaction is less than one percent on nickel. Since these traditional experiments were performed under high pressure, the surface could have been contaminated by the environment which would seriously effect the results of experiment. The importance of surface contaminants on this reaction over Ni has been recently demonstrated by Robertson, et al (8).

Recently, it has been shown that it is possible to use Auger Electron Spectroscopy (AES) to monitor the composition of the surface phase and to detect impurities within the top five monolayers of the surface. A simple review of AES will be given in Section 1-2.

The objective of this study is to obtain the kinetic parameters and quantitative information about the decomposition of formic acid on clean single crystal Ni (100) surface, in ultra-high vacuum, using Auger electron spectroscopy and flash desorption mass

spectrometry.

The temperature-programmed thermal desorption method (commonly termed flash desorption) has been extensively applied to the study of diatomic molecular adsorbed on both polycrystalline and single crystal surface. There are, however, very few reports of application of this technique to the investigation of more complicated molecules. The products of complex molecules are fragment desorption products, such as hydrogen, carbon monoxide and carbon dioxide from the desorption of formic acid on Ni surface. The theory of flash desorption will be discussed in Section 1-3.

1-2 Review of Auger Electron Spectroscopy

The Auger electron spectroscopy technique for chemical analysis of surface is based on the Auger electron emssion process. When an inner core vacancy of an atom is created by electron bombardment of the surface with electron energies 1-3 Kev, the atom will decay to a lower energy level. The electrons of the outer valence states are ejected with energies characterstic of the atom, as shown in Figure 1-1. These secondary electrons are known as Auger electrons after Pierre Auger who first described the process in 1925 (10).

The low-energy secondary Auger electrons have energies typically between 0-1000 ev and only those electrons can escape from the first several atom layers of a surface (11). This property gives Auger spectroscopy its high sensitivity to detect the composition of a surface.

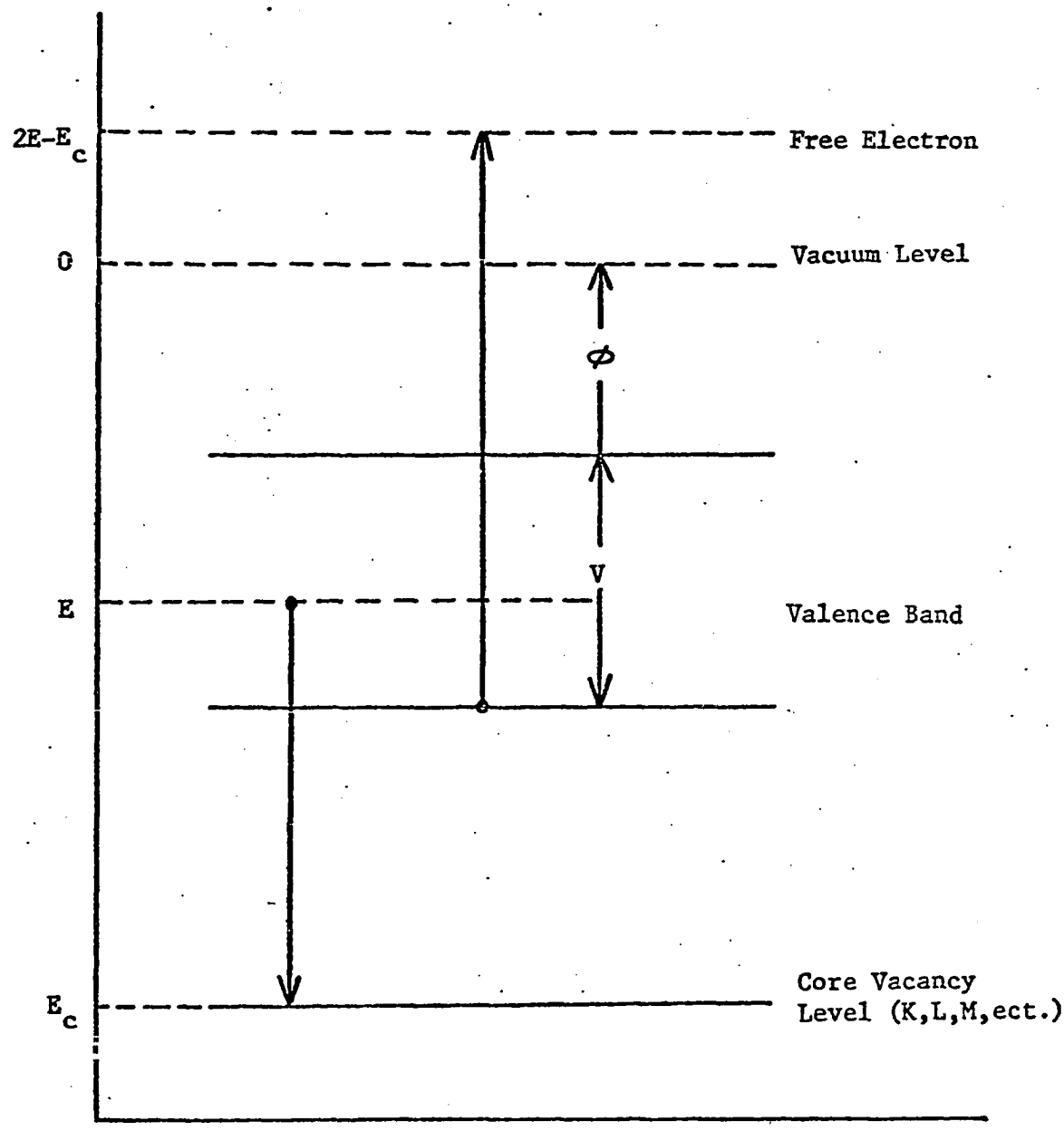

Figure 1-1 Auger electron from an excited atom. ϕ work function; V, width of the valence band, E_c, energy of the core electron level, E, original energy of the emitted electron.

The apparatus of an Auger electron spectroscopy system consists of an ultra-high vacuum chamber, an electron gun for target excitation and an electron-energy analyzer for detection of the Auger electron peaks in the total secondary electron energy distribution. Unfortunately Auger peaks are difficult to distinguish from a rather large continuous background. They are more easily detected by differentiating the energy distribution function N(E). Electronic differentiation can be obtained with a velocity analyzer by applying a small a.c. voltage on the energy selecting voltage and synchronously detecting the output of the electron multiplier. The consequent dN(E)/dE vs. E curves greatly reduces the continuous background. It is generally assumed that the peak to peak magnitude of Auger peak in the differentiated spectra is proportional to the concentrations of the element wich produces the electrons on a surface. Quantitative information may be obtained by comparing the peak heights of any specimen with those from pure elemental standards or from compounds with known composition. Very detailed discussions of all aspects of Auger electron spectroscopy may be found elsewhere (11,12).

1-3 Theory of Flash Desorption

The flash desorption technique has been often used to study desorption phenomena, and has been described by many authors, particular by Ehrlich (13) and Redhead (14). This technique has been developed such that both qualitative and quantitative information about the kinetics of desorption may be obtained from the date. First- and second-order desorption reactions

can be distinguished immediately. Quantitative values for activation energies, rate constants and the desorption rate are deduced from the partial pressure of the adsorbate as the temperature of the adsorbent is varied.

The important part of flash desorption procedure is concerned with the calculation of the desorption rate from measured pressure-time curves which are termed flash desorption spectra. The pressure-time curves also can be expressed as ion current signal of mass spectroscopy vs. time during the desorption process.

During the flash desorption, the sample is initially at temperature T_o and the initial surface coverage is σ_o. The sample is then heated rapidly through a temperature range where all the adsorbed molecules desorb. Simultaneously, the partial pressure of one of the desorption product and the temperature are recorded as a function of time. Readsorption during a flash is assumed to be negligible. The rate of the number of molecules desorbed per unit surface area can be expressed as

$$-A\frac{d\sigma}{dt} = KSp + KV\frac{dp}{dt} \qquad (1\text{-}8)$$

where σ = surface coverage (molecules/cm^2)
K = 3.27×10^{19} molecules/l-torr at 295°K
S = pumping speed (l/sec)
p = partial pressure (torr)
V = volume of the vacuum system (l)
A = surface area (cm^2).

Integrating Equation (1-8) yields

$$A(\sigma_o - \sigma) = KS\int_o^t pdt + KV(p - p_o) \qquad (1\text{-}9)$$

where p_o is initial partial pressure. When $t \rightarrow \infty$, $\sigma \rightarrow 0$, $p \rightarrow p_o$ and

$$A\,\sigma_o = KS\int_o^\infty p\,dt. \qquad (1\text{-}10)$$

Then Equation (1-9) becomes

$$\sigma = \frac{KS}{A}\int_t^\infty p\,dt - \frac{KV}{A}(p - p_o). \qquad (1\text{-}11)$$

Equation (1-11) shows that σ is a function of time. If the temperature increases linearly with time ($T = T_o + \beta t$), an alternative expression of Equation (1-11) as a function of temperature is

$$\sigma = \frac{KS}{\beta A}\int_T^\infty p\,dT - \frac{KV}{A}(p - p_o). \qquad (1\text{-}12)$$

The σ can be obtained from $\int_t^\infty p\,dt$ or $\int_T^\infty p\,dT$ which may be measured directly from the area under the pressure-time curve or pressure-temperature curve respectively. The desorption rate, $d\sigma/dt$, can also be calculated from the flash desorption spectrum.

If it is assumed that gas desorption from surface obeys Arrhenius' equation, then

$$-\frac{d\sigma}{dt} = \gamma_n \sigma^n \exp\left(-\frac{E}{RT}\right) \qquad (1\text{-}13)$$

where n = order of the desorption reaction

γ = rate constant or pre-exponential factor

E = activation energy of desorption (Kcal/g-mole).

With a linear change of sample temperature with time ($T = T_o + \beta t$) and a constant activation energy, E, Equation (1-13) can be solved by finding the temperature at which the desorption rate is a maximum, then

$$\frac{E}{RT_p^2} = \left(\gamma_1/\beta\right)\exp(-E/RT_p); \text{ for } n = 1 \qquad (1\text{-}14)$$

and

$$\frac{E}{RT_p^2} = \frac{\sigma_o \nu_2}{\beta} \exp(-E/RT_p); \text{ for } n = 2 \quad (1\text{-}15)$$

where T_p = temperature at which desorption rate is maximum (^oK).

Equation (1-14) shows that T_p is independent of surface coverage. For a first order desorption reaction with constant E, Redhead suggested that the activation energy can be obtained directly from Equation (1-14) by a measurement of T_p and by assuming a value of ν_1. The assumed value of pre-exponential factor is 10^{13} s^{-1} for a typical first order reaction. The accuracy of calculated activation energy is within $\pm$ 1.5 per cent which is estimated by Redhead (14).

For a second order reaction, Equation (1-15) shows that T_p depends on the surface coverage. The activation energy may be obtained from Equation (1-13) which can be rewritten as

$$\ln\left(-\frac{1}{\sigma^2}\frac{d\sigma}{dt}\right) = \ln(\nu_2) - \frac{E}{RT}. \quad (1\text{-}16)$$

Since the temperature change is a linear function of time, the time-dependent Equation (1-16) may be changed into temperature-dependent equation, i.e.

$$\ln\left(-\frac{1}{\sigma^2}\frac{d\sigma}{dT}\right) = \ln(\nu_2/\beta) - \frac{E}{RT} \quad (1\text{-}17)$$

A plot of $\ln(-1/\sigma^2 \cdot d\sigma/dT)$ vs. $1/T$ can be constructed in order to obtain a straight line with a slope $-E/RT$.

CHAPTER II

EXPERIMENTAL

2-1 Experimental Equipment

The experimental system used in this study is a sputter ion pumped stainless steel chamber, OFHC copper gasket sealed, bakeable to 250°C, and capable of acheiving ultra-high vacuum (10^{-9}torr). Figure 2-1 shows the arrangement of apparati employed in performing experiment.

The whole system is first pumped down to 1.0 x 10^{-3} torr by a Varian sorption pump (model 941-6001). During this rough pumping, the system pressure is measured by a Hasting thermocouple gauge (type DV-6M) and control unit (model DV-6). Two sources for ultra-high vacuum pumping are Varian 50 l/sec ion-getter pump (model 912-6000) and Varian titanium sublimation pump (model 916-0017). The power supply units for the ion pump and TSP are Varian VacIon control unit (model 921-0012) and Varian TSP power supply (model 922-0006) respectively. After a 48 hours bake-out to 200°C, the pressure of the system can reach $\backsim$ 1.0 x 10^{-9} torr. The system pressure is measured by a Bayer-Alpert type Varian ionization gauge (model UHV-24) and a Granville-Phillips ionization gauge controller (series 236, model 01).

A Physical Electronics Industries Auger electron

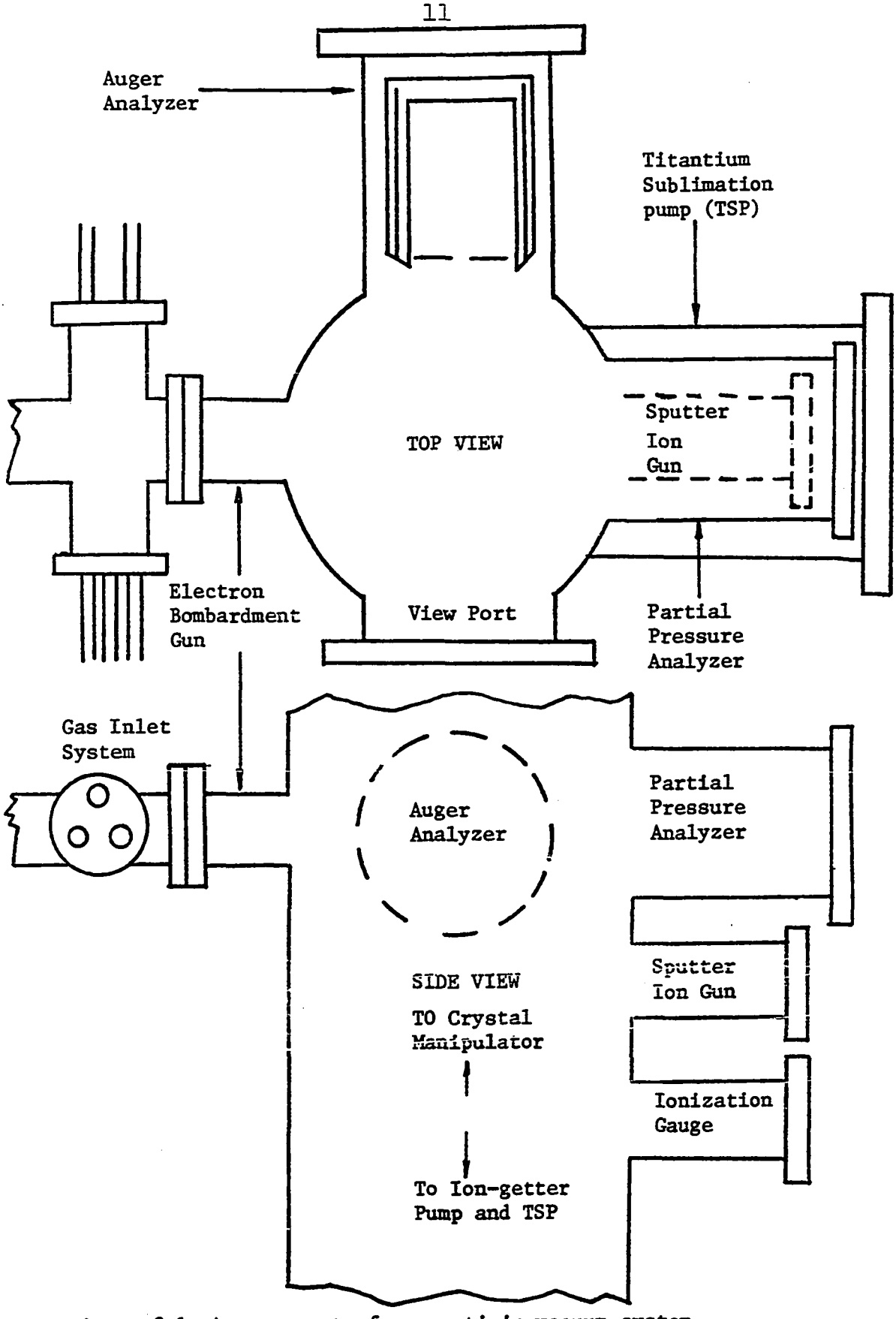

Figure 2-1 Arrangement of apparati in vacuum system.

spectrometer is used to monitor the elemental composition of the surface. This system consists of cylindrical-Auger electron optics (model 10-234G), Auger system control unit (model 11-500) and electron gun control unit (model 18-010). This cylindrical analyzer contains a coaxial electron gun and a thirteen-stage electron multiplier. A Kiethley high voltage supply is used to furnish the power for electron gun. After the electron bombardment of the crystal surface, backscattered secondary electrons are detected and enhanced by the electron multiplier. This potential voltage of electron multiplier is furnished by a Fluke high voltage power supply (model 423A). Also the secondary electron energy distribution is differentiated with respect to the electron kinetic energy by a Princeton Applied Research lock-in amplifier (model 120). The Auger spectrum is recorded as dN(E)/dE vs. E on an x-y recorder.

The crystal in the vacuum chamber is attached to a Physical Electronics Industries specimen manipulator (model 10-501M) which enables specimen movement by means of several mechnical motions such as lateral translation, rotation, linear vertical travel and tilt. This manipulator also includes four electrical feedthroughs.

A Physical Electronics Industries sputter ion gun (model 04-131) and control unit (model 20-005) are used for crystal surface cleaning. This system is capable of operating with the vacuum chamber back-filled to a pressure 5×10^{-5} torr of an inert gas, such as argon.

A home-made electron bombardment gun and a Physical Electronics Industries specimen heater control (model 20-025) are used to heat the crystal in order to desorb contaminants, such as oxygen, nitrogen and sulfur from the crystal surface.

During flash desorption, the crystal is heated by a well-focused light beam through the view port from an external projector lamp (1000 watts). This method can heat crystal up to 350°C with linear heating rate of 4°C per second. This temperature is high enough to perform flash desorption studies of decomposition of formic acid on Ni (100) surface. The temperature change of the crystal is monitored and recorded. Simultaneously, the partial pressure change of one of the desorbable gases is measured with a General Electric monopole partial pressure analyzer (model 22pc162). The ion current signal readout is through a Keithley high-speed pico-ammeter (model 416) and is recorded vs. temperature change of crystal by an x-y recorder.

2-2 Measurement of System Volume

The volume V, of the experimental chamber, was determined by measuring the pressure change when a known amount of gas was introduced into system. This was done by measuring the pressure in a known volume, opening the valve between the two volumes and measuring the change in pressure. The arrangement for making the measurement is shown in Figure 2-2.

The measurements were made as follows: the volume, V_1, of an emptied propane gas cylinder, the volume of a thermocouple gauge V_2, the volume, V_3, of a valve and the volume, V_4, of pipe were determined by measuring the amount of water required to fill each. Several trials were made the results are given in Table 2-1.

The total average volume, V_c, of the apparatus shown in Figure 2-2 is 380.5 ml. This average value was used to measure the chamber volume.

Next, the thermocouple gauge was calibrated according

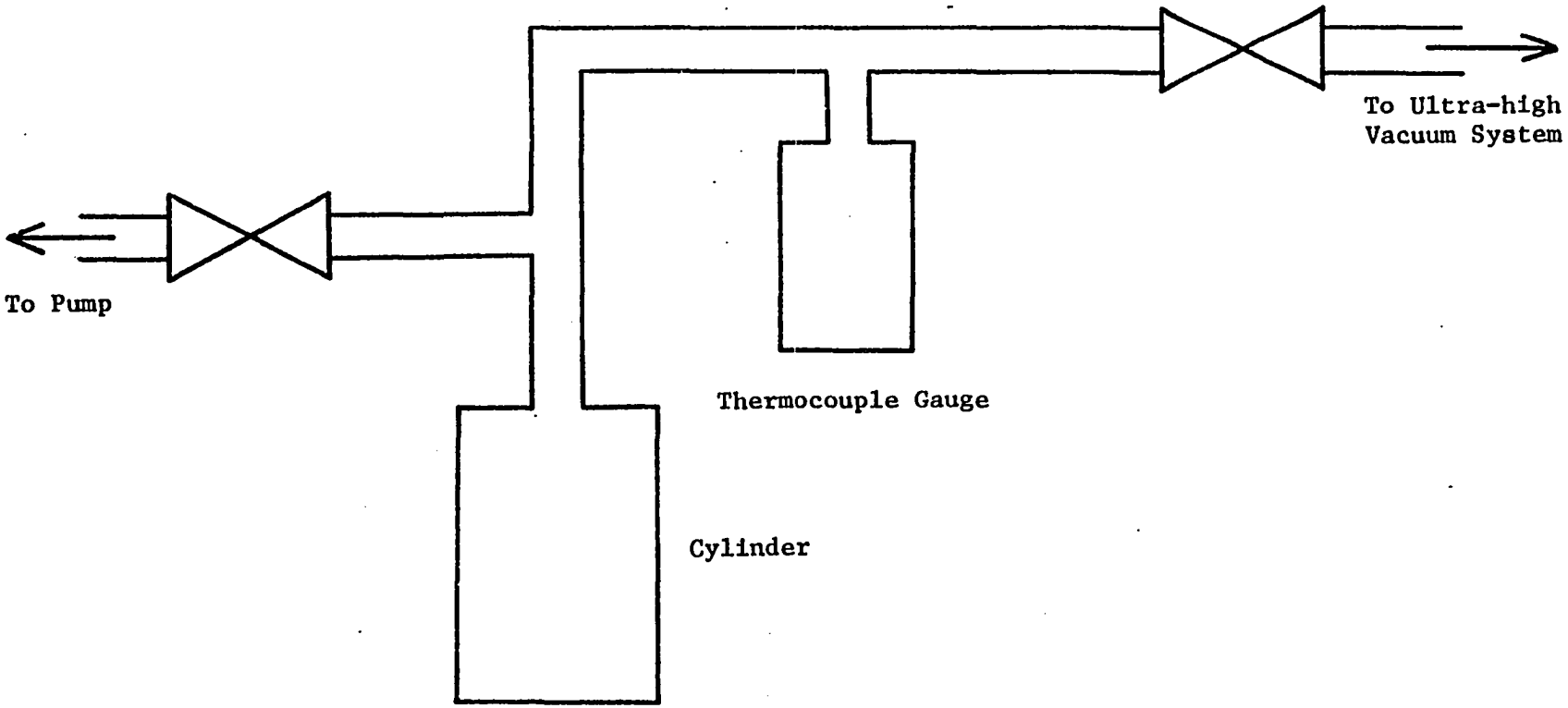

Figure 2-2 Arrangement of apparatus for measuring system volume.

Table 2-1

Volume of Apparatus for Measuring Vacuum System Volume

Trial	1	2	3	4	5	Average
Volume of cylinder, V_1, ml	345.0	342.0	347.0	347.0	347.0	345.6
Volume of T.C., V_2, ml	5.8	5.5	5.9	5.8	5.8	5.76
Volume of valve, V_3, ml	27.5	28.0	28.0	27.5	-	27.63
Volume of pipe, V_4, ml	11.1	12.0	11.2	11.5	11.8	11.52

to instructions supplied by the manufacturer (15). The experimental chamber, V, was pumped down to pressure of approximately 0 micron and the predetermined volume, V_c, was pumped down to 500 micron. The valve between these two volumes was opened and the pressure allowed to reach equilibrium. Then the valve was closed and the cylinder filled with air to the pressure of 500 micron again. This consecutive procedure was repeated eight times. It is important to note that the initial pressure of the chamber for each consecutive step equals the equilibrium pressure of previous step. Table 2-2 and Figure 2-3 show the pressures of cylinder and chamber at each consecutive step.

The following derivation leads to the calculation of the volume of chamber. When the pressure reaches equilibrium between the two volumes, cylinder and chamber, the pressure-volume relationship can be expressed as

$$P_n(V + V_c) = P_cV_c + P_oV \qquad (2\text{-}1)$$

where n = step number

P_n= equilibrium pressure of step n and also is the chamber pressure for next step, i.e., step n+1

P_o= initial pressure of chamber

P_c= pressure of cylinder, 500 micron.

When n=1,

$$P_1 = \frac{P_cV_c + P_oV}{V + V_c} . \qquad (2\text{-}2)$$

When n=2,

$$P_2 = \frac{P_cV_c + P_1V}{V + V_c} . \qquad (2\text{-}3)$$

Table 2-2

Pressures of Cylinder and Chamber
at Each Consecutive Step

Step, n	Cylinder pressure P_c (micron)	Chamber pressure P_n (micron)
0	500	0.0
1	500	4.0
2	500	10.0
3	500	17.0
4	500	26.5
5	500	35.0
6	500	43.0
7	500	51.0
8	500	59.0

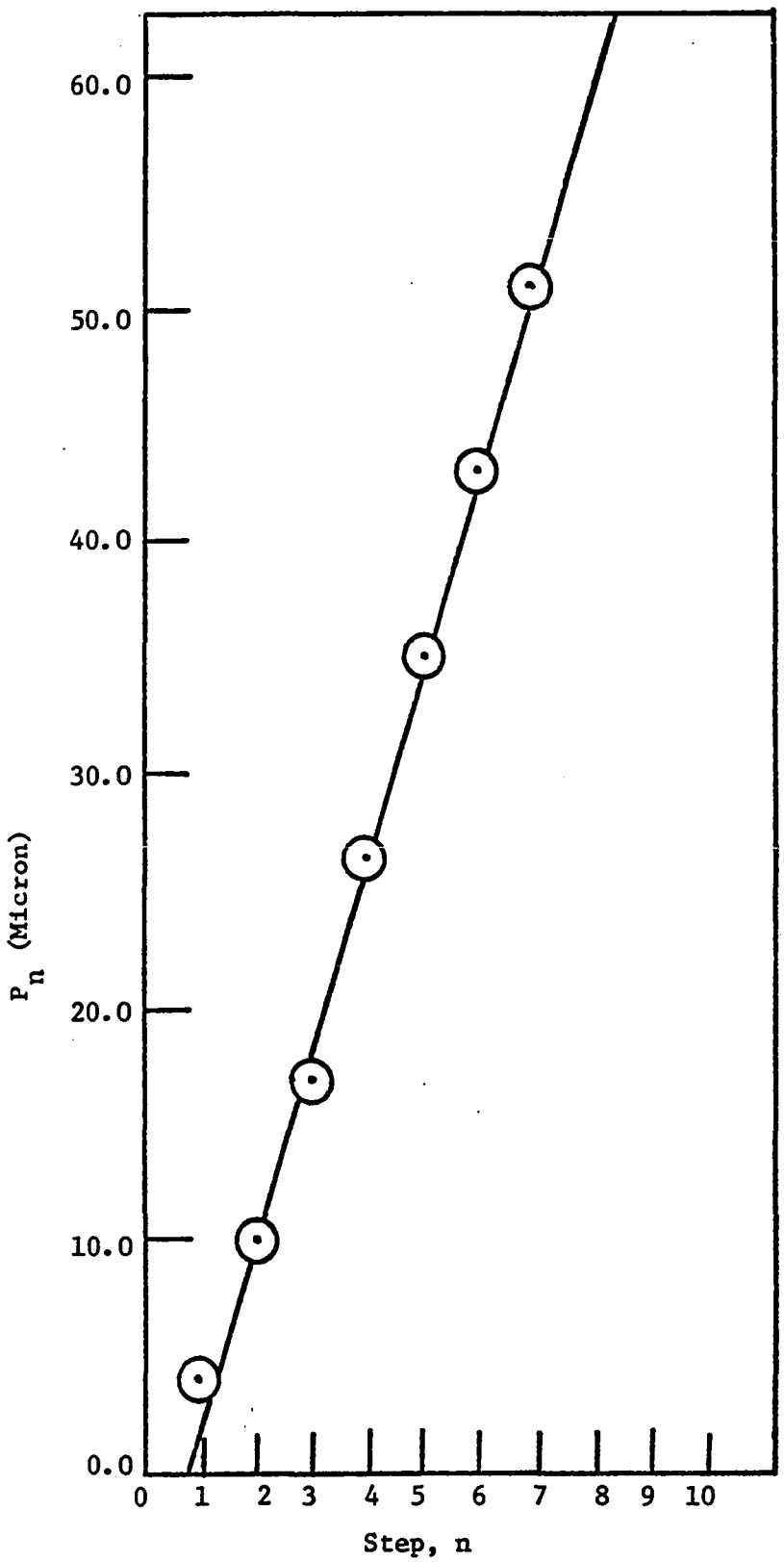

Figure 2-3 Pressure of vacuum system at each consecutive step.

Substitute Equation (2-2) into Equation (2-3)

$$P_2 = \frac{P_c V_c}{V + V_c}\left(1 + \frac{V}{V + V_c}\right) + P_o\left(\frac{V}{V + V_c}\right)^2 . \qquad (2\text{-}4)$$

When n=3,

$$P_3 = \frac{P_c V_c + P_2 V}{V + V_c} . \qquad (2\text{-}5)$$

Substitute Equations (2-2) and (2-4) into Equation (2-5)

$$P_3 = \frac{P_c V_c}{V + V_c}\left[1 + \frac{V}{V + V_c} + \left(\frac{V}{V + V_c}\right)^2\right] + P_o\left(\frac{V}{V + V_c}\right)^3 . \qquad (2\text{-}6)$$

From Equations (2-2), (2-4) and (2-6), at n step we get

$$P_n = \frac{P_c V_c}{V + V_c}\left[1 + \frac{V}{V + V_c} + \left(\frac{V}{V + V_c}\right)^2 + \cdots + \left(\frac{V}{V + V_c}\right)^{n-1}\right] + P_o\left(\frac{V}{V + V_c}\right)^n . \qquad (2\text{-}7)$$

If $P_o = 0$ and $V \gg V_c$, the final form of Equation (2-7) is

$$P_n = P_c\left(\frac{V_c}{V + V_c}\right)n \qquad (2\text{-}8)$$

This equation shows that the slope of the straight line in Figure 2-3 is equal to $P_c V_c/(V+V_c)$. After least squares fitting of the data in Table 2-2, the slope was found to be 8.1 and the volume of the experimental chamber is 24.3 liters.

2-3 Determination of Pumping Speed

The pump down curves of a particular gas can be expressed by the following equation (16)

$$V\frac{dP}{dt} + SP - \frac{L}{K} = 0 \qquad (2\text{-}9)$$

where L = constant leak rate (molecules/sec).
After integrating of Equation (2-9),

$$(P - P_B)/(P_o - P_B) = \exp(-t/\tau) \qquad (2\text{-}10)$$

where P_B = base pressure = L/KS
τ = time constant =V/S
From Equation (2-10) if the time constant for a particular gas can be measured, the pumping speed can be calculated by the relation τ=V/S. Since the left-hand side of Equation (2-10) is dimensionless, any measurable output that is linear in pressure can be used, i.e., an uncalibrated mass spectrometer or an ionization gauge. In fact, the GE partial pressure analyzer was used to make the measurement. The measurements were made as follows: the base pressure of the system was first determined. The experimental chamber was then backfilled with a particular gas to a known pressure, i.e., the initial pressure, P_o. Next, the valve between the particular gas and experimental chamber was closed and the pressure vs. time curve of the system recorded. The measurement of the time constant were performed for hydrogen, carbon monoxide and carbon dioxide.

However, before one can record the pump-down curve, it must be determined that the decay which is measured is that of the pressure in the experimental chamber and not the decay curve of the detection circuitry. In order to ascertain that the response being measured was

the true response, the GE partial pressure analyzer was set to sweep back and forth across the m/e=28 peak, and the time between repetitive sweep cycle was measured. A typical such curve is shown in Figure 2-4. The slope of the peaks may be controlled by one of two things; (i) the width of mass peak itself, (ii) the time response of detect system. If the slope is due to the former then the quantity

$$(\frac{H}{t})\ (\frac{1}{T}) \qquad (2\text{-}11)$$

where H = peak height in amps
t = time required to fall
T = period of the sweep cycle

will be constant while varying the sweep rate. This quantity was measured several times and the results are shown in Figure 2-5. It shows that the decay of the peak is due to the sweep rate only for a period of at least 1.969 seconds, which corresponds to a decay time of 0.203 seconds.

The pressure versus time curves for H_2, CO and CO_2 were then taken. The time constant was determined from these curves. A typical curve for CO is shown in Figure 2-6. The results of the time constant and pumping speed at various of P_o are given in Table 2-3. The values obtained for the pumping speed are quite reasonable because, (i) the ion pump is rated at 50 l/sec by the manufacturer (17), (ii) the fact that the pumping speed is reduced at lower pressure is typical and expected of getter-ion pumps (16), (iii) the pumping speeds of H_2, CO, and CO_2 are around 2.7, 1.0, and 1.0 times the pumping speed of nitrogen respectively (17).

2-4 Composition for Various Gases

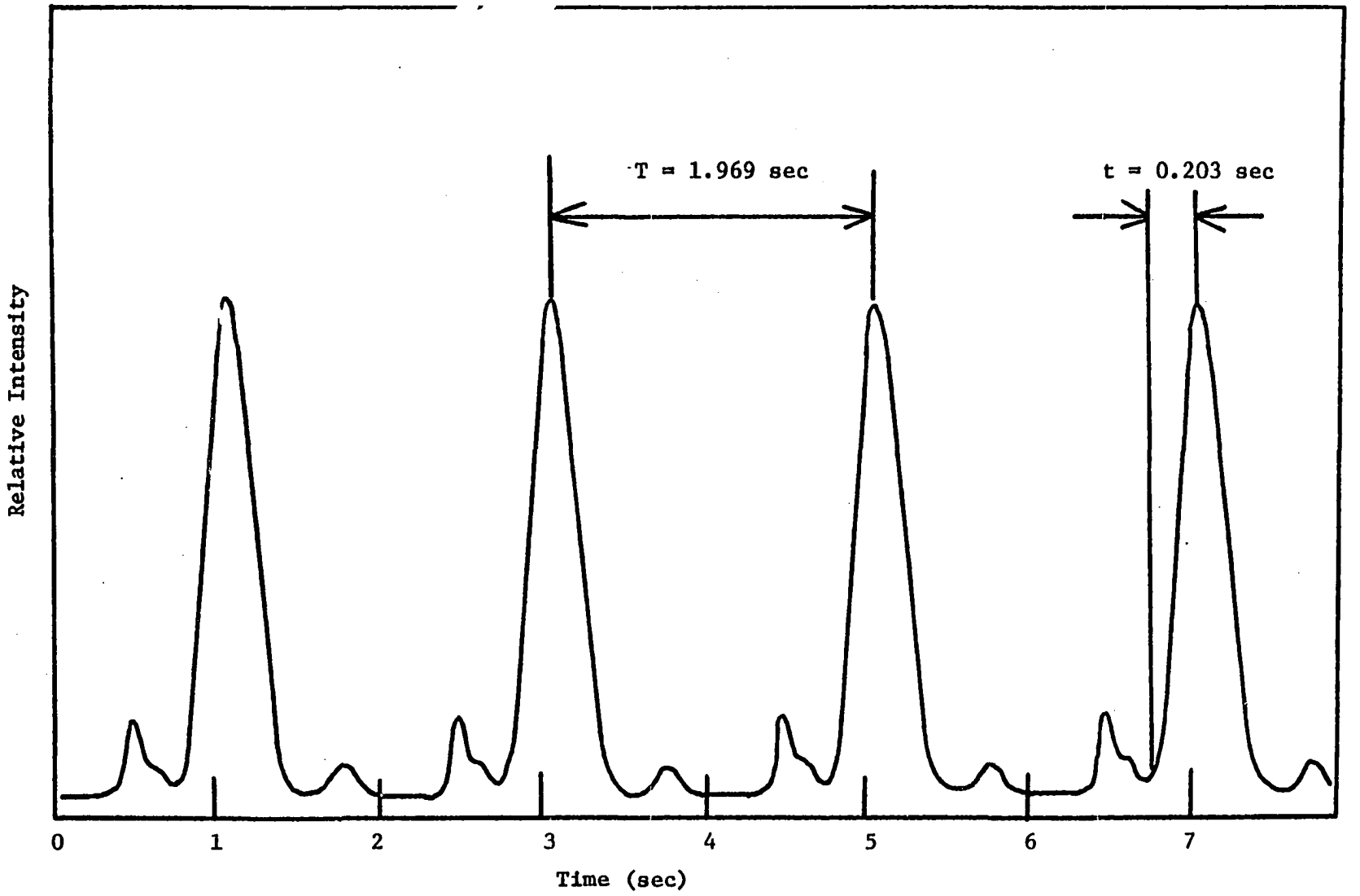

Figure 2-4 Repetitive scans of the m/e = 28 signal.

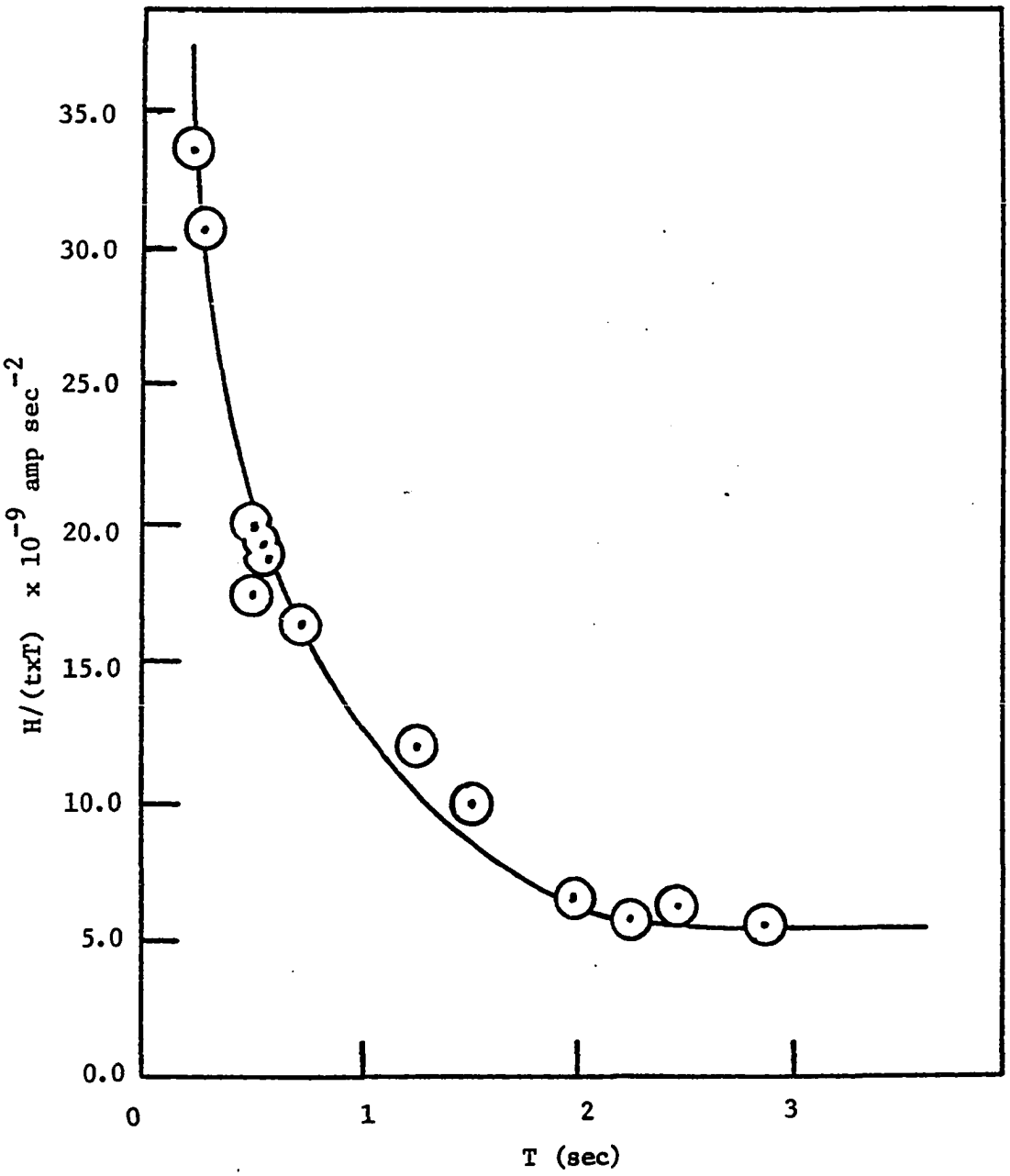

Figure 2-5 Response constant H/(txT) versus time.

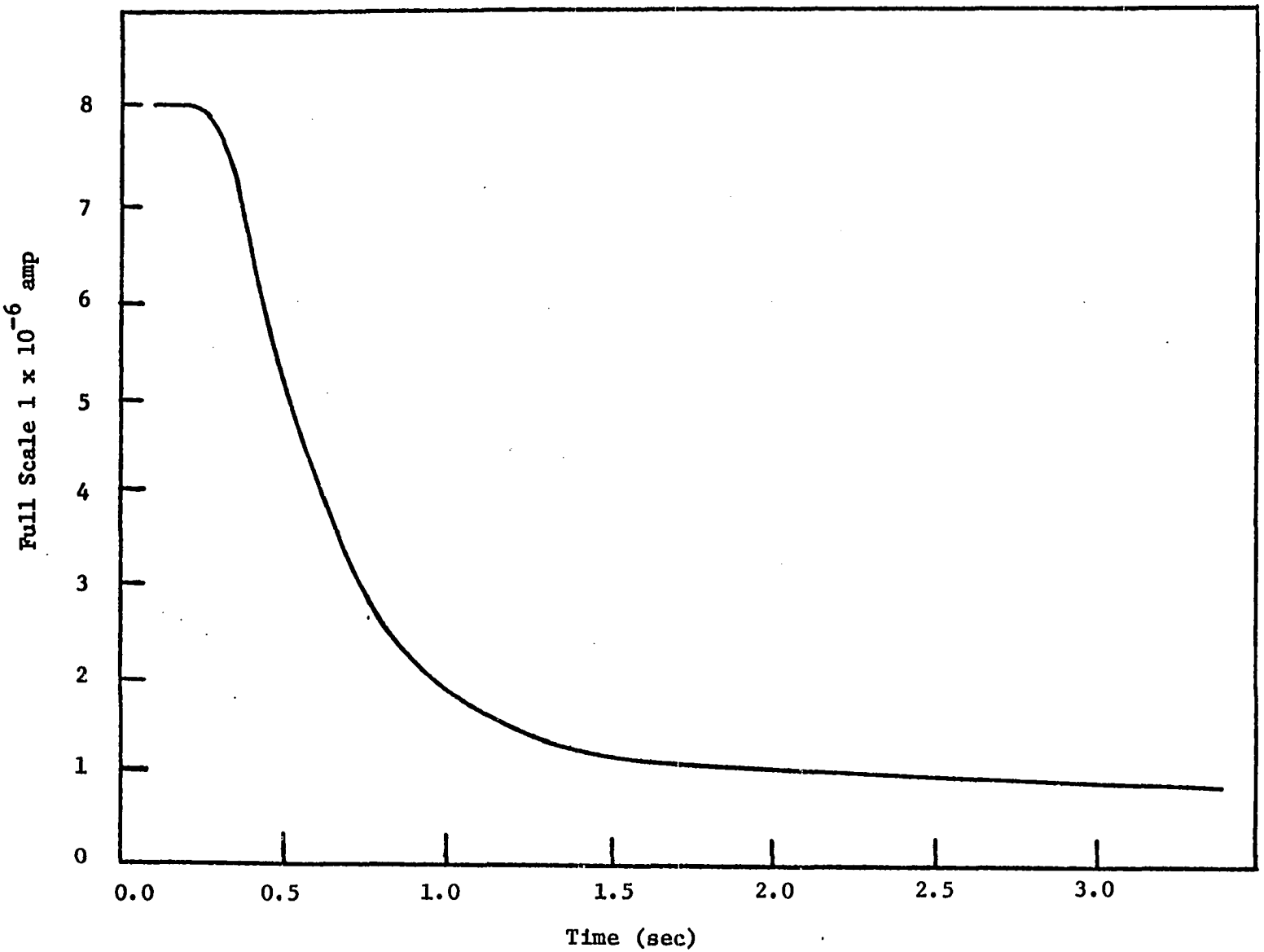

Figure 2-6 Typical carbon monoxide pump-down curve.

Table 2-3

Time Constant and Pumping Speed
for Various Gas

Initial pressure P_o (amp)	Time constant (sec)	Pumping speed S (liter/sec)
Carbon monoxide		
8.00×10^{-8}	0.36	67.5
7.93×10^{-7}	0.30	81.0
7.25×10^{-6}	0.27	90.0
Hydrogen		
7.90×10^{-8}	0.118	203.0
7.20×10^{-7}	0.100	243.0
Carbon dioxide		
9.60×10^{-8}	0.53	45.8
9.80×10^{-7}	0.488	49.5
9.10×10^{-6}	0.487	49.9

The purities of the gases used for this study are as follows; (i) hydrogen, Airco research grade 99.9995%, (ii) argon, Airco research grade 99.9995%, (iii) carbon monoxide, Airco research grade 99.9%, (iv) carbon dioxide, Airco research grade 99.995%.

Formic acid (Matheson Coleman & Bell Manufacture Chemists regent grade, 98% minimum assay) has been used for this study. The maximum impurities and specification of this formic acid are listed in Table 2-4. The formic acid contains approximately 1.5% water and 0.4% acetic acid as the major impurities.

The decomposition of formic acid on a single crystal nickel (100) surface is performed in a controlled ultra-high vacuum environment and a very small quantity of formic acid is needed to saturate the nickel surface. A small impurity with a high vapor pressure, such as water or acetic acid, could drastically effect the adsorption of formic acid on the nickel surface. Therefore, the formic acid is required to be very pure. Impurities of 1.5% water and 0.4% acetic acid are not acceptable. Formic acid of 99.99-100% purity cannot be obtained by simple distillation of aqueous product since two constant-boiling azeotropes are formed (18). In addition, formic acid becomes unstable and decomposes around 35°C (18). This complicates the purification of formic acid through ordinary distillation since the formic acid vapor cannot be generated by heating the liquid. A special purification procedure is required to acheive anhydrous or nearly anhydrous formic acid. The 98% minimum assay formic acid was purified by fractional crystallization, vacuum distillation and prolonged pumping on the solid. The purity of the resulting formic acid was checked by mass spectrometer.

Table 2-4

Maximum Impurities and Specification of Formic Acid

Assay	98% minimum
Acetic acid	0.4%
Ammonium	0.0005%
Chloride	Passes test
Dilution test	Passes test
Color (APHA)	Not less than 15
Evaporation residue	0.003%
Heavy metals	0.001%
Iron	0.001%
Sulfate	0.003%
Sulfite	Passes test

In fractional crystallization, the starting formic acid is immersed in an ice water bath. Two thirds of the formic acid was frozen. The remaining liquid was discarded and the solid was remelted at room temperaure. This procedure was repeated four times until the formic acid reached a constant freezing point of $-8.4^{o}C$ which is the freezing point of pure formic acid (18). The resulting formic acid was then vacuum distilled in the apparatus shown in Figure 2-7. The whole system was pumped to 10^{-5} torr in order to lower the boiling point of formic acid and generate the formic acid vapor. The vapor was passed through a packed column of solid anhydrous calcium sulfate which was used as a drying agent to remove the water. The dry vapor was collected and condensed in a storage container immersed in a liquid nitrogen bath. Finally several cycles of melting and freezing of the solid formic acid were performed to remove additional impurities. The cold trap in Figure 2-7 was filled with liquid nitogen to isolate the system from mechanical and diffusion pumps.

The resulting formic acid was sealed under vacuum and mounted to the ultra-high vacuum system which was at a pressure of less than 2.0×10^{-9} torr. The formic acid gas was leaked into the system at room temperature until pressure 1.0×10^{-8} torr reached. The GE partial pressure analyzer was used to take the mass spectrum of the resulting formic acid. This spectrum is shown in Figure 2-8. The impurity concentration is low and the cracking pattern is very similar to those in the literature (19,20,21,22).

2-5 Calibrations

In most cases the sensitivities of an ionization

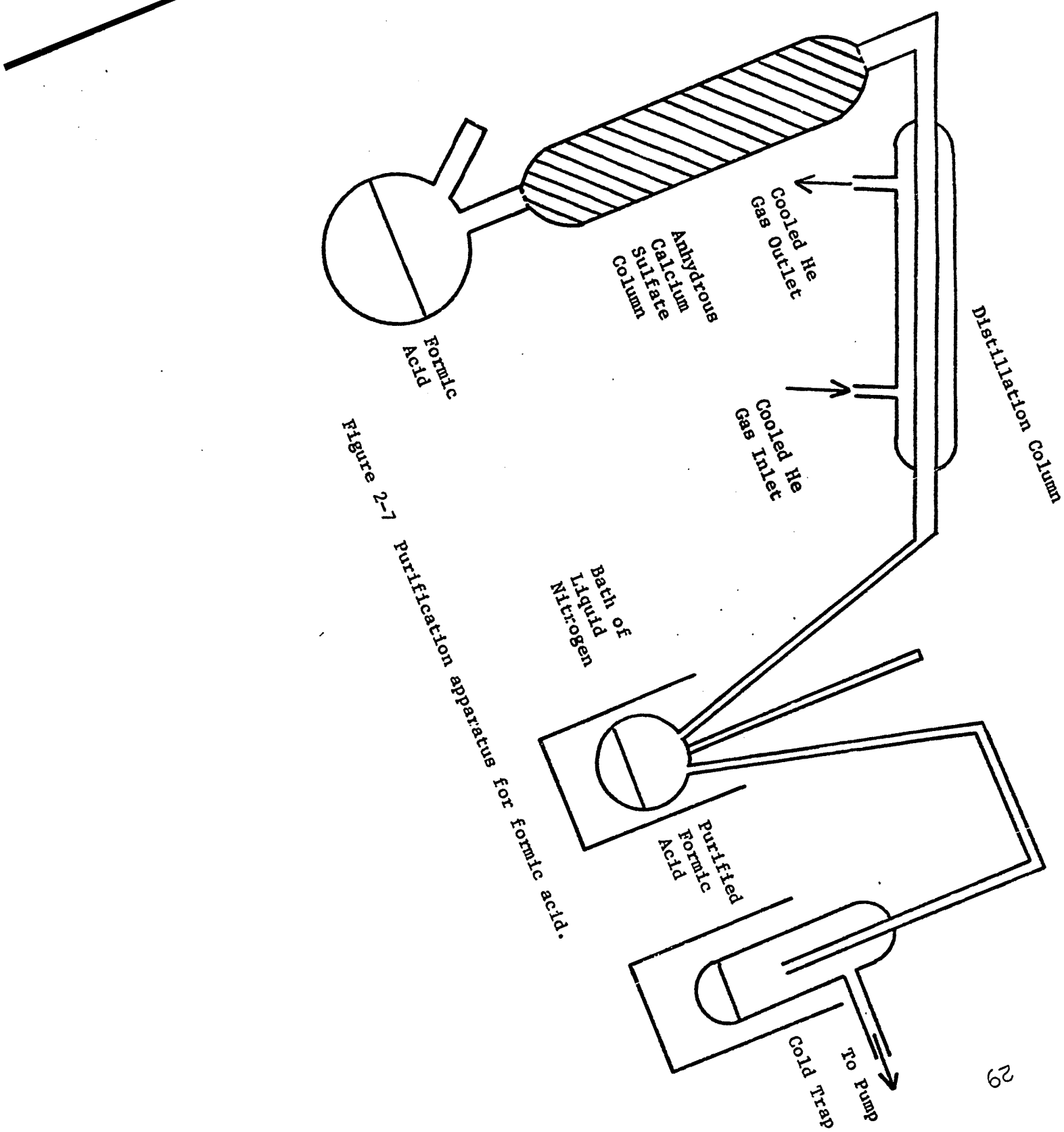

Figure 2-7 Purification apparatus for formic acid.

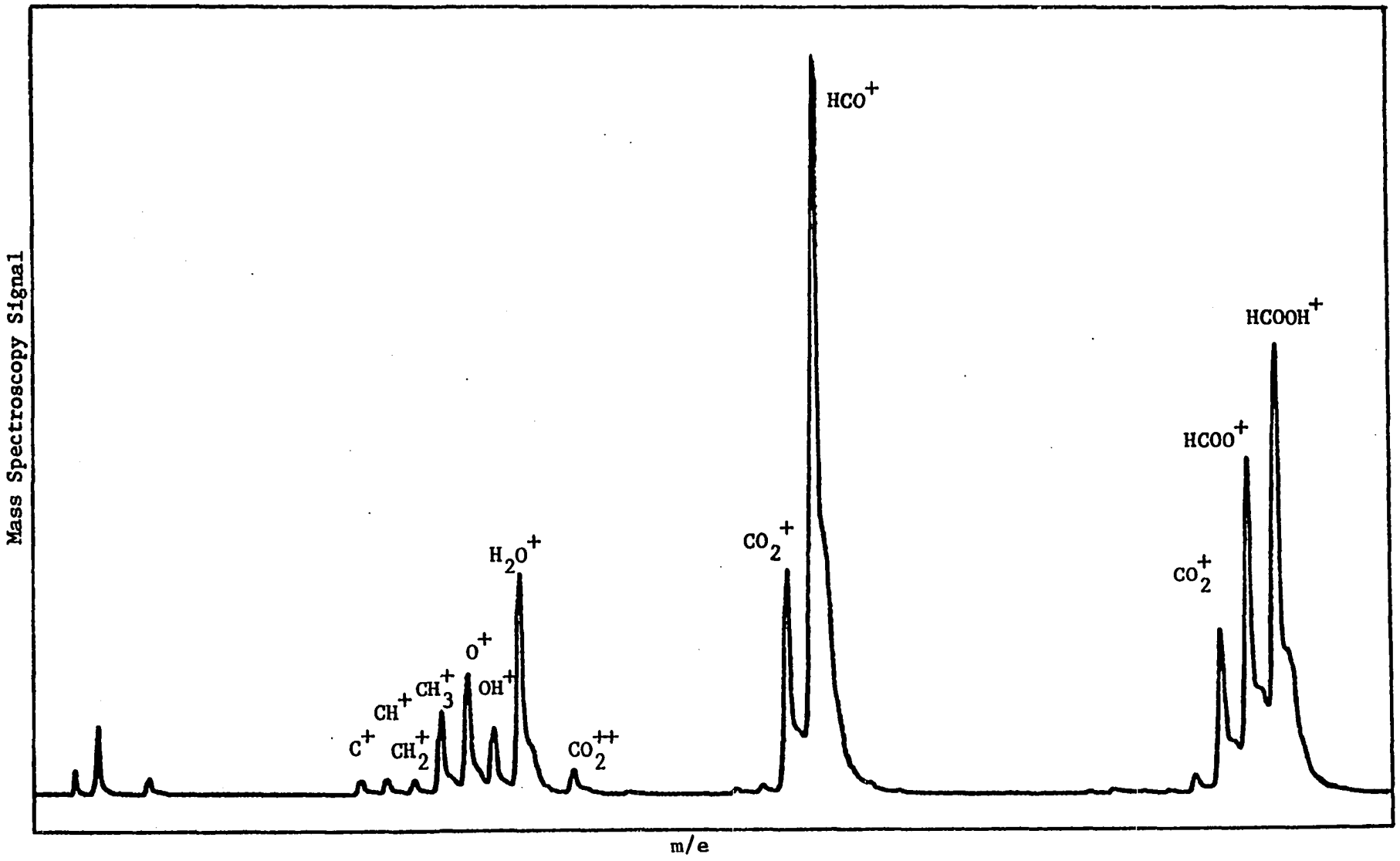

Figure 2-8 Mass spectrun of purified formic acid.

gauge are normalized to argon or nitrogen. In the study of the decomposition of formic acid on the surface of Ni (100), the actual pressure of formic acid is necessary in order to calculate the number of molecules which impinge upon the surface. A calibration method for an ionization gauge was needed to obtain the true pressure of formic acid. A Varian ionization gauge was installed on the ultra-high vacuum system and the following procedure was used to calibrate the ionization gauge.

For any particular temperature, the formic acid vapor pressure over the liquid and solid is known (23). Thus, by a judicious choice of temperature, the vapor pressure in the vacuum chamber can be selected, and, if it is of the correct order of magnitude, it can be used to calibrate an ionization gauge. If the temperature of the mixture of actone and dry ice is used ($-86^{o}C$), the vapor pressure of formic acid is 3.95×10^{-5} torr (23). For the Varian Bayer-Alpert ionization gauge with a 4 ma emission current, the actual pressure is linearly proportional to the emission current in the pressure region between 10^{-5}-10^{-10} torr (17). Thus, the correct pressure reading can be obtained by adjusting the emission current.

A calibration prccedure of the Varian Bayer-Alpert ionization gauge for formic acid is described as follows:

(i) The original pressure reading of the ultra-high vacuum system is 2.0×10^{-9} torr based on the emission current of 4 ma of ionization gauge. Then, when the ion pump is turned off, the pressure increases. The pressure change with time is recorded as shown in Figure 2-9. After 38 minutes have elapsed, the pressure reaches equilibrium at a reading value 2.0×10^{-6} torr. At this pressure, the major component (95%) is

CH_4 in the gas phase. The sensitivity of Bayer-Alpert ionization gauge for CH_4, normalized to nitrogen is 1.5 (24). So the actual equilibrium reading should be 1.33×10^{-6} torr approximately.

(ii) The formic acid bottle is immersed in a bath of acetone and dry ice mixture. The temperature of formic acid is -86°C. The formic acid vapor is leaked into the system. Again the pressure increases with time. This change is recorded as shown in Figure 2-10. This pressure reading is also based on the emission current of 4 ma in the ionization gauge. After 32 minutes, the pressure reaches an equilibrium value of 1.4×10^{-5} torr.

(iii) The equilibrium pressure of formic acid at -86°C is 3.95×10^{-5} torr. Thus, the gauge pressure reading at 1.4×10^{-5} torr is not the correct pressure. At this point, the total actual pressure in the system should be the background pressure, 1.33×10^{-6} torr, plus the equilibrium vapor pressure of formic acid at -86°C, 3.95×10^{-5} torr, and the total actual pressure is 4.08×10^{-5} torr. The pressure reading is changed from 1.4×10^{-5} torr to 4.08×10^{-5} torr by adjusting emission current until it reaches a value of 10.95 ma.

The ionization gauge is now calibrated to read the actual pressure of formic acid, if an emission current 10.95 ma is used.

This Varian ionization gauge has already been calibrated, with nitrogen as a reference, by the manufacturer (17). Because of different ionization probabilities, corrections must be made for different gases such as H_2, CO and CO_2. To obtain the actual pressure,

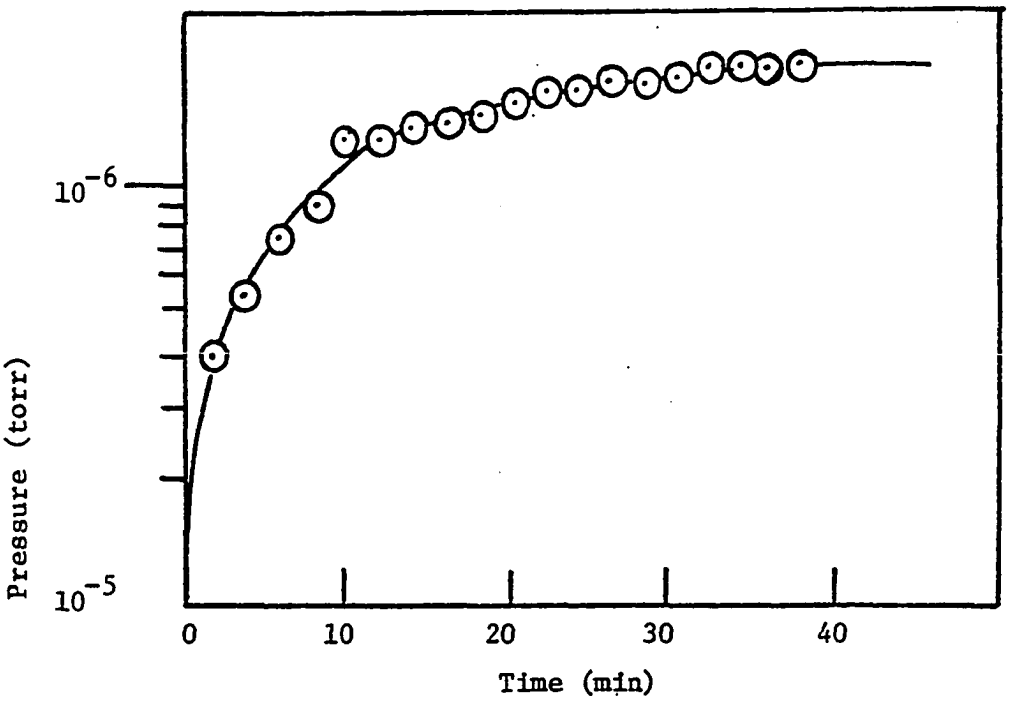

Figure 2-9 The pressure change with time after ion pump is turned off.

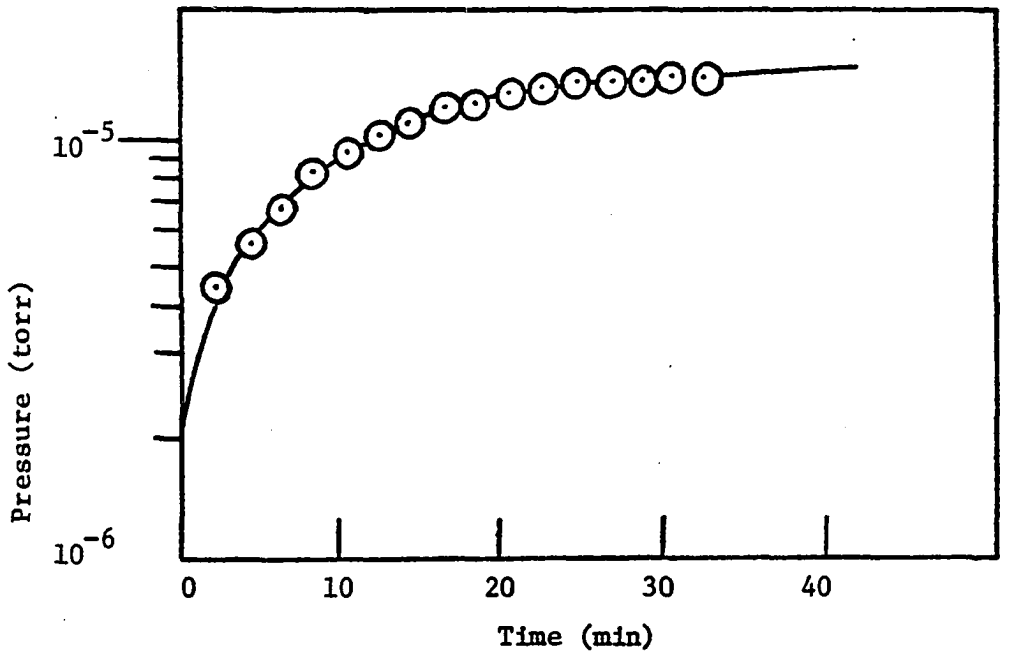

Figure 2-10 The pressure change with time after formic acid is leaked into system.

The gauge reading is multiplied by the ionization probabilities 2.0, 0.95 and 0.73 for H_2, CO and CO_2 respectively.

Since the flash desorption spectrum in this study is obtained from the mass spectrometer ion current signal, it is necessary to convert the ion current into pressure in order to obtain the total number of molecules desorbed from surface. The GE partial pressure analyzer is calibrated against the Varian ionization gauge for H_2, CO and CO_2 for this purpose. Log-log plots of ion current in amp. vs. pressure in torr are given in Figure 2-11 for H_2, CO and CO_2. The pressures shown in Figure 2-11 have already been calibrated according to the above discussions.

2-6 Preparation of Crystal Ni (100)

The nickel single crystal (100) was obtained from Ames Laboratories. It had been checked for orientation to within $\pm$ 1 degree by the back reflection Laue method. The final polishing preparation was done on a mechanical wheel using 50 $\overset{\circ}{A}$ alumina powder. No etching treatment was used for polishing. The Ni (100) used for this study has dimensions of 0.6 cm x 1.25 cm x 0.01 in with a total area of 1.5 cm^2 and a negligible edge effect. This crystal was suspended in the vacuum chamber by the tungsten-rhenium thermocouple wires which monitor the temperature. The wires were 0.005 inch in diameter and the prepared junctions were spot-welded directly to one side of the crystal. The other end of these two wires were connected to two of the electric feed-throughs of the specimen manipulator separately.

After the Ni (100) crystal was installed in the system, the nickel surface composition was monitored by AES. A typical Auger spectrum of comtaminated Ni (100) is shown in Figure 2-12. It is important to note that

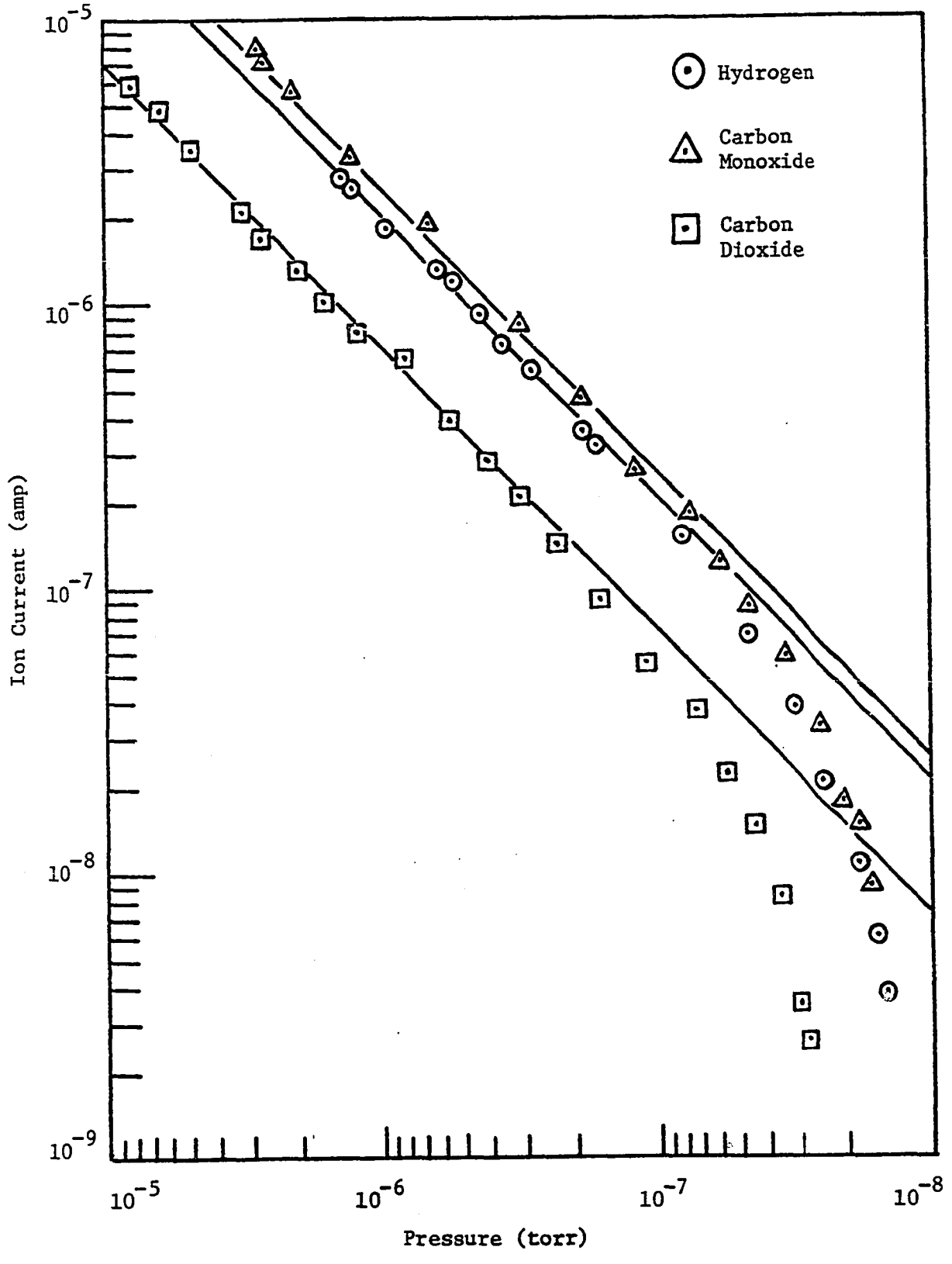

Figure 2-11 The calibration of mass spectroscopy ion current against ionization gauge pressure.

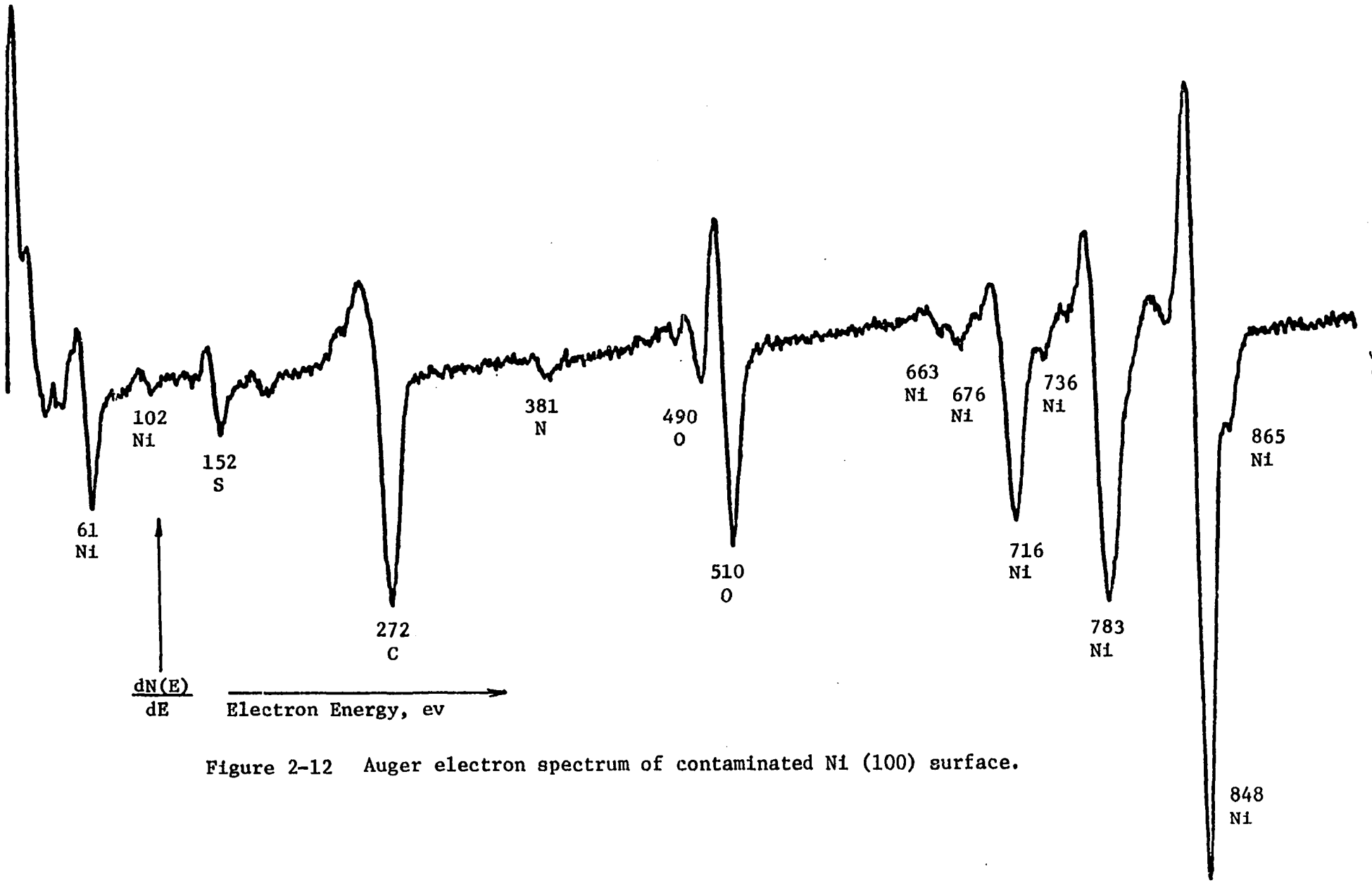

Figure 2-12 Auger electron spectrum of contaminated Ni (100) surface.

significant amounts of sulfur, nitrogen, oxygen and carbon appear on Ni (100) surface. Initial cleaning of both side surface of Ni (100) crystal were made by heating and and sputtering cycles. The crystal was first heated by the electron bombardment gun. The nitrogen and carbon AES peaks totally disappeared from the surface after it was heated 30 minutes at a temperature of 800°C. Oxygen and sulfur remained on the surface but the amount of oxygen was significantly decreased. Then the crystal was sputtered with a beam current of 10.5 μa of argon ions at energy of 500 ev for 30 minutes. This removed the residual sulfur and the Auger spectrum of a clean Ni (100) surface is shown in Figure 2-13.

Once nitrogen was removed by heating at 800°C, it reappeared infrequently and at amounts too small to have an effect on the subsequent experiments. Sulfur can be totally removed by sputtering and does not return to the surface. However, if new thermocouple wires are attached, the sulfur does reappear in significant quantity on the surface. This suggests that a majority of sulfur has diffused from the thermocouple wires onto the crystal rather than sweating out from the bulk. Oxygen is the most difficult species to remove. In agreement with other investigators (25,26), oxygen cannot be removed by heating or sputtering, but the atomic percentage of oxygen on Ni (100) surface is less than 2.44%. Carbon also disappears after heating and does not reappear on the surface for a period of up to two hours at room temperature under normal operating pressure. In conclusion, it is believed that the clean Ni (100) surface is relatively stable in the environment of ultra-high vacuum at 2.0×10^{-9} torr.

2-7 Experimental Procedure

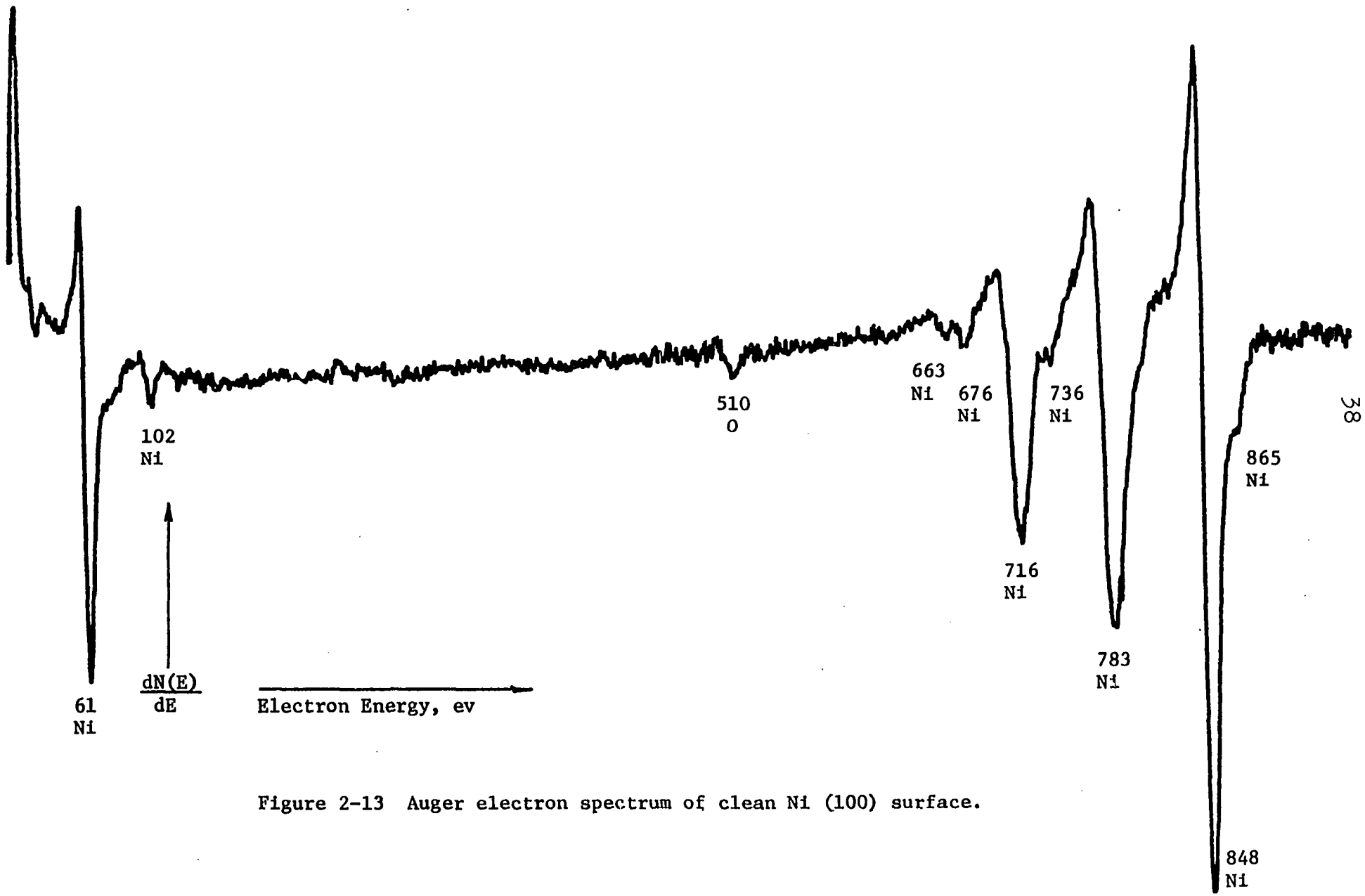

Figure 2-13 Auger electron spectrum of clean Ni (100) surface.

After the Ni (100) crystal was cleaned by heating and argon ion bombardment, the experiments were performed in the following sequence.

(i) A particular gas is leaked into system and the pressure change is recorded vs. time. The area under this recorded curve represents the exposure of the gas to surface. After this area is measured, the number of gas molecules striking per unit surface area can be calculated according to the method described in Appendix A.

(ii) The Ni crystal is heated with a linear heating rate by using a well-focused light beam and this particular gas starts to desorb from Ni surface. The partial pressure of this gas is recorded vs. surface temperature change by monitoring mass spectrometer ion current. The area under this flash curve is related to the coverage of this gas for this particular exposure on the Ni surface. This curve itself represents the desorption rate of this gas as a function of temperature.

(iii) After flashing, the Auger electron spectrum is taken periodically to monitor the composition of the surface.

(iv) The crystal is heated again by electron bombardment to 800°C for several minutes to remove the major contaminants such as hydrogen, oxygen and carbon. This cleaning procedure does not include an argon ion bombardment step, since the sulfur does not reappear on Ni (100) surface after first argon ion bombardment treatment.

(v) After this cleaning of the crystal surface by heating alone, the surface is checked by the

Auger electron spectroscopy to make sure the surface is free of contaminants. In most cases, this step is omitted, because the surface is clean enough after step (iv).

(vi) The crystal is allowed to cool to room temperature.

These six steps consist of an adsorption-desorption experimental cycle. After a number of data points are obtained, a plot of surface coverage vs. exposure is constructed and the sticking coefficient of this particular gas is calculated according to procedure outlined in Appendix B.

CHAPTER III

RESULTS AND DISCUSSIONS

3-1 Adsorption and Desorption of Hydrogen

The hydrogen flash desorption spectra after hydrogen adsorption on clean Ni (100) surface at 46°C show two maxima occuring at 378 and 460°K. After hydrogen desorption, the Auger electron spectrum of the Ni surface remained essentially the same as that before adsorption. Figure 3-1 shows a series of typical hydrogen flash desorption spectra at various hydrogen exposures. The total hydrogen coverage of these two peaks vs. hydrogen exposure is given in Table 3-1 and shown in Figure 3-2. The full coverage of these two peaks reaches a limiting value of 1.11×10^{14} molecules/cm^2.

The shape of α state peak, which is the flash peak at lower temperature, is symmetric about the peak temperature 378°K, a symmetric peak is characteristic of second order desorption kinetics (14). A plot of the natural logrithm of the desorption rate divided by the α state coverage as a function of the inverse temperature is presented in Figure 3-3. According to Equation (1-13), this curve should be linear, if the hydrogen desorption reaction is first order. Since the line in Figure 3-3 is nonlinear, this indicates that α state hydrogen desorption is not first order. Therefore, a plot of the natural logrithm of desorption rate divided by the square

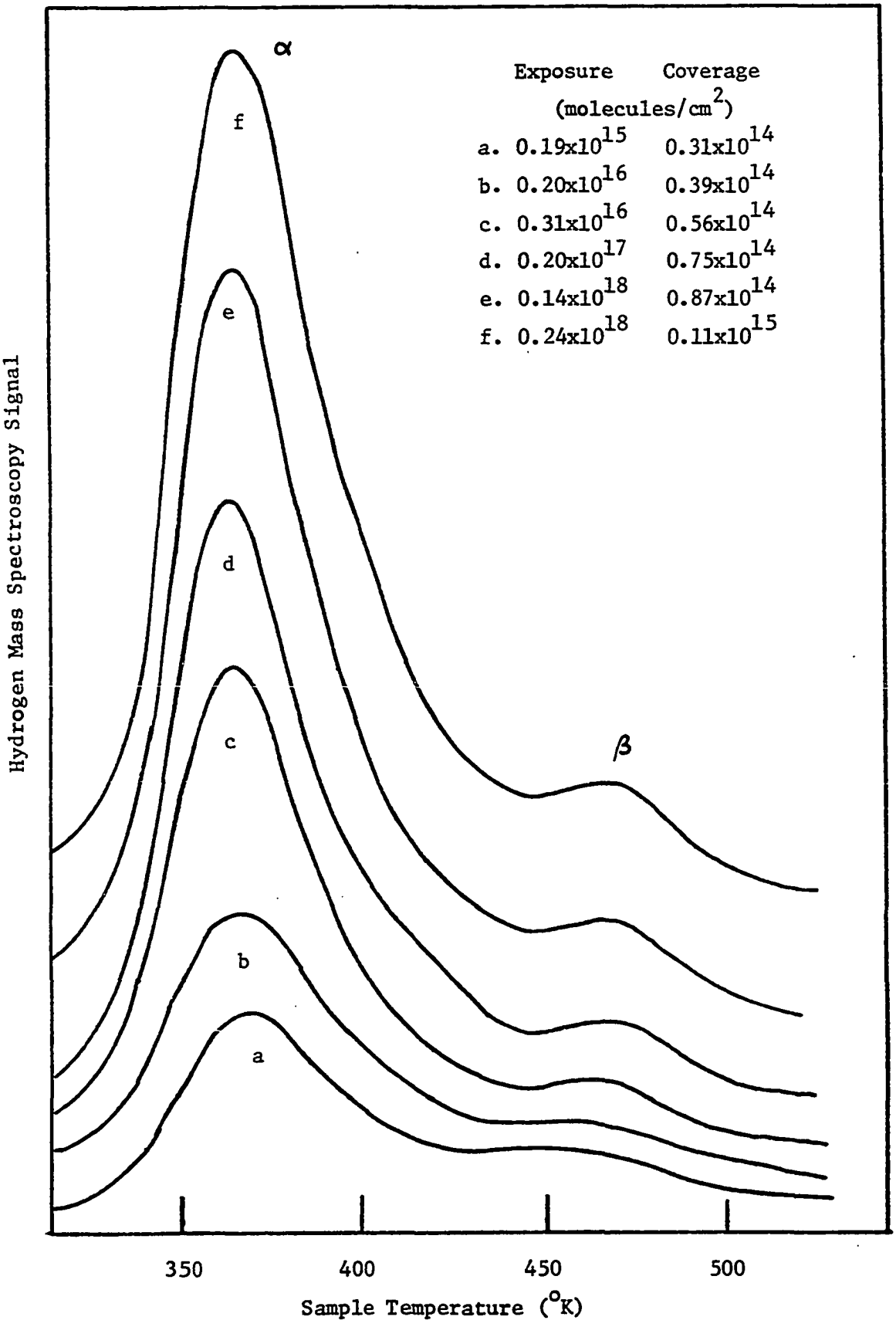

Figure 3-1 Typical hydrogen flash desorption spectra at various hydrogen exposure.

Table 3-1

Total Hydrogen Coverage Versus Hydrogen Exposure

Hydrogen exposure (10^{16} mole./cm^2)	Hydrogen coverage (10^{14} mole/cm^2)	Hydrogen exposure (10^{16} mole./cm^2)	Hydrogen coverage (10^{14} mole./cm^2)
0.009	0.18	2.9	0.76
0.019	0.13	3.9	0.83
0.020	0.35	4.6	0.75
0.032	0.37	5.5	0.78
0.050	0.33	7.0	0.83
0.068	0.41	7.9	0.74
0.11	0.49	8.8	0.80
0.19	0.39	9.5	0.82
0.25	0.39	10.0	0.84
0.31	0.56	12.0	0.85
0.32	0.65	13.0	0.96
0.43	0.74	14.0	0.87
0.55	0.68	15.0	0.97
0.62	0.69	17.0	1.00
0.64	0.57	19.0	0.98
0.67	0.56	22.0	1.11
1.20	0.69	24.0	1.11
1.50	0.64	26.0	1.11
2.00	0.75	30.0	1.11
2.90	0.63	35.0	1.11

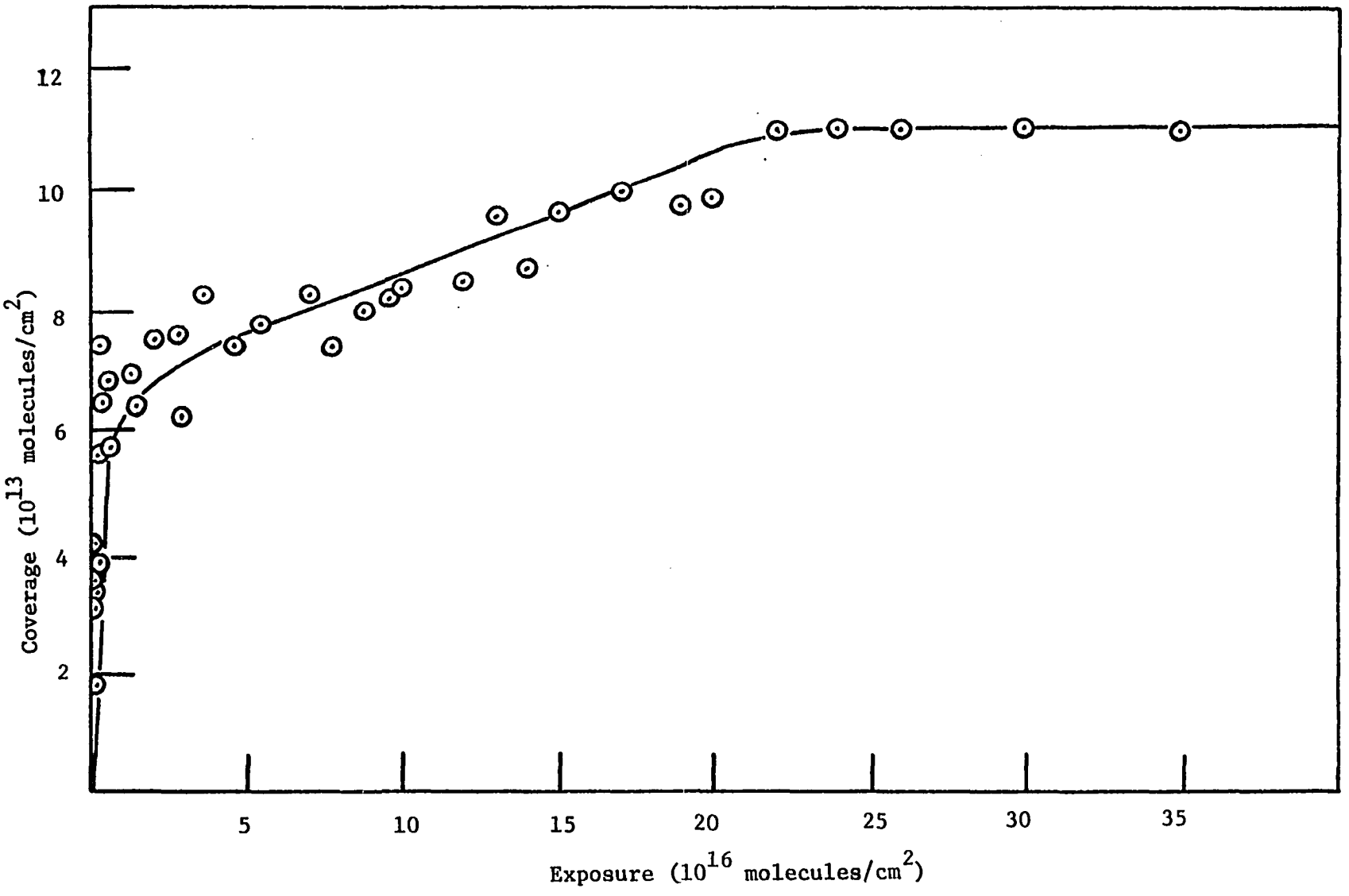

Figure 3-2 Total hydrogen coverage versus hydrogen exposure

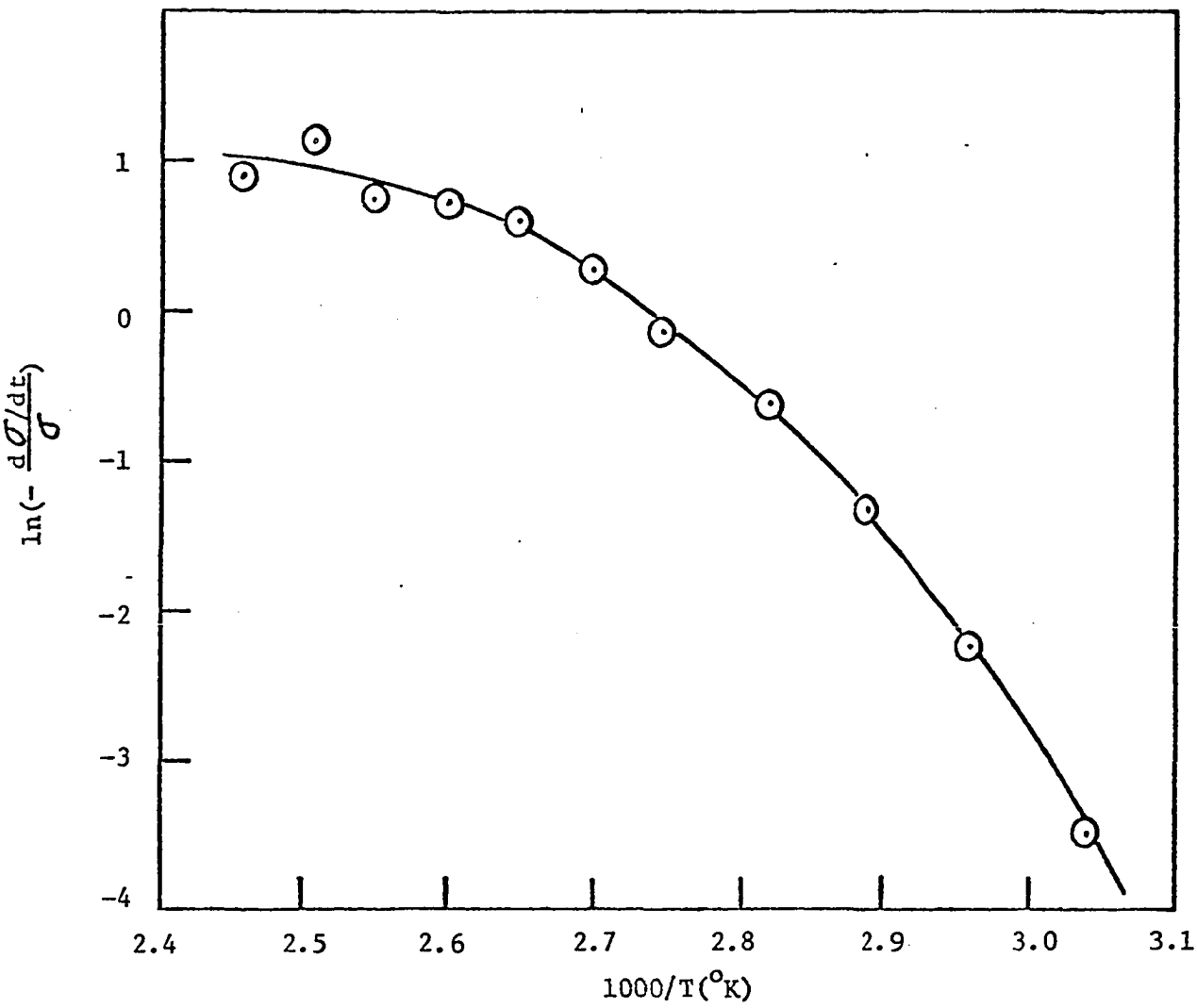

Figure 3-3 Logrithm of the ratio of desorption rate to α state coverage versus inverse temperature for hydrogen desorption after hydrogen exposure.

of the α state coverage as a function of the inverse temperature has been constructed in Figure 3-4. In accordance with Equation (1-17), the linear correlation in Figure 3-4 strengthens the assumption of second order desorption kinetics with a fixed activation energy for the hydrogen. The activation energy and pre-exponential factor of this reaction can be obtained from slope and intercept of the straight line in Figure 3-4. A linear least-squares fitting yields an activation energy of 21.78 ± 0.3 Kcal/g-mole and a pre-exponential factor of 0.128 cm^2/atom-sec. Two theoretical α state peaks, which correspond to the flash spectra c and f in Figure 3-1, have been generated by computer simulation with above values of activation energy and pre-exponential factor, using Equation (1-13). The peak temperature of the theoretical flash peaks differs from that of the experimental flash peaks by about 20°C. When an activation energy of 23.0 Kcal/g-mole is used without changing the value of the pre-exponential factor, the peak temperature of theoretical flash peak generated by computer is identical to that of experimental flash peak. However, the peak height of the theoretical flash peak at the peak temperature is lower than that of experimental flash peak. This difference of peak height is about a factor of 1.3 and 1.2 for the flash peaks c and f in Figure 3-1 respectively. This peak height difference is probably due to inaccuracies in the measurement of the pumping speed for hydrogen.

The hydrogen coverage of the α state versus hydrogen exposure is given in Table 3-2 and shown in Figure 3-5. The saturated coverage of α state is 1.0×10^{14} molecules/cm^2. This curve with two segments in Figure 3-5 is similar to that in Figure 3-2. The first segment occurs below

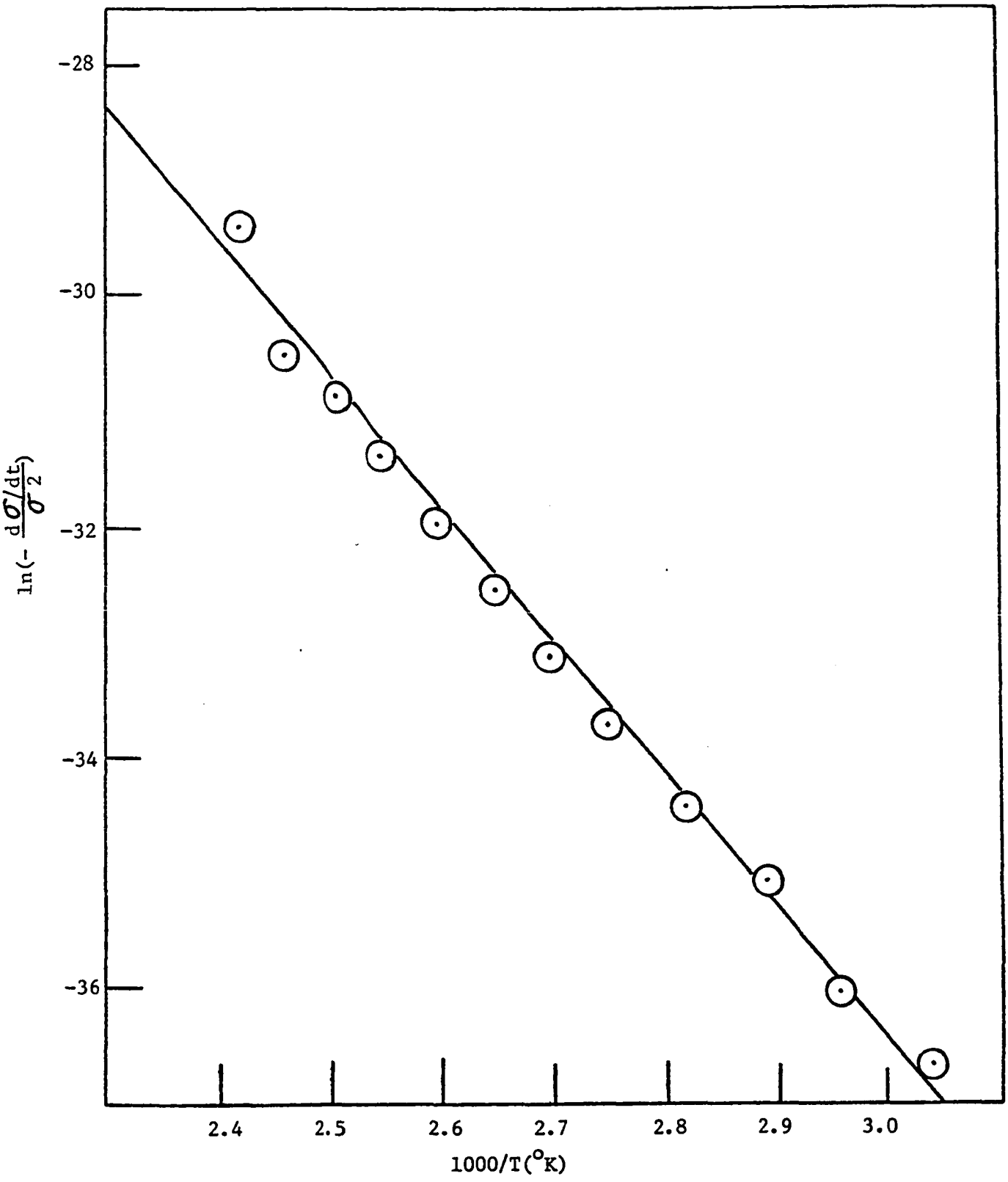

Figure 3-4 Logrithm of the ratio of desorption rate to square of α state coverage versus inverse temperature for hydrogen desorption after hydrogen exposure.

Table 3-2

Hydrogen Coverage of α State Versus Hydrogen Exposure

Hydrogen exposure (10^{16} mole./cm^2)	Hydrogen coverage (10^{14} mole./cm^2)	Hydrogen exposure (10^{16} mole./cm^2)	Hydrogen coverage (10^{14} mole./cm^2)
0.009	0.14	4.6	0.64
0.019	0.21	5.5	0.68
0.050	0.23	7.9	0.60
0.068	0.36	8.8	0.71
0.19	0.33	9.5	0.71
0.25	0.31	10.0	0.68
0.31	0.50	12.0	0.74
0.62	0.57	14.0	0.80
0.64	0.50	15.0	0.86
0.67	0.49	19.0	0.87
1.20	0.56	20.0	0.94
1.50	0.55	24.0	0.94
2.00	0.68	26.0	0.97
2.90	0.54	30.0	1.00

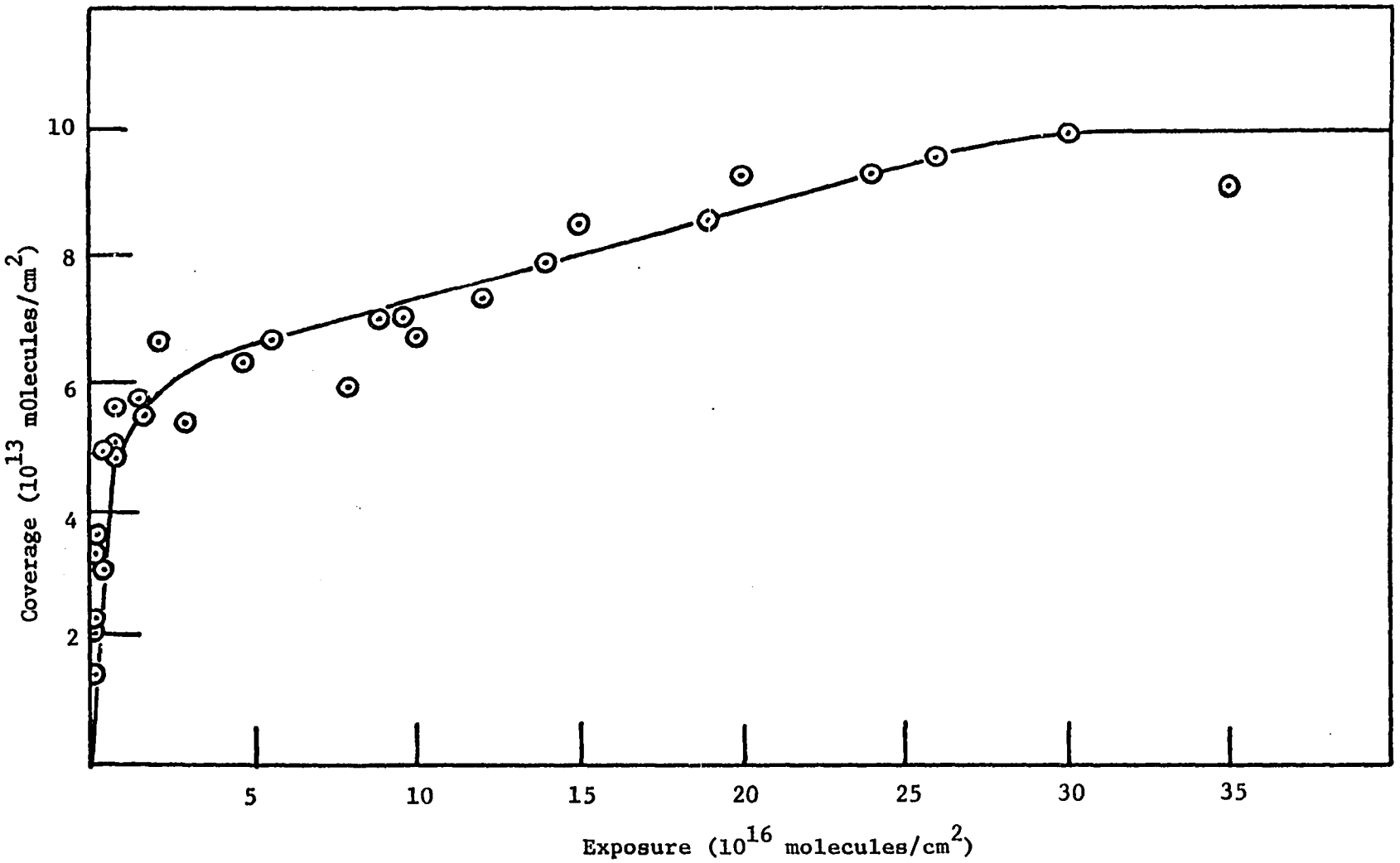

Figure 3-5 Hydrogen coverage of α state versus hydrogen exposure.

2.0×10^{16} molecules/cm^2 exposure and the second one is between 2.0×10^{16} and 3.0×10^{17} molecules/cm^2 exposure. These two segments in α state coverage-exposure curve could be interpreted as two regions with different sticking coefficients. In accordance with Equation (B-7) in Appendix B, the sticking coefficients are estimated by two plots of $\ln(1-\theta)$ versus the exposure divided by the hydrogen coverage of α state and are given in Figures 3-6 and 3-7. A linear least-squares fitting straight line in Figure 3-6 gives a slope of $0.4 \times 10^{-2} \pm 0.6 \times 10^{-3}$. This slope is the sticking coefficient for the α state below a hydrogen exposure of 2.0×10^{16} molecules/cm^2. In the same manner, the straight line in Figure 3-7 indicates a sticking coefficient of $0.1 \times 10^{-2} \pm 0.1 \times 10^{-3}$ for the hydrogen exposure above 2.0×10^{16} molecules/cm^2.

In Figure 3-8, the α state (dashed line) is separated from the remainder of the hydrogen flash desorption spectrum. This separation is based on the theoretical α state flash peak by multiplying this peak by the factor due to inaccurate measurement of pumping speed of hydrogen. It is intresting to note that the β state, which is the flash peak at higher temperature, consists of more than one state. Since the quantity of β state is small (1.1×10^{13} molecules/cm^2), it is impossible to make any quantitative analysis for this state. Also, the β state contains at least two peaks and these peaks are superimposed each other. This increases the difficulty in analyzing the β state. Part of the β peak may be due to the adsorption on the crystal edges. The hydrogen coverage of β state vs. hydrogen exposure is given in Table 3-3 and shown in Figure 3-9. The saturated coverage of this β state is 1.1×10^{13} molecules/cm^2. According to Equation (B-7), the $\ln(1-\theta)$ vs. the hydrogen exposure divided by the saturated coverage of β state is

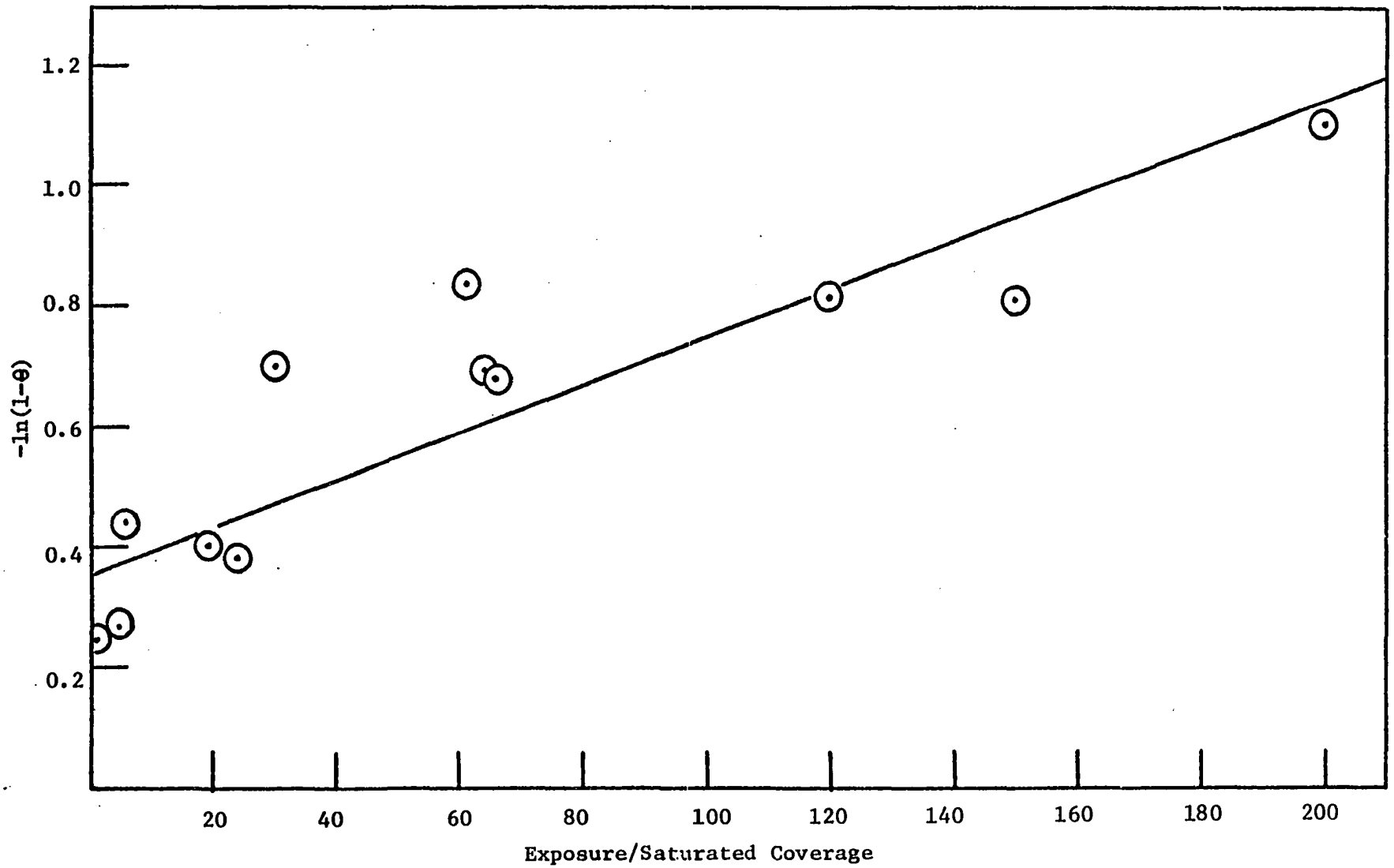

Figure 3-6 Hydrogen sticking coefficient of α state for hydrogen exposure below 2.0×10^{16} molecules/cm^2.

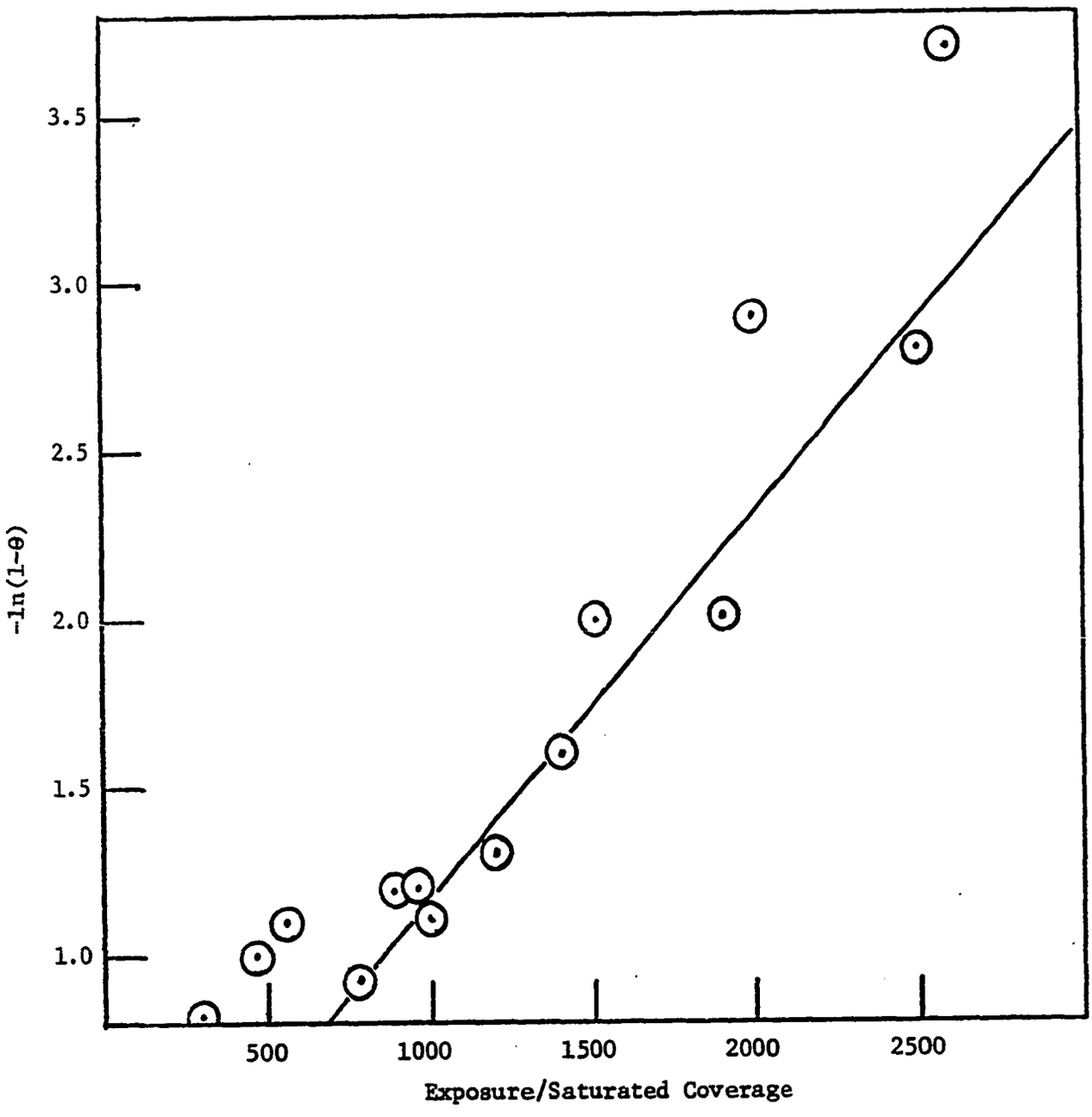

Figure 3-7 Hydrogen sticking coefficient of α state for hydrogen exposure higher than 2.0×10^{16} molecules/cm^2.

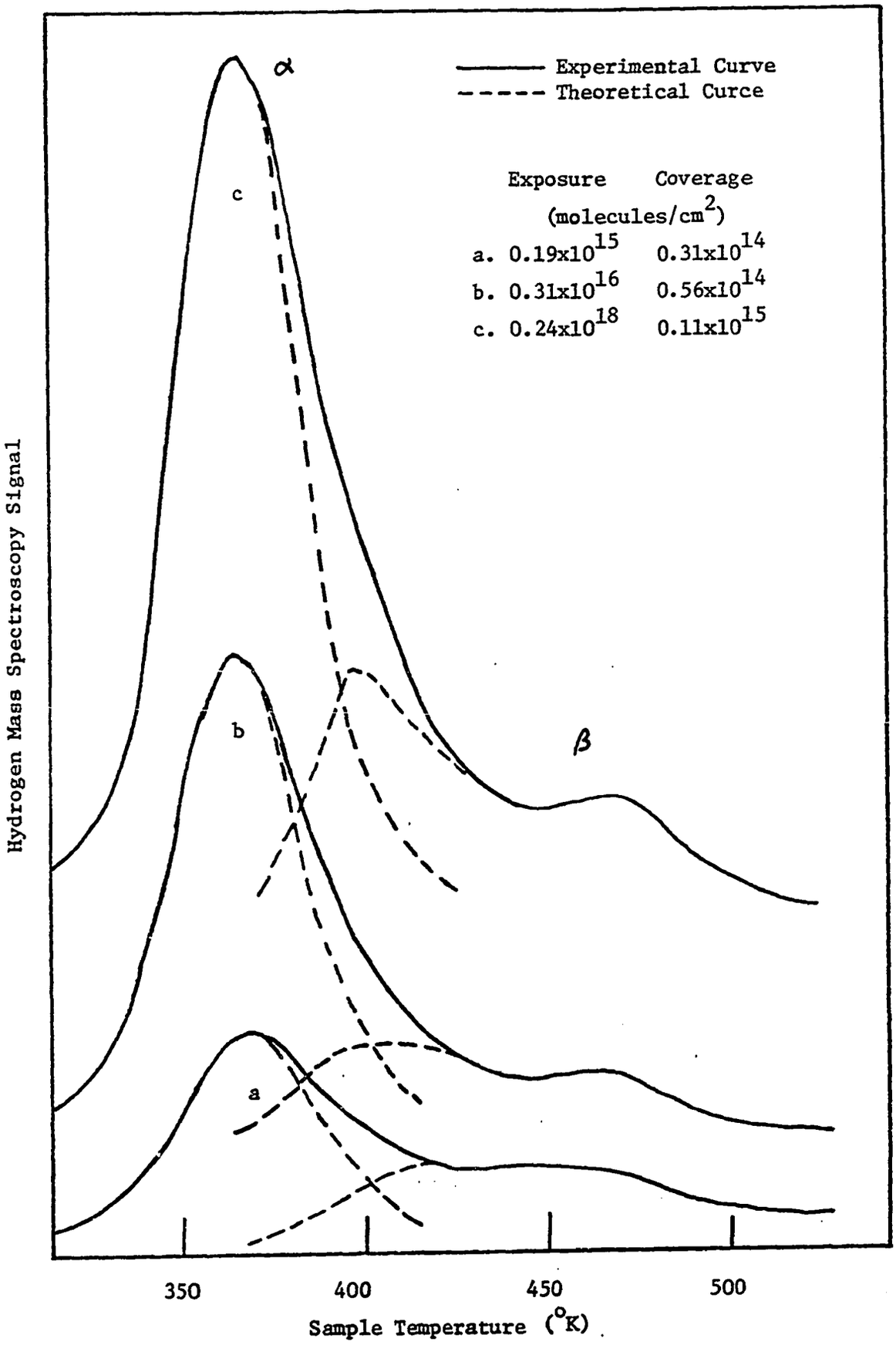

Figure 3-8 Theoretical hydrogen flash desorption spectra at various hydrogen exposure.

Table 3-3

Hydrogen Coverage of β State Versus Hydrogen Exposure

Hydrogen exposure (10^{16} molecules/cm^2)	Hydrogen coverage (10^{14} molecules/cm^2)
0.009	0.036
0.068	0.057
0.19	0.060
0.25	0.072
0.31	0.058
0.64	0.074
0.67	0.065
1.5	0.068
2.0	0.069
2.9	0.079
4.6	0.093
5.5	0.097
8.8	0.093
9.5	0.093
12.0	0.11
15.0	0.11
19.0	0.11
24.0	0.11
30.0	0.11

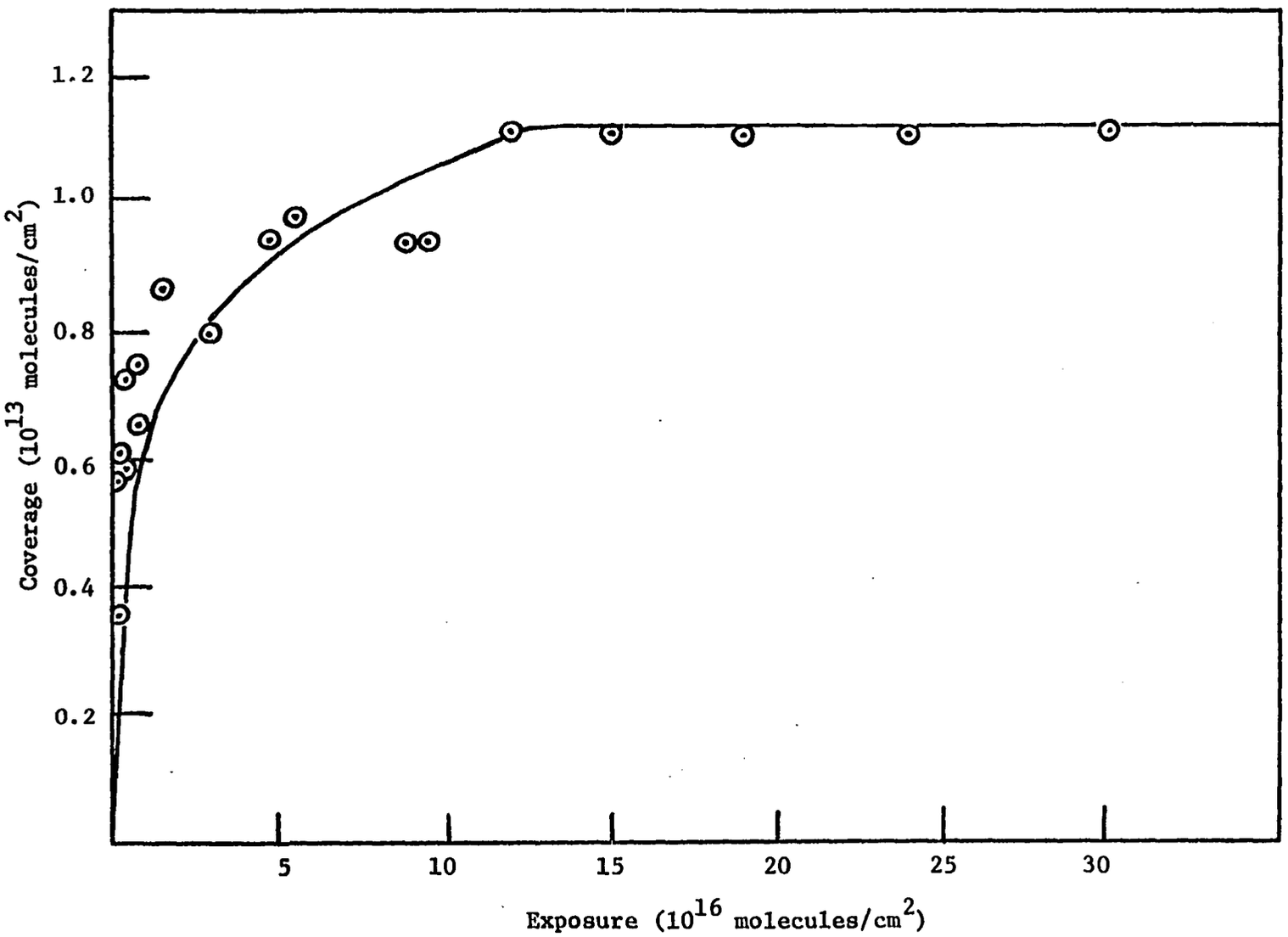

Figure 3-9 Hydrogen coverage of β state versus hydrogen exposure.

plotted in Figure 3-10. A linear least-squares fitting gives a sticking coefficient of $0.78 \times 10^{-4} \pm 0.5 \times 10^{-5}$.

The results of this study on H_2-Ni (100) system are in agreement with previous work. Lapujoulade and Neil (27) have studied this system by using the flash desorption technique. They reported a second order desorption reaction with an activation energy of 23.1 Kcal/g-mole and a pre-exponential factor of 2.5×10^{-1} cm^2/atom-sec. They also observed a sticking coefficient of 0.06 and a full coverage of 3.3×10^{14} atoms/cm^2 which corresponds to 1.15×10^{14} molecules/cm^2. The only disagreement is that only one hydrogen flash peak was observed by them. Two flash desorption peaks have been detected in the study. However, other investigators (28,29) also reported a second peak in hydrogen flash desorption spectrum on polycrystalline nickel surface. This disagreement is probably due to different surface treatment. Lapujoulade and Neil cleaned their surface only by heating. As other investigators (26) and this study have indicated it is impossible to remove sulfur from the Ni (100) surface by heating alone. The sulfur on Ni (100) surface can only be removed by ion bombardment. Also the Ni (100) surface used by Lapujoulade and Neil was not subjected to analysis by Auger electron spectroscopy to monitor the composition of the surface. Therefore, their Ni (100) surface was probably contaminated by sulfur which could account for the difference in the observed flash desorption spectrum. The sticking coefficient (0.06) obtained by Lapujoulade and Neil is a little bit higher than that of this study. Horgan and Daline (30) stated that the contaminants on low index planes of Ni surface will effect the measurement of sticking coefficient and concluded that the sticking coefficient of hydrogen should be less than or equal to

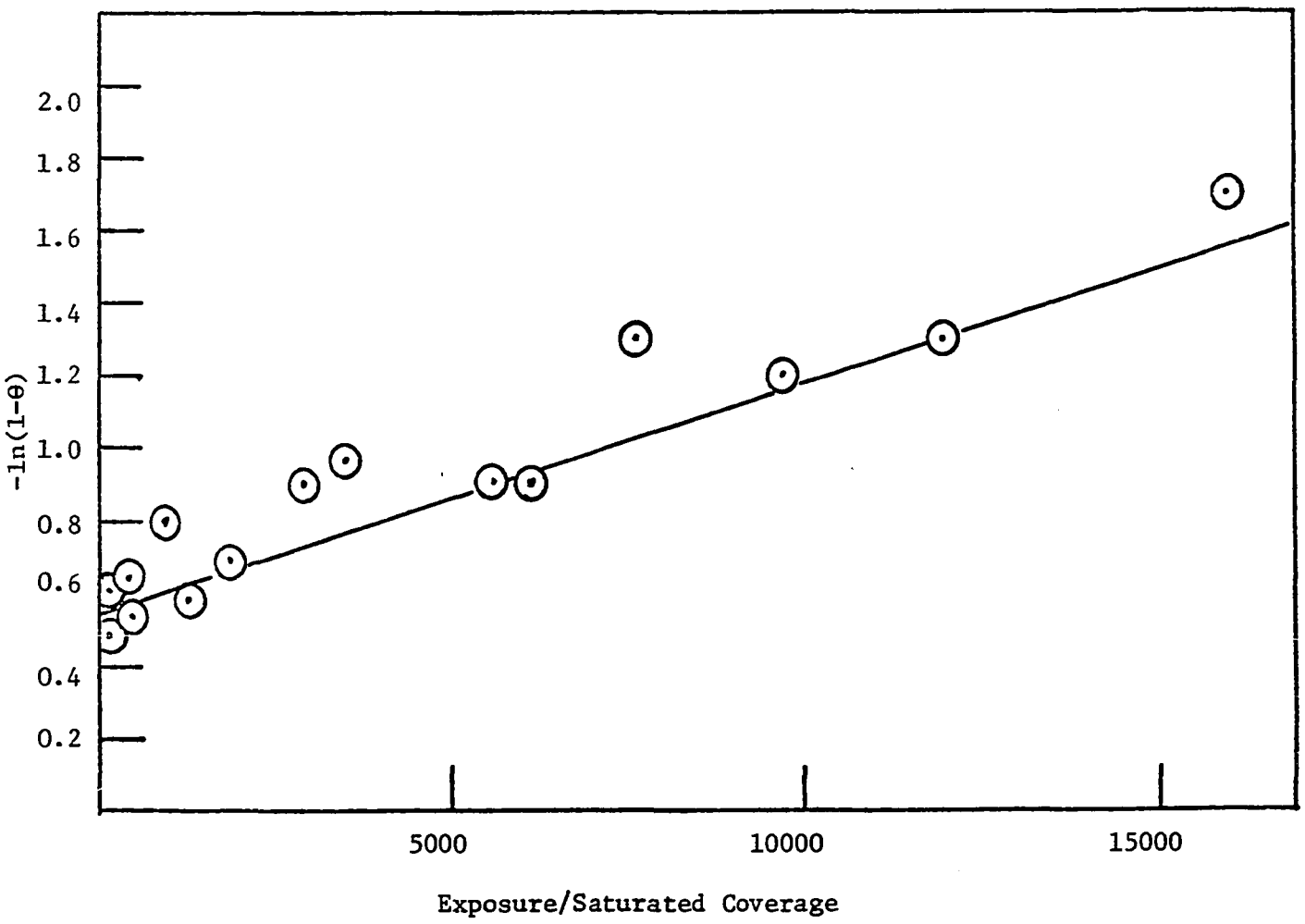

Figure 3-10 Hydrogen sticking coefficient of β state.

10^{-2} for Ni (100) and Ni (111). Again the high sticking coefficient obtained by Lapujoulade and Neil could be correlated with a contaminated surface.

3-2 Adsorption and Desorption of Carbon Monoxide

Figure 3-11 shows a series of carbon monoxide flash desorption spectra at various carbon monoxide exposures on the clean Ni (100) surface at 46°C. Only a single desorption peak has been observed at a temperature 407°C with a half width of 71.3±6.1°C at full coverage. The carbon monoxide coverage vs. carbon monoxide exposure is given in Table 3-4 and shown in Figure 3-12. The curve in Figure 3-12 is generated by a polynomial regression computer program and expressed as

$$\sigma = 1.468 + 40.205N - 108.455N^2 + 138.798N^3 - 83.366N^4 + 18.852N^5 \qquad (3\text{-}1)$$

where σ = coverage of carbon monoxide (10^{14} molecules/cm^2)
N = exposure of carbon monoxide (10^{16} molecules/cm^2).
It shows that the maximum coverage is 7.7×10^{14} molecules /cm^2 which corresponds to 0.48 monolayer based on an adsorption site density of 1.61×10^{15} atoms/cm^2 for Ni (100). After a CO adsorption and flash desorption cycle, the Auger electron spectrum is essentially the same as before adsorption indicating a negligible buildup of carbon and oxygen.

Since the peak shape is asymmetric and does not shift with peak temperature, this state can be characterized by first order desorption kinetics. An activation energy of 25.1 Kcal/g-mole has been obtained by solving Equation (1-14) based on the experimental peak temperature and

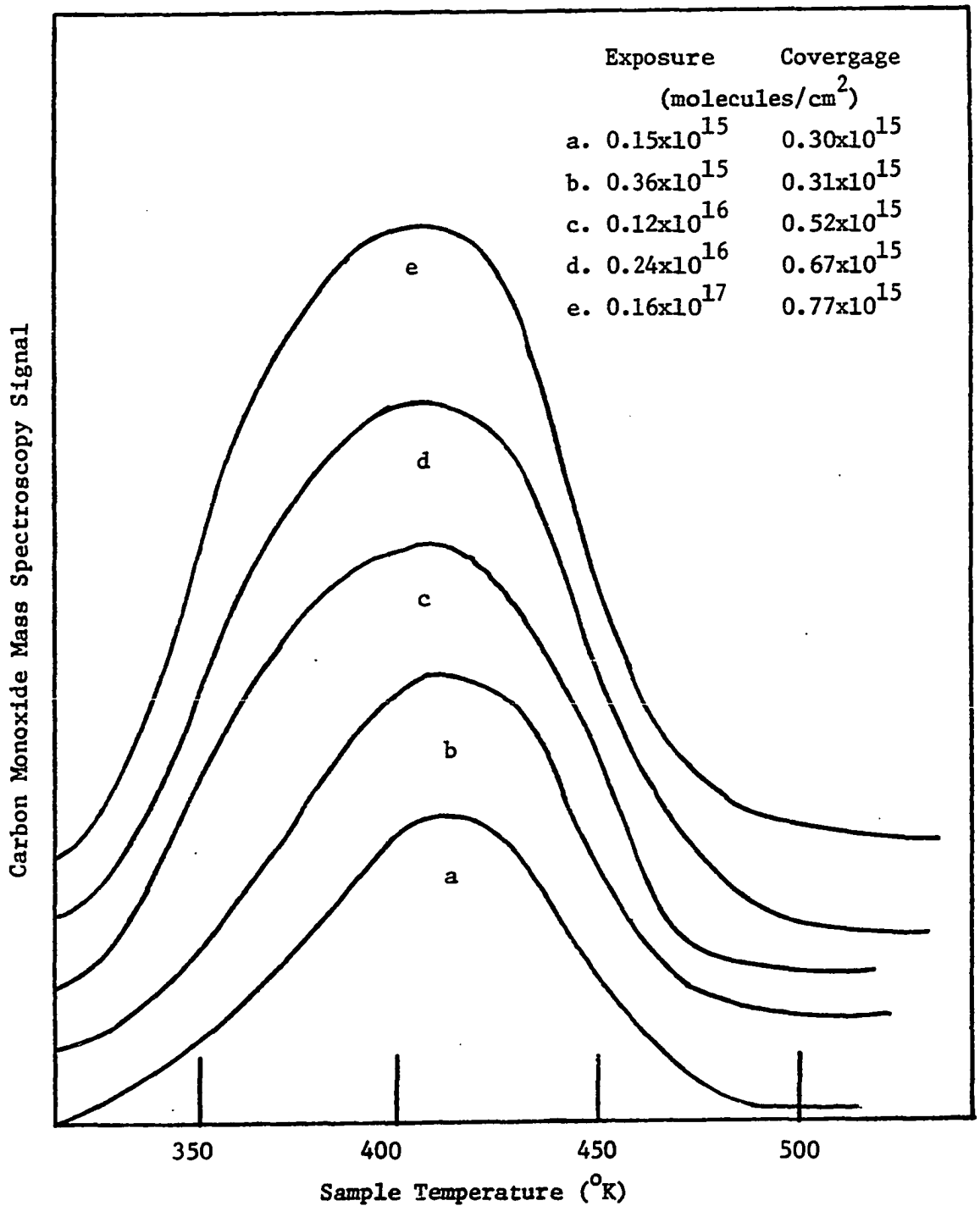

Figure 3-11 Typical carbon monoxide flash desorption spectra at various carbon monoxide exposure.

Table 3-4

Carbon Monoxide Coverage Versus
Carbon Monoxide Exposure

Carbon monoxide exposure (10^{16} mole./cm^2)	Carbon monoxide coverage (10^{15} mole./cm^2)	Carbon monoxide exposure (10^{16} mole/cm^2)	Carbon monoxide coverage (10^{15} mole/cm^2)
0.0001	0.036	0.24	0.54
0.0062	0.093	0.24	0.67
0.014	0.12	0.25	0.60
0.015	0.30	0.29	0.70
0.019	0.16	0.50	0.73
0.019	0.26	0.51	0.75
0.023	0.34	0.75	0.73
0.032	0.21	0.83	0.74
0.036	0.31	0.89	0.76
0.040	0.42	0.98	0.74
0.057	0.29	1.0	0.72
0.070	0.47	1.1	0.77
0.10	0.47	1.2	0.73
0.11	0.51	1.6	0.77
0.12	0.52		

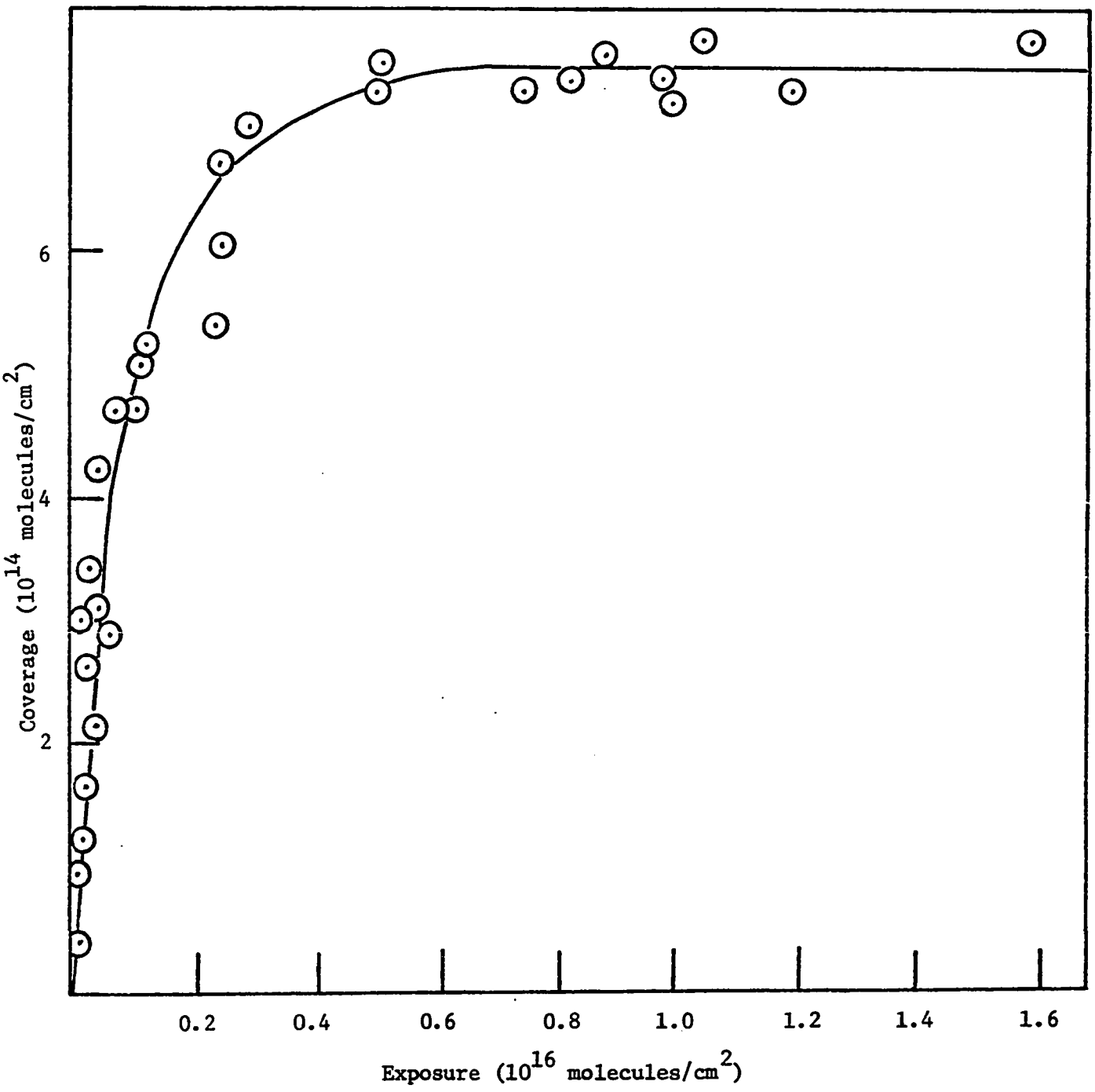

Figure 3-12 Carbon monoxide coverage versus carbon monoxide exposure.

an assumed pre-exponential factor 10^{13} sec^{-1}. Using Equation (1-13), a theoretical CO flash peak (as shown in Figure 3-13), which corresponds to the flash desorption spectrum e in Figure 3-11, has been generated by computer simulation with the above values of activation energy and pre-exponential factor. The peak temperature of this theoretical flash peak is identical to that of the experimental flash peak. However, the shape of the theoretical flash peak is narrower than that of the experimental flash peak at same CO coverage. This difference suggests that there are several states contributing to the experimental flash desorption spectrum.

In Appendix B, the sticking coefficient of CO has been discussed and a simple site occupation model has been introduced to calculate the sticking coefficient for CO. Therefore, a plot of $\ln(1-\theta)$ vs. the exposure divided by the saturated coverage has been constructed in Figure 3-14 in order to obtain the sticking coefficient. After a linear least-square fitting, the slope is found to be 0.42 ± 0.023, which corresponds to the value of sticking coefficient of carbon monoxide.

Earlier results of the study of the Ni (100)-CO interaction are reviewed and discussed here with reference to the results of this study. Park and Farnsworth (31) studied the adsorption of CO on Ni (100) using Low-Energy Electron Diffraction (LEED) and observed a c(2x2) pattern. Litchman, et al (32) examined this study by using electron probe surfacemass spectrometry and reported that there were no ions traceable to adsorbed CO on the Ni (100) surface. However, as first pointed out by Onchi and Farnsworth (33) a Ni (100) surface which is prepared by heating alone may not be sufficiently clean to adsorb CO. Onchi and Farnsworth (34) again confirmed the c(2x2) pattern first observed

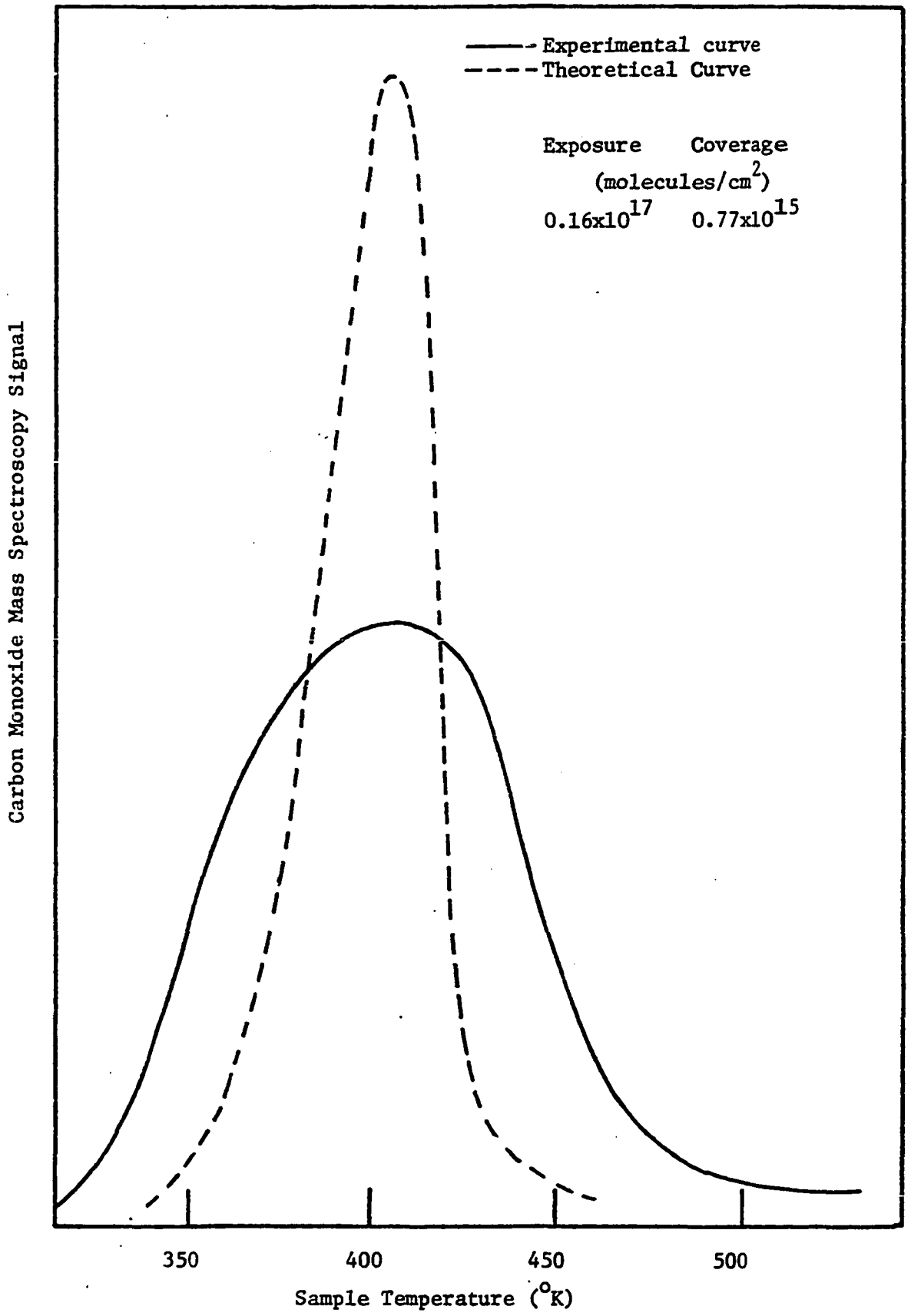

Figure 3-13 Theoretical carbon monoxide flash desorption spectrum of carbon monoxide adsorption.

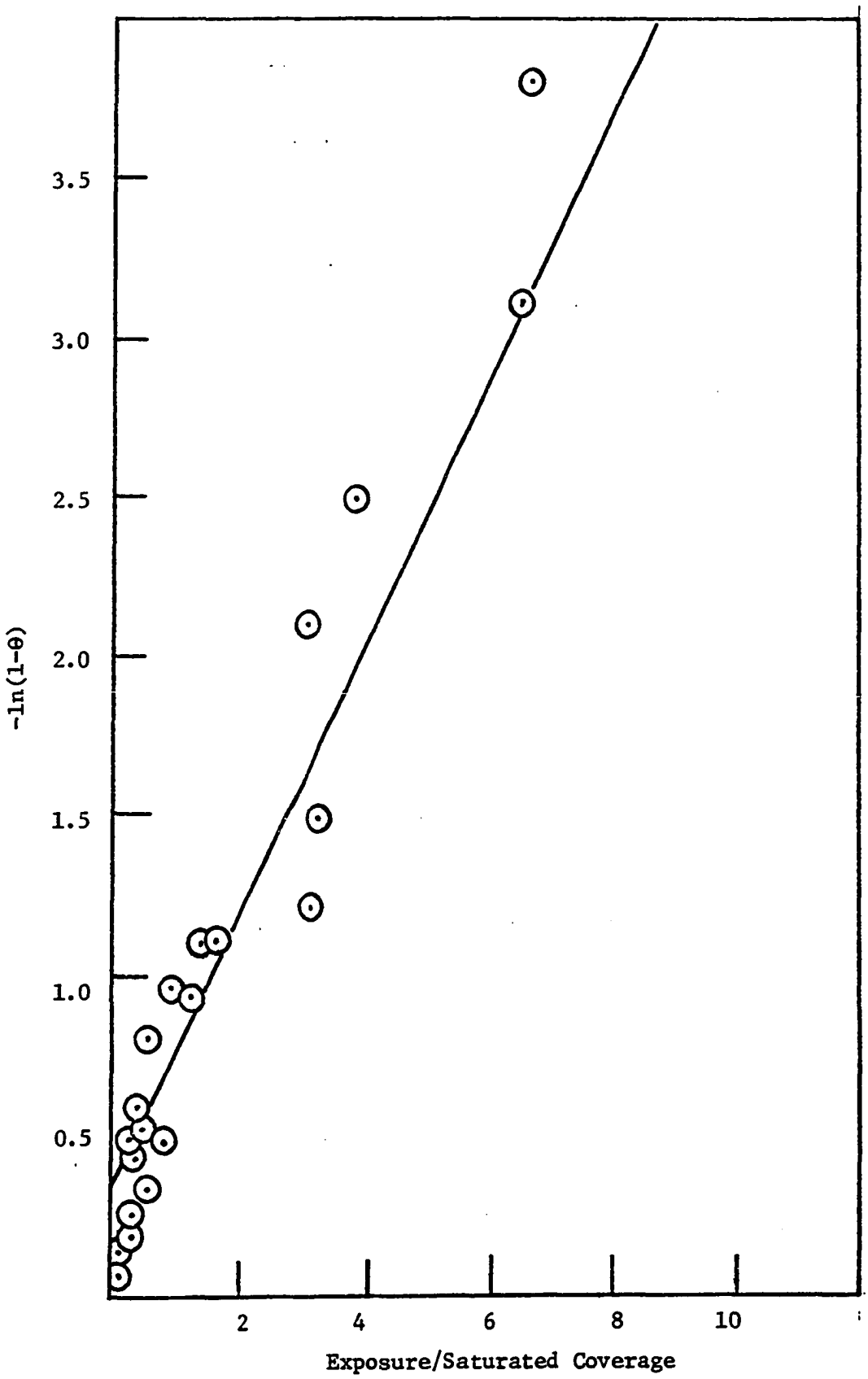

Figure 3-14 Carbon monoxide sticking coefficient.

by Park and Farnsworth and also reported flash desorption spectra with three peaks at 200, 400 and 600°K respectively. Tracy (35) observed that there was only one single flash desorption peak at 400°K which is very close to the result of this study at 407°K. Also Tracy pointed out that the 600°K peak reported by Onchi and Farnsworth was so broad as to possibly suggest desorption from the sample support. Futhermore, Tracy's LEED observations showed that in the submonolayer region the CO-Ni (100) system is characterized by three phases: (i) a disordered structure formed at a sufficiently low coverage and/or high temperature, (ii) a c(2x2) structure which exists at a low temperature and/or high coverage up to and including 0.5 monolayers, and (iii) a compressed hexagonal structure which exists for coverage of 0.61 to 0.69 monolayers. corresponding to a saturated coverage of 1.11×10^{15} molecules/cm^2. Klier, et al (36) have made equilibrium studies of CO adsorption on Ni (100). They reported a saturated coverage of 1.10×10^{15} molecules/cm^2 and a binding energy of 26.1 Kcal/g-mole which are in agreement with results of Tracy. The maximum coverage of this study is only 0.48 monolayers. The results of this study are compatible with the phase (ii) as characterized by Tracy. The maximum coverage 7.7×10^{14} molecules/cm^2 in this study then agrees with Tracy's phase (ii) coverage of 8.05×10^{14} molecules/cm^2.

3-3 Adsorption of Carbon Dioxide

After adsorption of carbon dioxide on the clean Ni (100) surface at 46°C, only the carbon monoxide was observed upon flashing. The CO flash desorption spectra at various CO_2 exposure is shown in Figure 3-15. The maximum desorption rate occured at 433°K. The CO

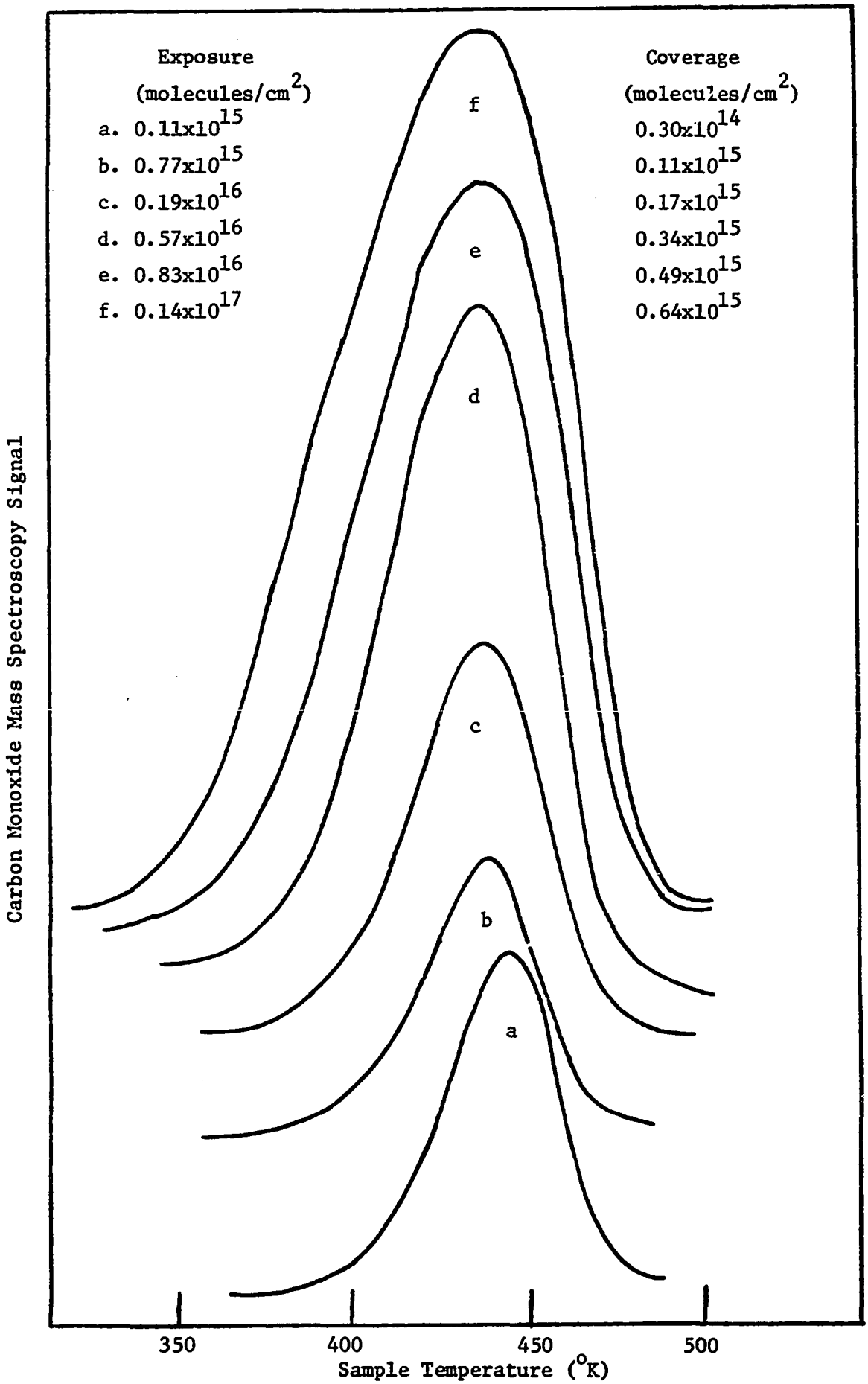

Figure 3-15 Typical carbon monoxide flash spectra at various carbon dioxide exposure.

coverage vs. CO_2 exposure is given in Table 3-5 and shown in Figure 3-16. The curve in Figure 3-16 is generated by a polynomial regression computer program and expressed as

$$\sigma = 0.309 + 6.832N - 1.904N^2 \qquad (3\text{-}2)$$

where σ = coverage of CO (10^{14} molecules/cm^2)
N = exposure of CO_2 (10^{16} molecules/cm^2).
The saturated coverage of CO is 6.4×10^{14} molecules/cm^2.

Since the peak shape is asymmetric and does not shift with peak temperature, this state can also be assigned to first order desorption kinetics. An activation energy of 26.9 Kcal/g-mole has been obtained by solving Equation (1-14) using the peak temperature and an assumed pre-exponential factor of 10^{13} sec^{-1}. Two theoretical flash peaks which correspond to the flash desorption spectra c and f in Figure 3-15, have been generated by computer simulation with the above values of activation energy and pre-exponential factor using Equation (1-13). In figure Figure 3-17, these two theoretical flash peaks are shown as dashed lines. The shape of the theoretical peak (curve a in Figure 3-17) reproduces the experimental flash peak at a CO coverage of 0.17×10^{15} molecules/cm^2. It is intresting to note that the shape of theoretical flash peak (curve b in Figure 3-17) is narrower than that of the experimental flash peak at a CO coverage of 0.64×10^{15} molecules/cm^2. This suggests that there is only one CO state for low CO_2 exposures ($<0.19 \times 10^{16}$ molecules/cm^2) and that there several CO states contributing to the experimental flash desorption spectrum for high CO_2 exposures. However, the peak temperature of the theoretical peak is identical to that of the experimental flash peak.

In Appendix B, the calculations for the sticking

Table 3-5

Carbon Monoxide Coverage Versus
Carbon Dioxide Exposure

Carbon dioxide exposure (10^{16} mole./cm^2)	Carbon monoxide coverage (10^{15} mole./cm^2)	Carbon dioxide exposure (10^{16} mole./cm^2)	Carbon monoxide coverage (10^{15} mole./cm^2)
0.0042	0.037	0.41	0.26
0.011	0.030	0.42	0.29
0.012	0.031	0.56	0.33
0.025	0.027	0.57	0.34
0.052	0.039	0.59	0.37
0.075	0.077	0.61	0.43
0.077	0.11	0.83	0.49
0.17	0.14	1.0	0.52
0.19	0.17	1.1	0.51
0.24	0.20	1.1	0.54
0.26	0.15	1.4	0.62
0.29	0.25	1.4	0.64
0.37	0.25	1.7	0.64
0.37	0.21	1.9	0.64
0.38	0.25		

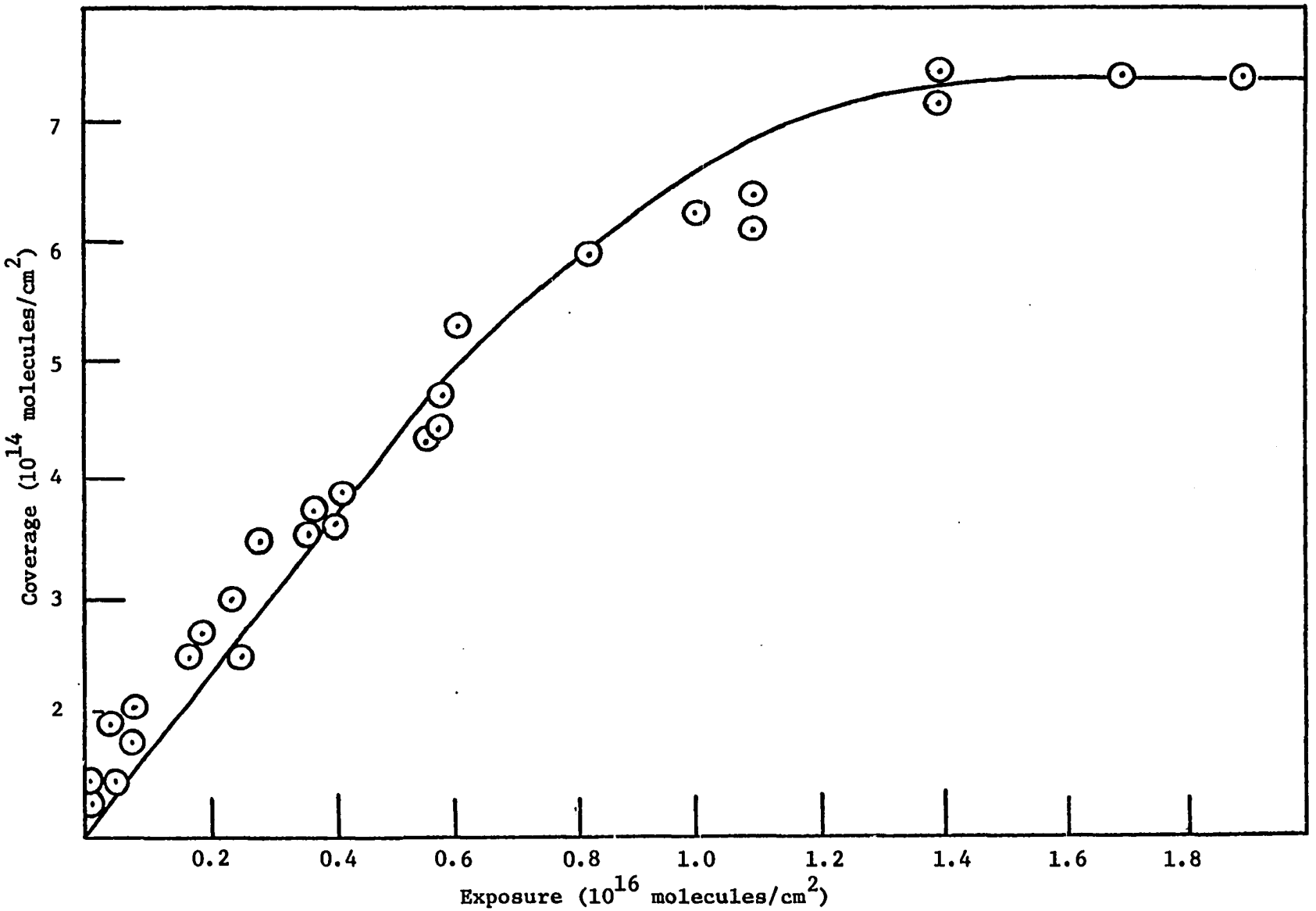

Figure 3-16 Carbon monoxide coverage versus carbon dioxide exposure.

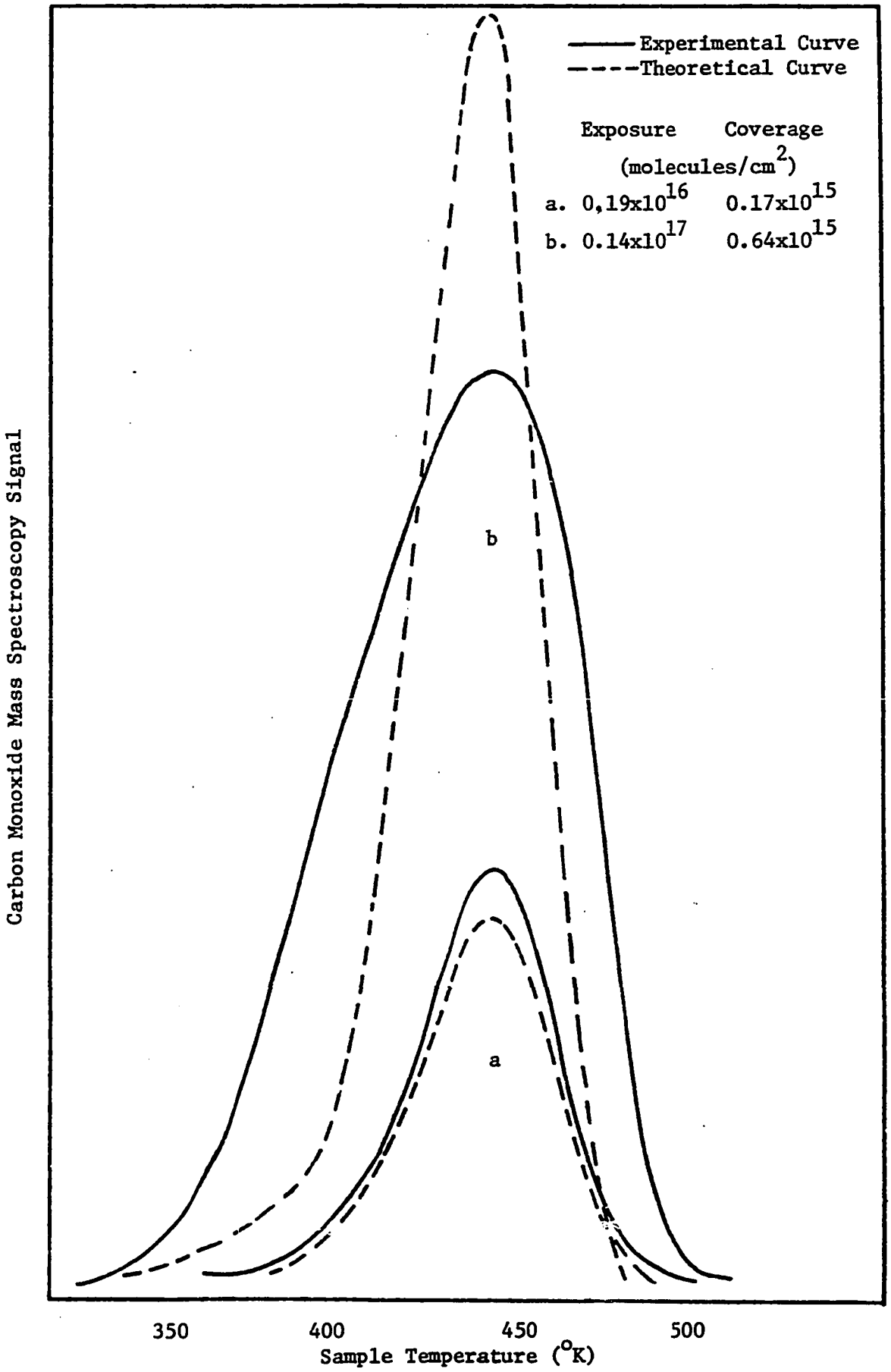

Figure 3-17 Theoretical carbon monoxide flash desorption spectra at at various carbon dioxide exposure.

coefficient for CO_2 has been discussed and an initial sticking coefficient of 0.07 has been reported based on Equation (B-2). In accordance with the simple site occupation model for the sticking coefficient, a plot of the $\ln(1-\theta)$ vs. CO_2 exposure divided by CO saturated coverage is given in Figure 3-18. A linear least-squares fitting of this plot gives a sticking coefficient of 0.1 ± 0.004 for CO_2 adsorption.

After the flash desorption, the Auger electron spectrum (as shown in Figure 3-19) was taken and indicated that oxygen builds up to an average oxygen atom percentage of 9.42% on Ni (100) surface.

Three facts indicate that the CO desorption following the adsorption of CO_2 on the Ni (100) surface is not due to background CO; (i) the CO peak shape is narrower than the shape of CO desorption peak from CO adsorption, (ii) the peak temperature is different, 433°K in comparison to 407°K which is the CO peak temperature after CO adsorption, and (iii) CO flash peak following adsorption of CO did not cause a buildup of oxygen on the surface, as was observed for CO_2 exposure. Also these three facts indicate that CO_2 molecule dissociated on a clean Ni (100) surface to yield adsorbed oxygen and CO. This is very similar to the study of decomposition of CO_2 on W (100) surface which is reported by Clavenna and Schmidt (40).

Unfortunatly, there is no report concerning flash desorption studies of CO_2 adsorption on a Ni (100) surface. McCarty, et al (41) observed that only a single first order CO peak at temperature 438°K with a desorption activation energy of 26.7 Kcal/g-mole after CO_2 adsorbed on Ni (110) surface which is in agreement with results of this study. Also McCarty, et al obtained a sticking coefficient of 0.15 ± 0.05, a value which agrees with the

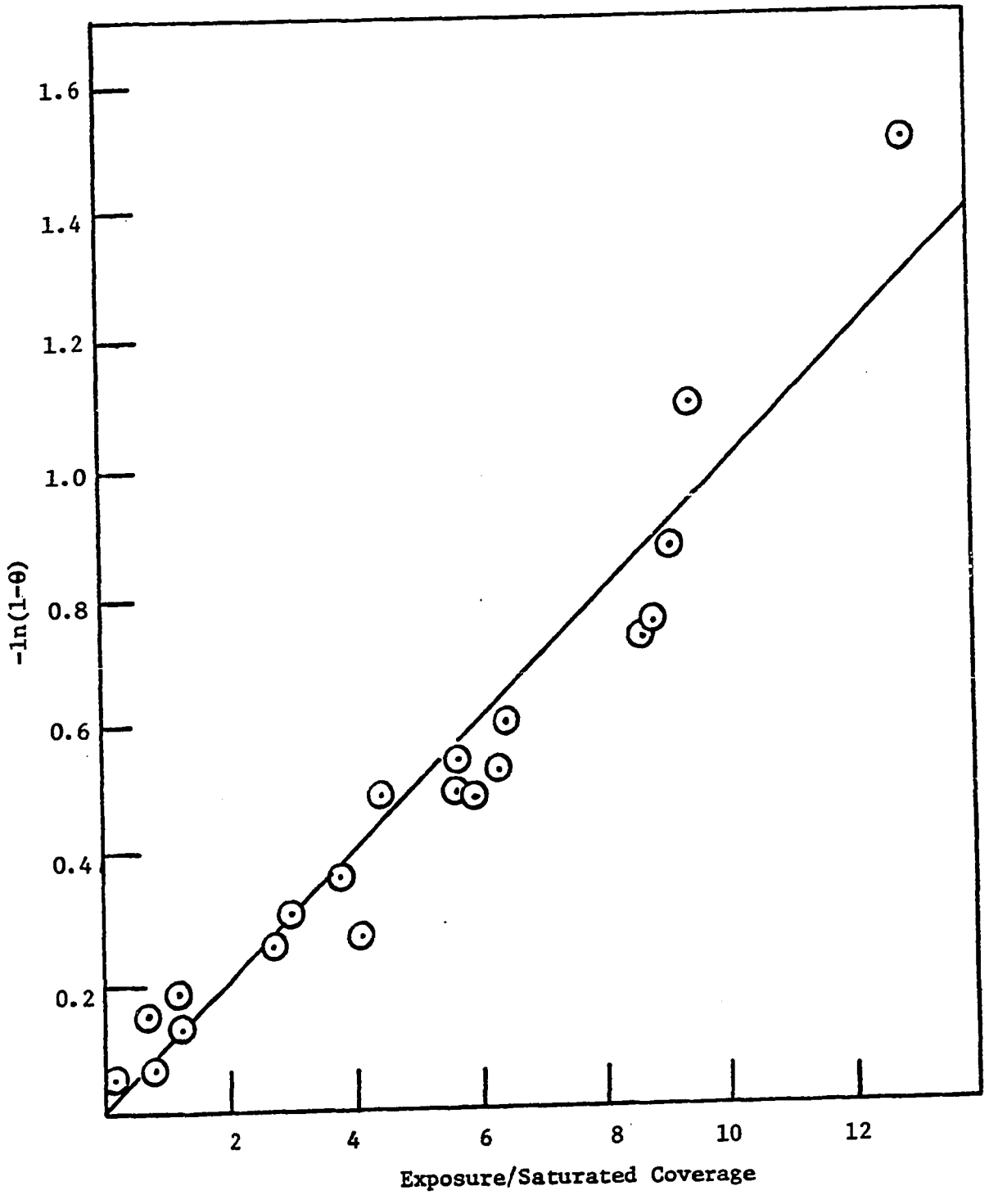

Figure 3-18 Carbon dioxide sticking coefficient.

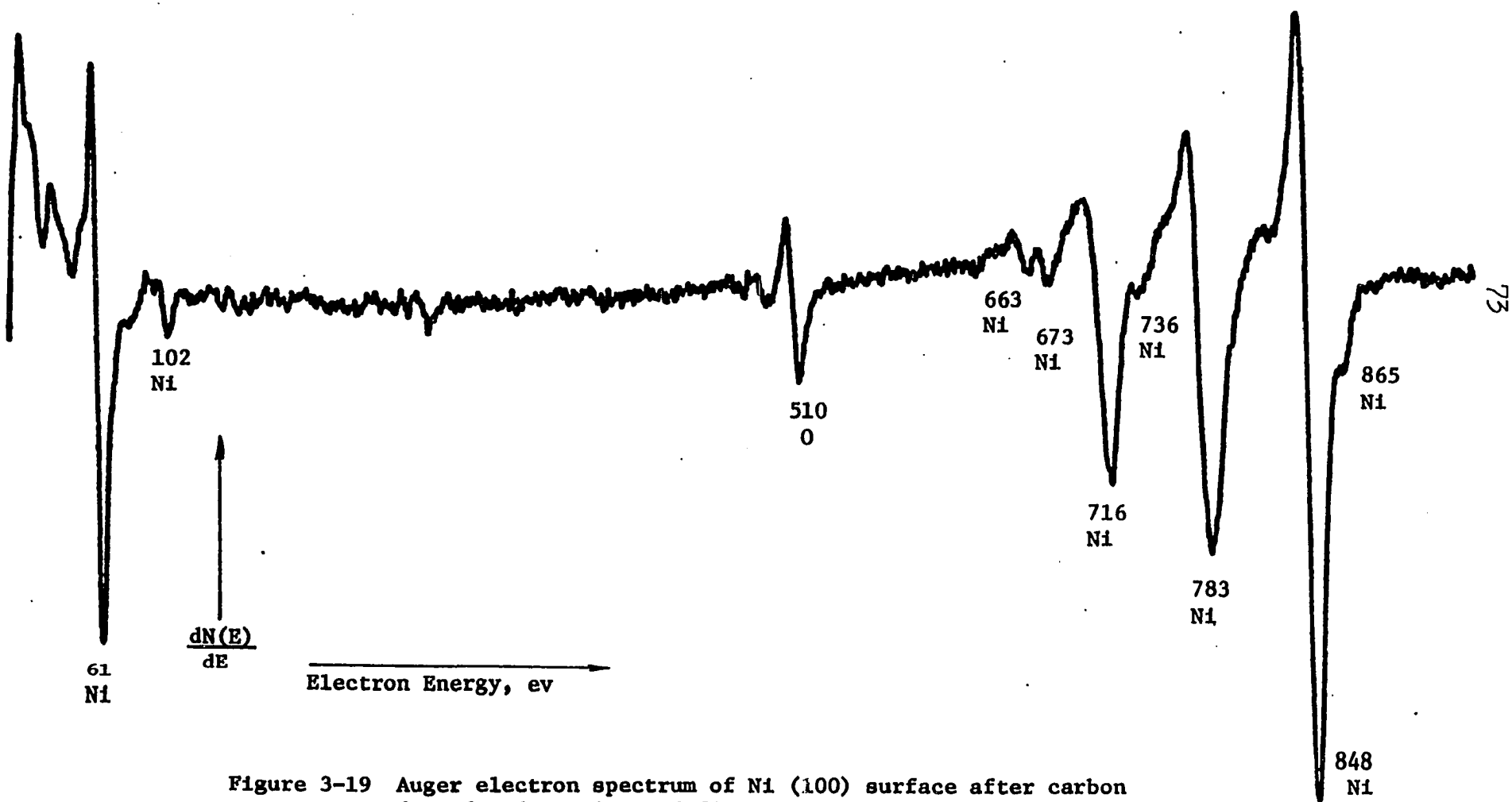

Figure 3-19 Auger electron spectrum of Ni (100) surface after carbon dioxide adsorption and flash.

sticking coefficient observed in this study.

3-4 Flash Decomposition of Formic Acid

After formic acid adsorption on Ni (100) surface at 46°C, the formic acid does not desorb from the surface directly. Only the reaction products H_2, CO and CO_2 were observed.

A series of typical flash desorption spectra of hydrogen at various formic acid exposure is shown in Figure 3-20. Two maximum desorption rates occured at 378 and 460°K. The total hydrogen coverage of these two peaks versus formic acid exposure is given in Table 3-6 and shown in Figure 3-21. The curve in Figure 3-21 generated by a polynomial regression program and expressed as

$$\sigma = 0.071 + 83.080N - 901.046N^2 + 4575.551N^3 - 8483.965 \qquad (3\text{-}3)$$

where σ = coverage of hydrogen (10^{14} molecules/cm^2)
N = exposure of formic acid (10^{16} molecules/cm^2).
The saturated coverage of these two peaks reaches a limiting value of 3.7×10^{14} molecules/cm^2. The coverage ratio between α state (the flash peak at 378°K) and the β state (the flash peak at 460°K) has a constant value of $1:0.47 \pm 0.05$.

The shape of α state hydrogen peak is symmetric about the peak temperature 378°K, a symmetric peak is characteristic of second order desorption reaction. A plot of the natural logrithm of the hydrogen desorption rate divided by the α state hydrogen as a function of the inverse temperature is presented in Figure 3-22.

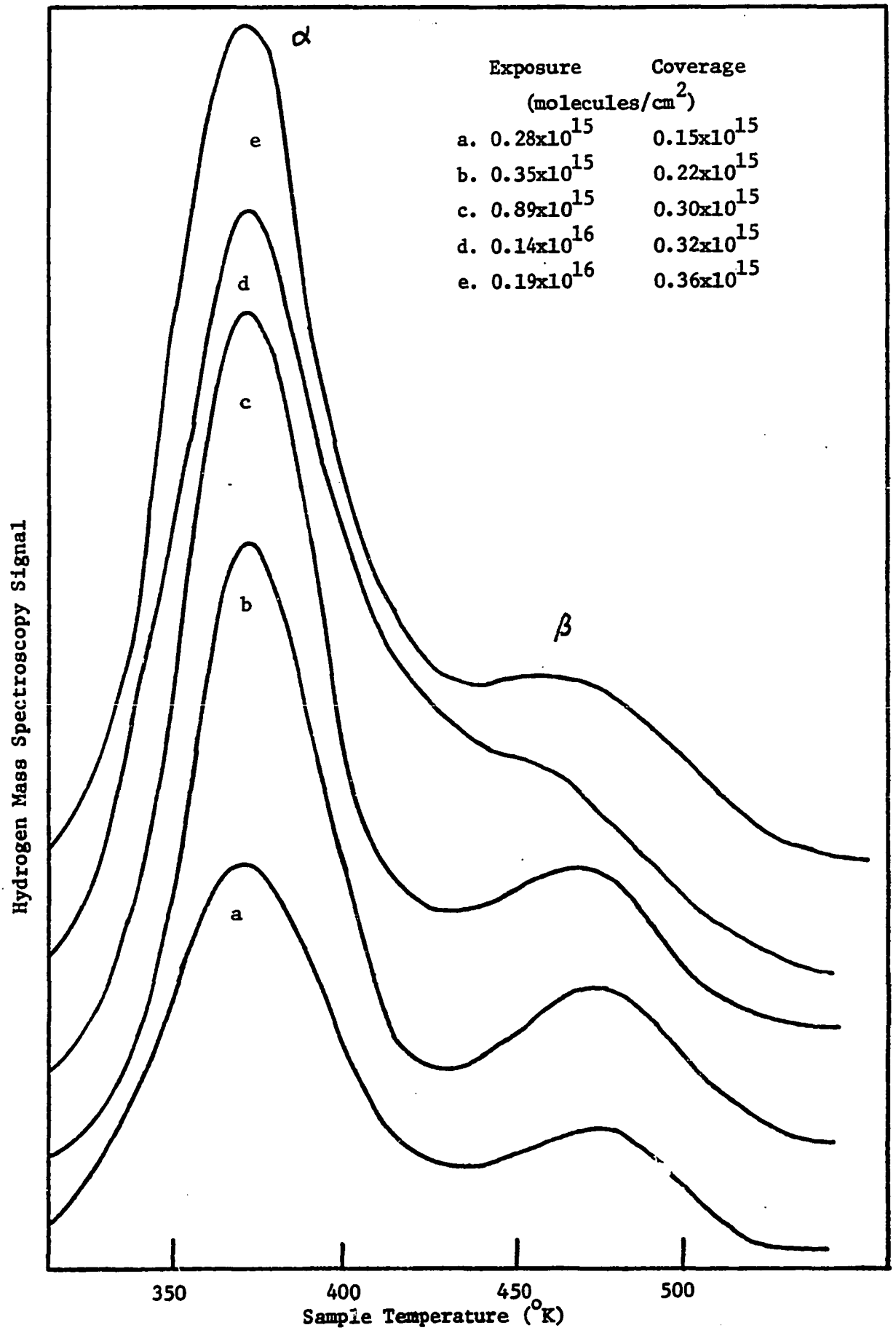

Figure 3-20 Typical hydrogen flash desorption spectra at various formic acid exposure.

Table 3-6

Hydrogen Coverage Versus Formic Acid Exposure

Formic acid exposure (10^{15} molecules/cm^2)	Hydrogen coverage (10^{15} molecules/cm^2)
0.088	0.084
0.16	0.11
0.28	0.15
0.35	0.22
0.52	0.28
0.54	0.25
0.81	0.29
0.85	0.28
0.89	0.30
0.91	0.34
0.96	0.29
1.1	0.31
1.3	0.32
1.4	0.32
1.4	0.35
1.6	0.36
1.9	0.36
2.0	0.37

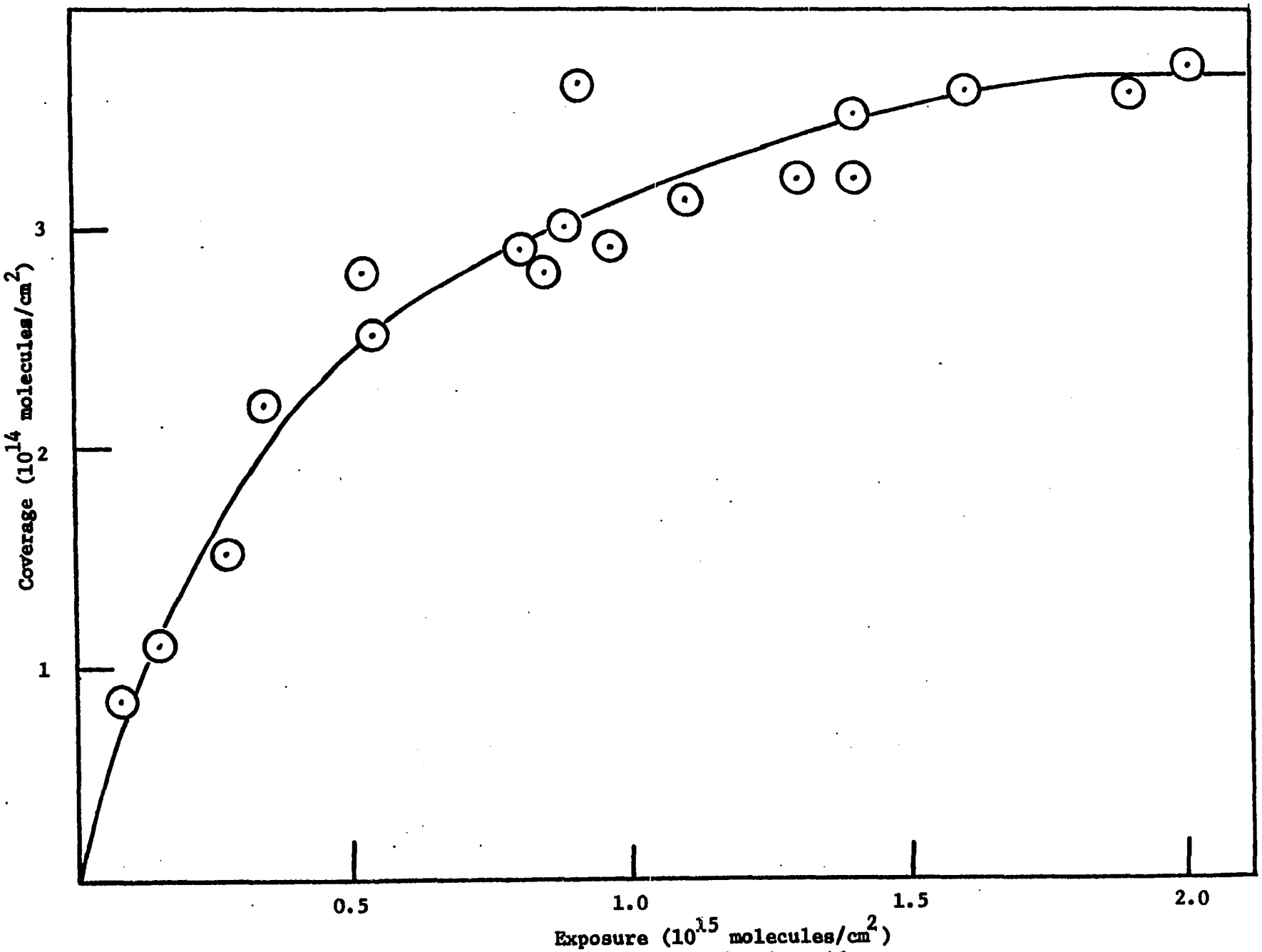

Figure 3-21 Hydrogen coverage versus formic acid exposure.

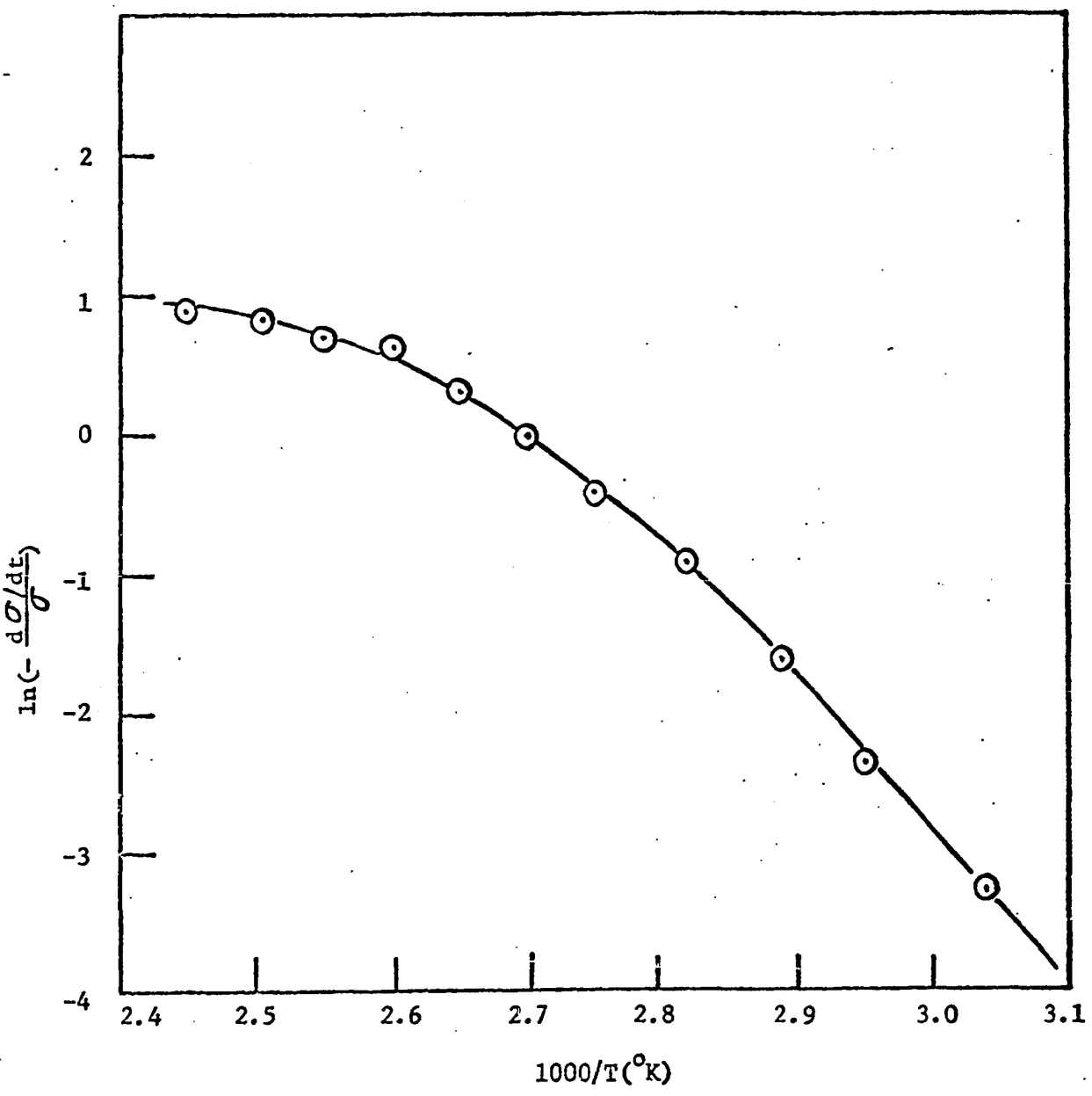

Figure 3-22 Logrithm of the ratio of desorption rate to α state coverage versus inverse temperature for hydrogen desorption after formic acid exposure

According to Equation (1-13), this curve should be linear, if this desorption reaction is first order. In fact, the line in Figure 3-22 is nonlinear and indicates that the α state hydrogen desorption is not first order. However, a plot of the natural logrithm of desorption rate divided by the square of the α state coverage as a function of the inverse temperature has been given in Figure 3-23. In accordance with Equation (1-17), the linear correlation in Figure 3-23 provides additional evidence of second order kinetics with a fixed activation energy for the hydrogen desorption following formic acid adsorption. The activation energy and pre-exponential factor of this reaction can be obtained from slope and intercept of the straight line in Figure 3-23. A linear least-squares fitting yields an activation energy of 21.5 ± 0.22 Kcal/g-mole and a pre-exponential factor of 0.057 cm^2/atom-sec. Two theoretical α state peaks, which correspond to the flash spectra b and e in Figure 3-20, have been generated by computer simulation with the above values of activation energy and pre-exponential factor using Equation (1-13). The peak temperature of the theoretical flash peaks differs from that of the experimental flash peak by about $30^{\circ}C$. When an activation energy of 23.5 Kcal/g-mole is used without changing the value of pre-exponential factor, the peak temperature of the theoretical flash peak generated by the computer is identical to that of the experimental flash peak. However, the peak height of the theoretical flash peak at peak temperature is lower than that of the experimental flash peak. This difference of peak height is about a factor of 1.4 and 1.2 for the flash peak b and c in Figure 3-20 respectively. This peak height difference is probably due to the inaccuracies in the measurement of pumping speed for hydrogen.

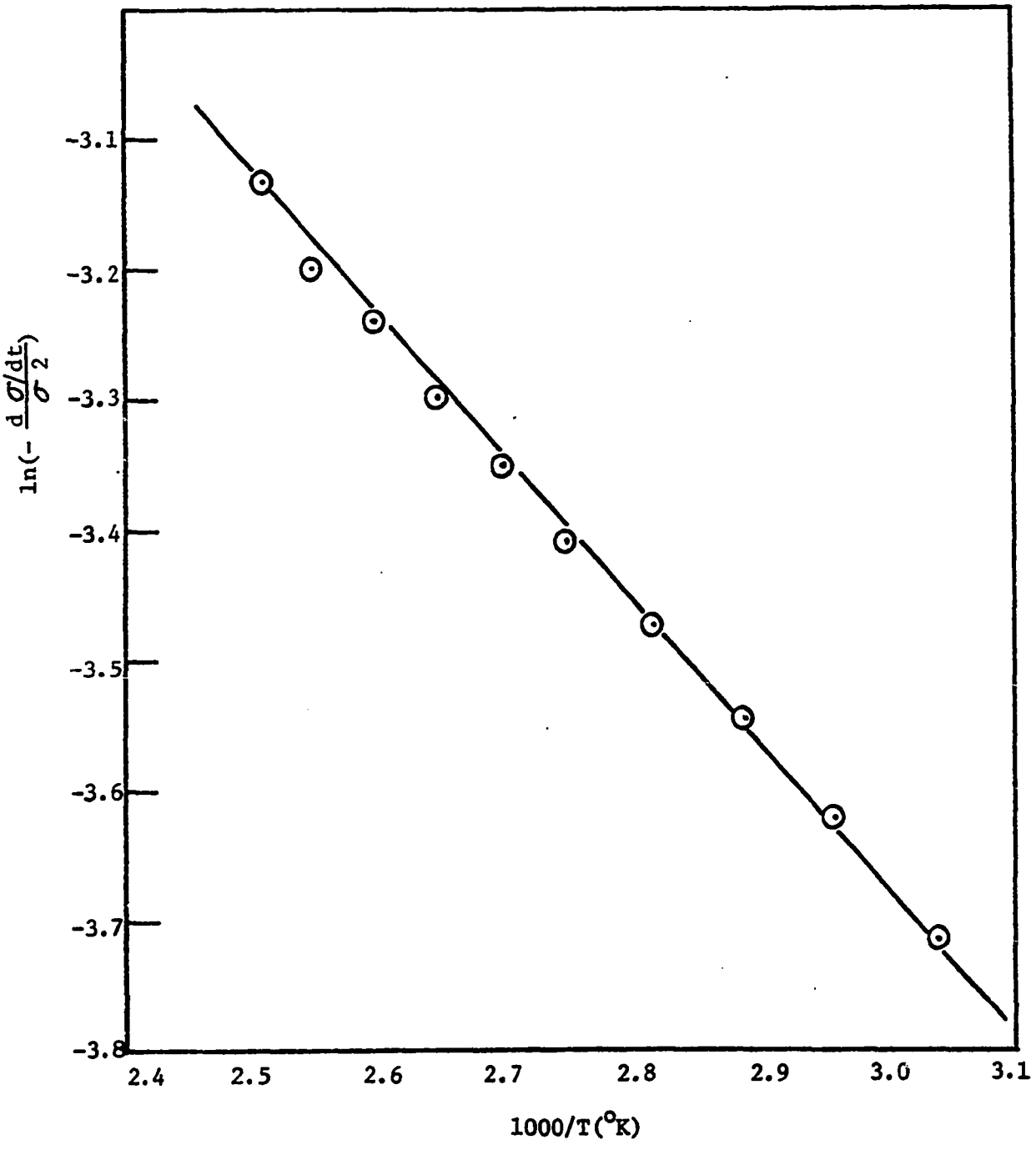

Figure 3-23 Logrithm of the ratio of desorption rate to square of α state coverage versus inverse temperature for hydrogen desorption after formic acid exposure.

In Figure 3-24, the α state (dashed line) is separated from the remainder of the hydrogen flash desorption spectrum. This separation is based on the theoretical α state flash peak by multiplying this peak by a factor correcting for the assumed measurement of pumping speed of hydrogen. The separated β state consists of more than one peak and these β state peaks are superimposed each other. Since the amount of β state is small (1.15×10^{14} molecules/cm^2), it is impossible to make any quantitative analysis for this state.

Comparing the H_2 flash desorption spectrum from HCOOH adsorption to that from H_2 adsorption, the following facts are observed; (i) both flash desorption spectra have two peaks occuring at identical temperatures of 378 and 460°K, (ii) both α state desorption peaks are second order reaction, and (iii) the only significant difference appears in the β state. The H_2 saturated coverage of the β state from H_2 adsorption is less than that from HCOOH adsorption by about an order of magnitude. The shape of H_2 β state from H_2 adsorption is different from that from HCOOH adsorption since there are probably several states within β state peak and it is not possible to determine the individual changes which occur between the H_2 adsorption and the HCOOH adsorption.

Figure 3-25 shows a series of carbon monoxide flash desorption spectra at various formic acid exposure. Only a single desorption peak has been observed at temperature 433°K. The CO coverage as a function of formic acid exposure is given in Table 3-7 and shown in Figure 3-26. The curve in Figure 3-26 is generated by a polynomial regression computer program and expressed as

$$\sigma = 0.591 + 113.090N - 2204.551N^2 + 20093.92N^3 - 65211.16N^4 \qquad (3-4)$$

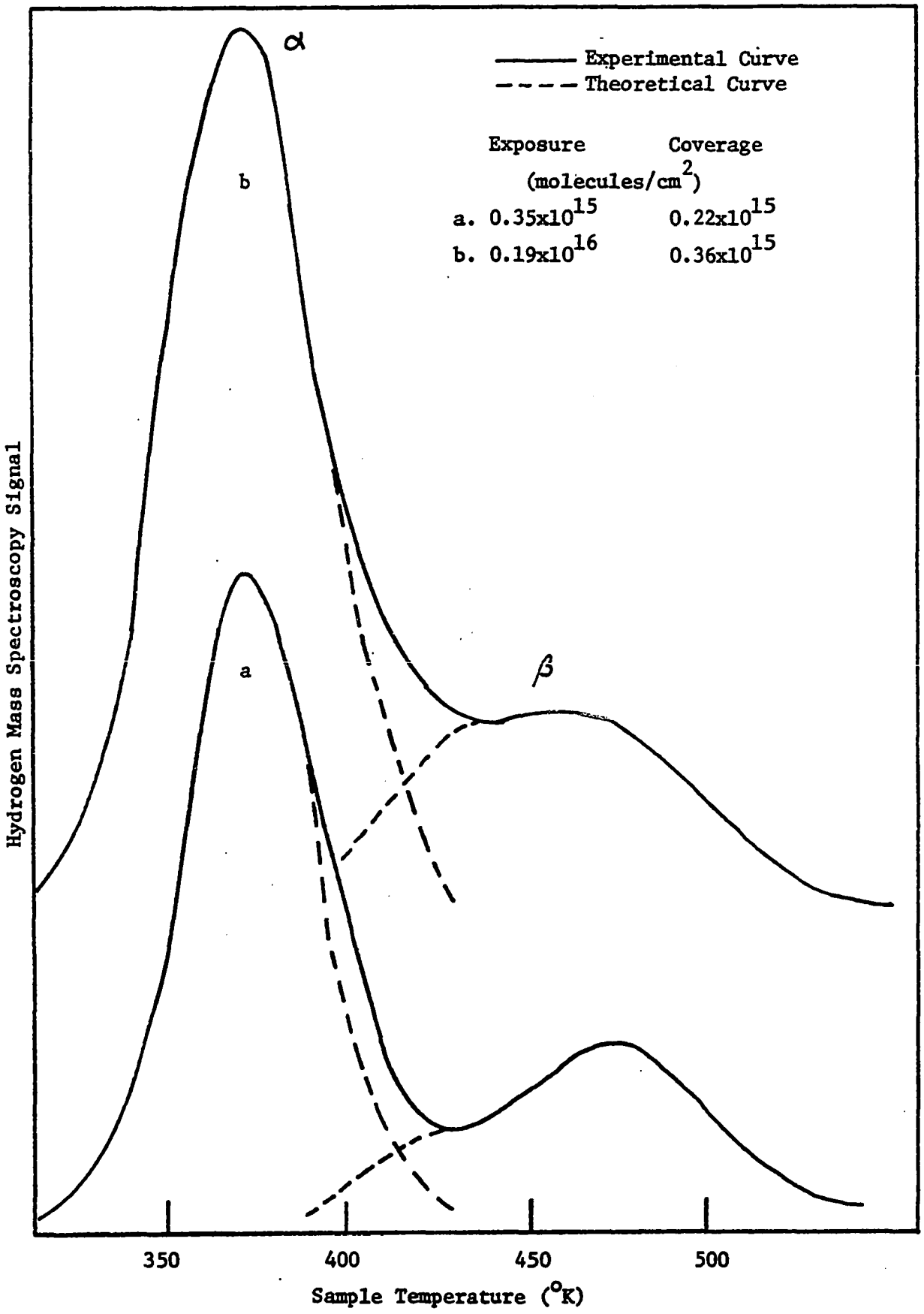

Figure 3-24 Theoretical hydrogen flash desorption spectra at various formic acid exposure.

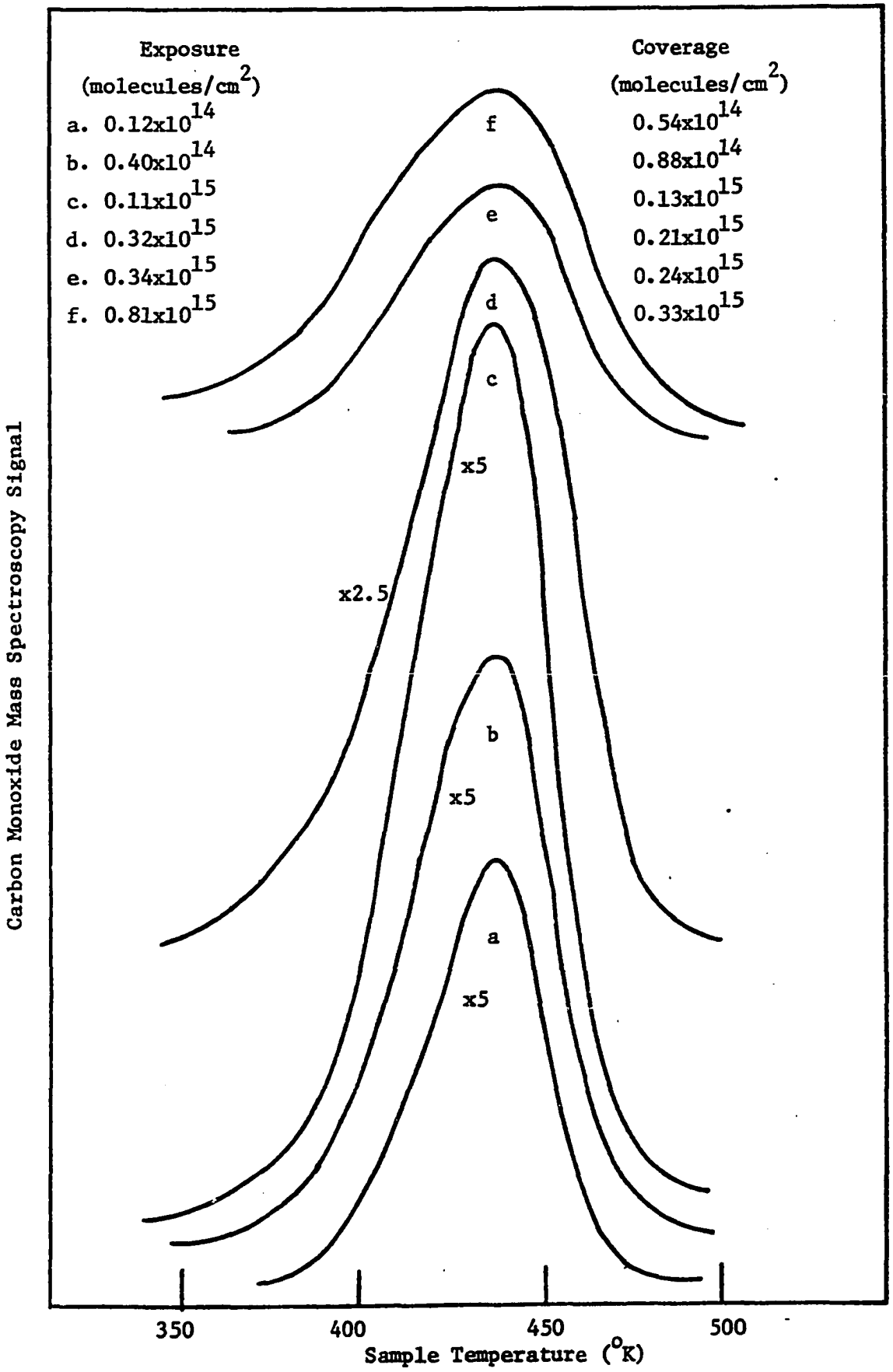

Figure 3-25 Typical carbon monoxide flash desorption spectra at at various formic acid exposure.

Table 3-7

Carbon Monoxide Coverage Versus Formic Acid Exposure

Formic acid exposure (10^{15} molecules/cm^2)	Carbon monoxide coverage (10^{15} molecules/cm^2)
0.012	0.054
0.040	0.088
0.056	0.12
0.057	0.11
0.11	0.13
0.12	0.20
0.12	0.21
0.28	0.26
0.32	0.21
0.34	0.24
0.44	0.29
0.56	0.29
0.73	0.31
0.81	0.33
1.1	0.34
1.3	0.36

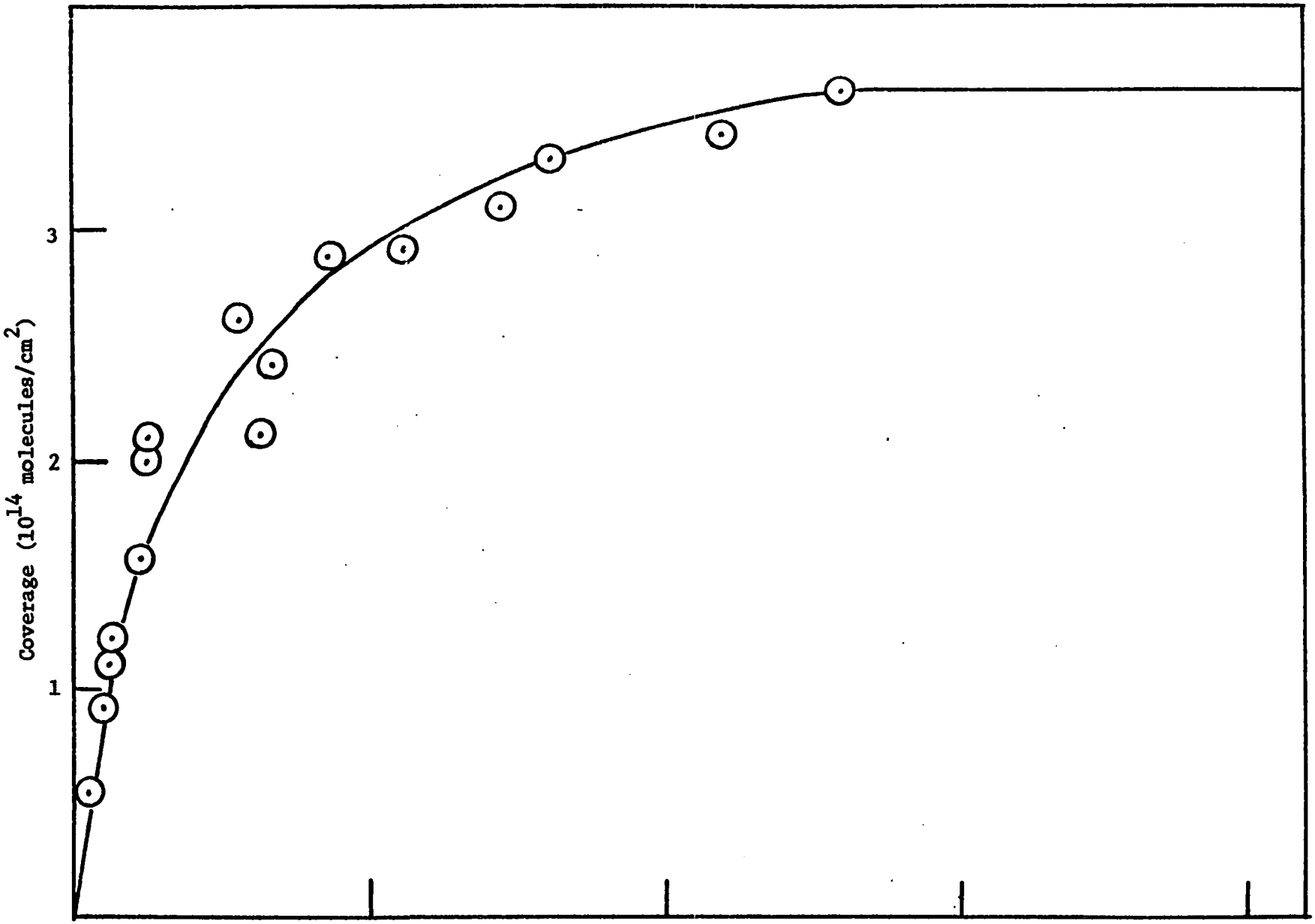

Figure 3-26 Carbon monoxide coverage versus formic acid exposure.

where σ = coverage of CO

N = exposure of formic acid.

The maximum coverage of CO is 3.6×10^{14} molecules/cm^2.

Since the CO peak shape is symmetric and does not shift with peak temperature, this state is probably associated with a first order desorption reaction. An activation energy of 26.9 Kcal/g-mole has been obtained by solving Equation (1-14) with the experimental peak temperature and an assumed pre-exponential factor of 10^{13} sec^{-1}. Two theoretical flash peaks, which correspond to the flash spectra c and f in Figure 3-25, have been generated by computer simulation with above values the activation energy and pre-exponential factor using Equation (1-13). These two CO theoretical flash peak are shown as dashed line in Figure 3-27. The shape of the theoretical peak (curve a in Figure 3-27) reproduces the experimental flash peak at a CO coverage of 0.13×10^{15} molecules/cm^2; however the shape of theoretical peak b in Figure 3-27 is narrower than that of the experimental flash peak at a CO coverage 0.33×10^{15} molecules/cm^2. This suggests that there is one CO state for low HCOOH exposures ($<0.11 \times 10^{16}$ molecules/cm^2) and possibly several CO states contributing to the experi-flash spectrum for high HCOOH exposures. However, the peak temperature of theoretical flash peak is identical to that of experimental flash peak.

It is very intresting to note that this CO flash peak is different from that following pure CO adsorption in both peak shape and peak temperature. The peak temperature from CO adscrption is 407°K and from HCOOH adsorption is 433°K. Also the CO peak of HCOOH adsorption is much narrower than that of CO adsorption. However, this CO peak from HCOOH adsorption is similar to that following CO_2 adsorption in peak shape and also

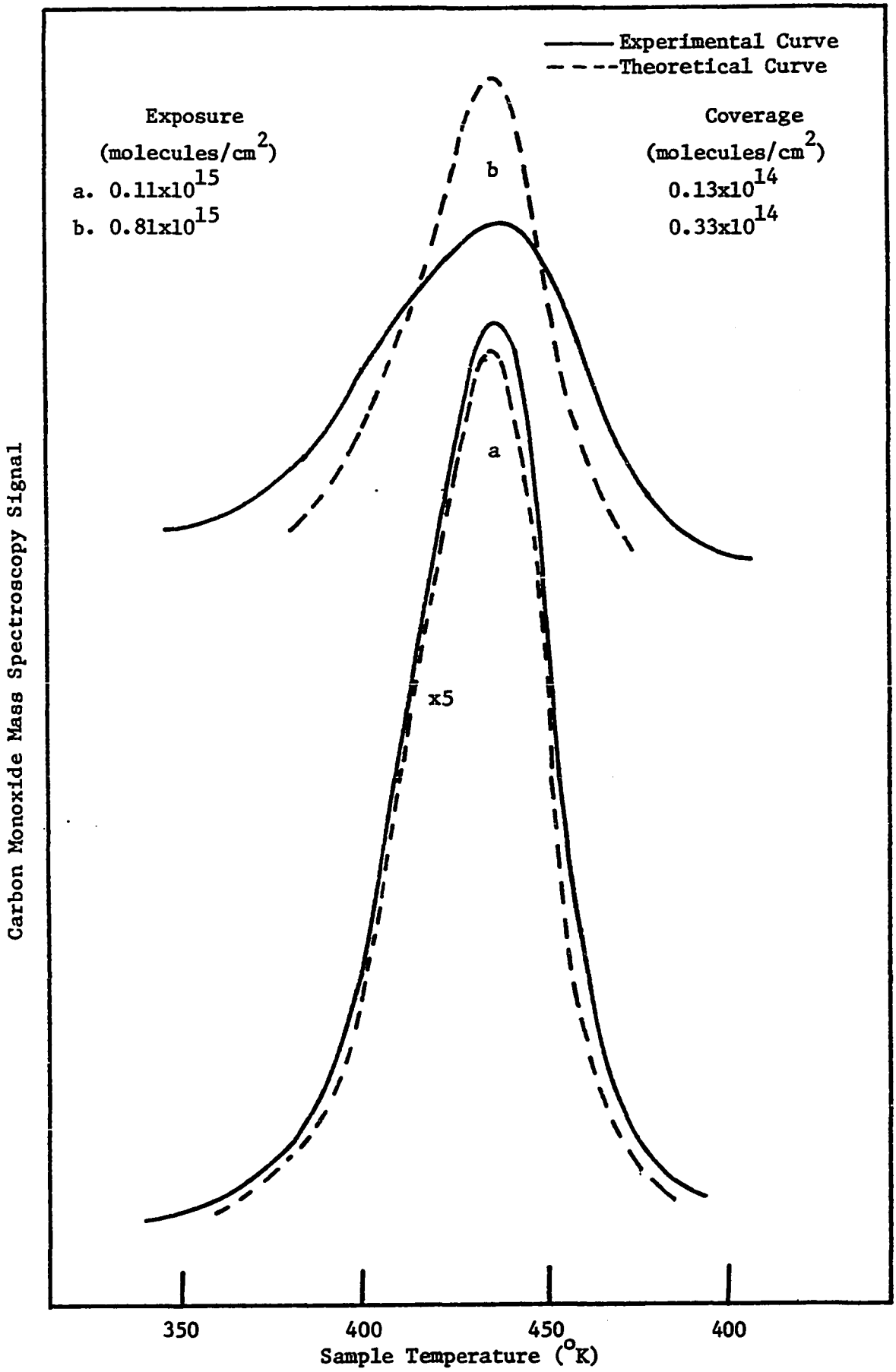

Figure 3-27 Theoretical carbon monoxide flash desorption spectra at various formic acid exposure.

both CO peaks have identical peak temperatures (433°K) These points will be discussed later in this section.

In contrast to the pure CO_2 adsorption on Ni (100) surface, where the CO_2 does not desorb from surface upon flashing, CO_2 is desorbed following HCOOH exposure to Ni (100) surface. A series of typical CO_2 flash desorption spectra at various formic acid exposure is shown in Figure 3-28. The maximum desorption rate occured at 378°K. Interestingly, this CO_2 desorption peak temperature is identical to the H_2 state peak temperature (378°K) following HCOOH adsorption. The CO_2 coverage versus formic acid exposure is given in Table 3-8 and shown in Figure 3-29. The curve in Figure 3-29 is generated by a polynomial regression computer program and expressed as

$$\sigma = -0.194 + 199.147N - 4028.690N^2 + 30483.68N^3 - 101309.3N^4 \qquad (3\text{-}5)$$

where σ = coverage of CO_2 (10^{14} molecules/cm^2)
N = exposure of CO_2 (10^{16} molecules/cm^2).
The full coverage of CO_2 is 3.6 x 10^{14} molecules/cm^2.

A plot of the natural logrithm of the CO_2 desorption rate divided by the CO_2 coverage as a function of the inverse temperature is shown in Figure 3-30. According to Equation (1-13), the nonlinearity of the curve in Figure 3-30 indicated that this desorption reaction is not first order. However, the shape of the CO_2 flash peak is symmetric about the peak temperature, a symmetric peak is characteristic of second order desorption kinetics. A plot of the natural logrithm of CO_2 desorption rate divided by the square of the CO_2 coverage as a function of the inverse temperature

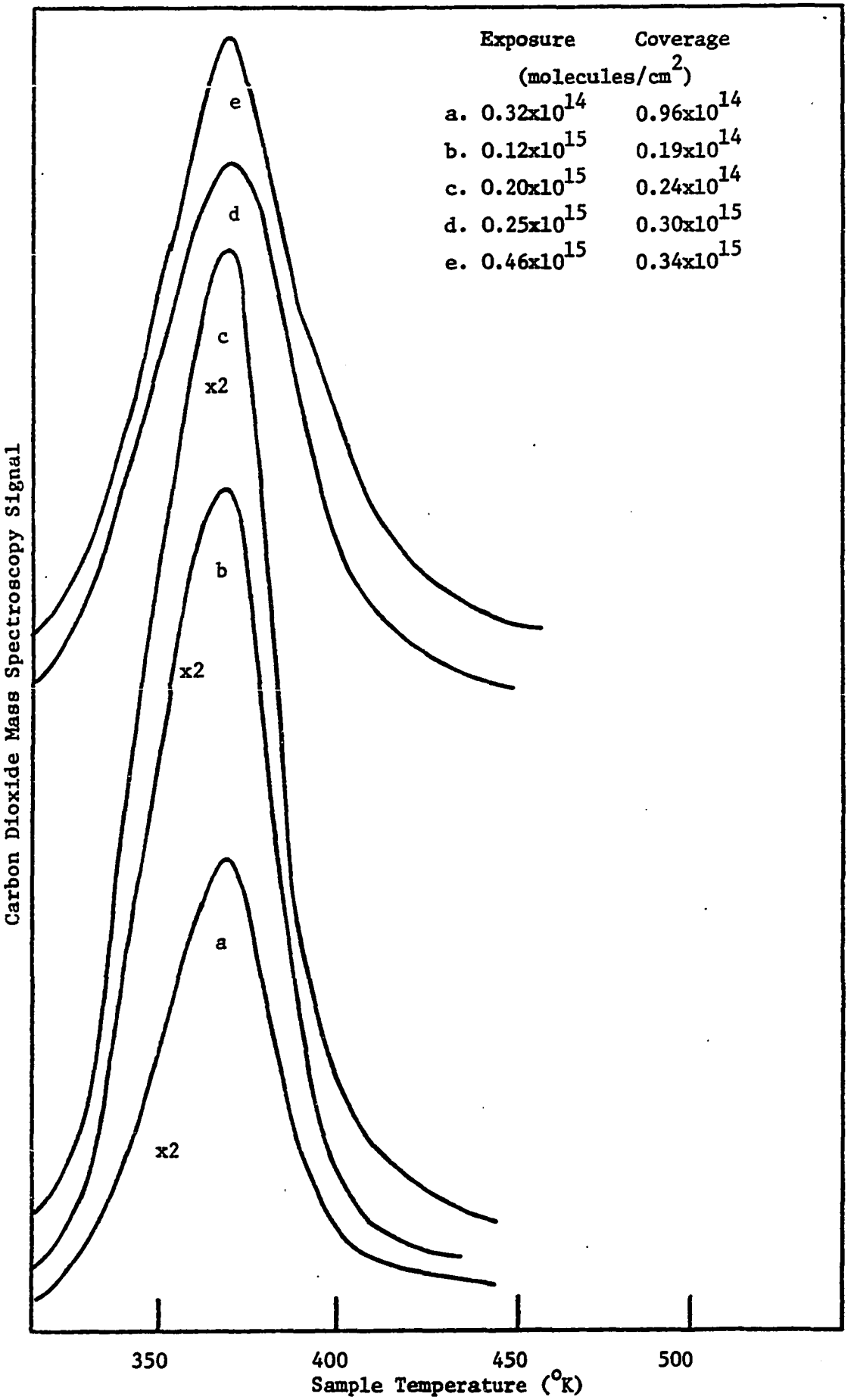

Figure 3-28 Typical carbon dioxide flash desorption spectra at various formic acid exposure

Table 3-8

Carbon Dioxide Coverage Versus Formic Acid Exposure

Formic acid exposure (10^{15} molecules/cm^2)	Carbon dioxide coverage (10^{15} molecules/cm^2)
0.019	0.0053
0.025	0.0074
0.032	0.096
0.051	0.11
0.054	0.17
0.091	0.19
0.12	0.19
0.17	0.22
0.20	0.24
0.25	0.30
0.34	0.29
0.36	0.31
0.44	0.31
0.46	0.34
0.57	0.34
0.74	0.34
0.92	0.32
1.2	0.36

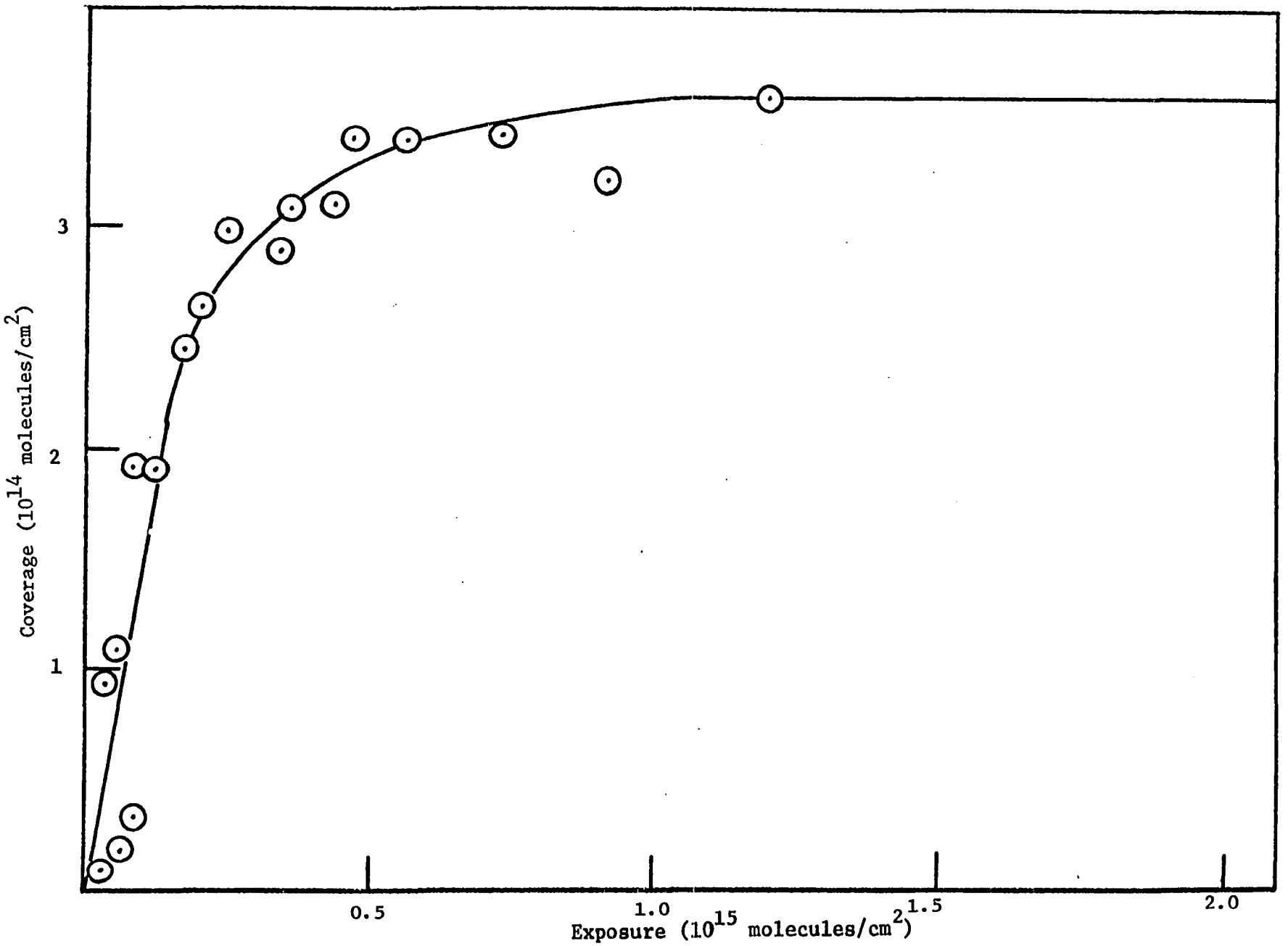

Figure 3-29 Carbon dioxide coverage versus formic acid exposure.

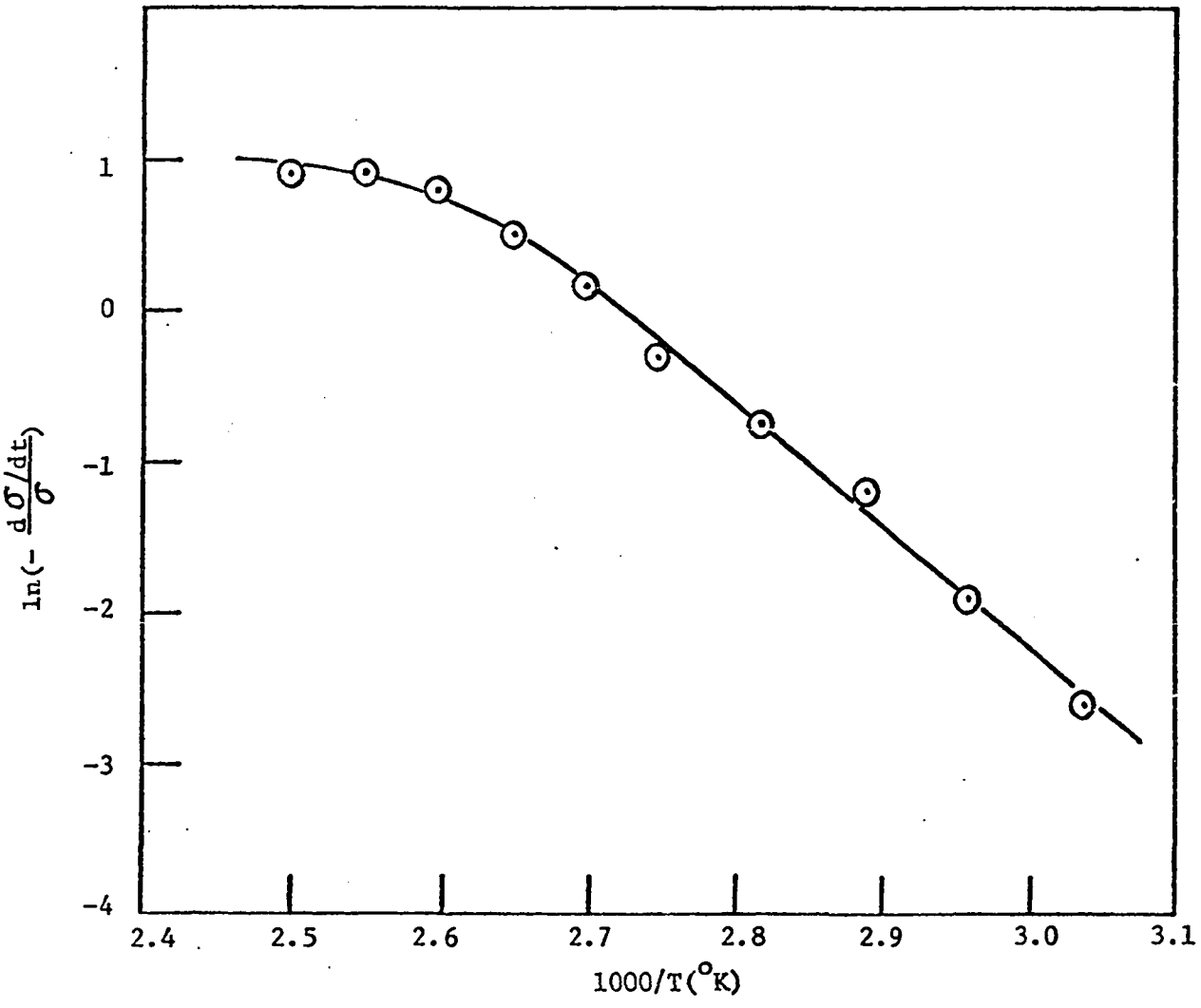

Figure 3-30 Logrithm of the ratio of desorption rate to coverage versus inverse temperature for carbon dioxide desorption after formic acid exposure.

is presented in Figure 3-31. In according with Equation (1-17), the linear correlation in Figure 3-31 suggests that this CO_2 desorption follows second order desorption kinetics with a fixed activation energy. A linear least-squares fitting of this straight line gives an activation energy of 21.0 ± 0.6 Kcal/g-mole and a pre-exponential factor of 0.068 cm^2/atom-sec. Using Equation (1-13), the theoretical CO_2 peaks have been generated by computer simulation with the above values of activation energy and pre-exponential factor. The CO_2 peak temperature of the theoretical flash peaks differs from that of the experimental flash peaks by about 20°K. However, the CO_2 theoretical flash peaks reproduce the experimental flash peaks when an activation energy of 23.5 Kcal/g-mole is used without changing the pre-exponential factor.

The sticking coefficient of formic acid has been calculated and a value of 1.98 is obtained. This value is unreasonable since the sticking coefficient should be less than 1.0 for any adsorption case. This controversy probably can be explained as follows. The calculation of the sticking coefficient of formic acid is based on the surface coverage of carbon and the formic acid exposure. The value of formic acid exposure is obtained from the formic acid vapor pressure reading of a ionization gauge calibrated against the formic acid vapor at -86°C. The vapor pressure of formic acid at -86°C is calculated by extropolating Coolidge's formic acid vapor pressure data near -5°C and using temperature relation (23) down to -86°C. Therefore this extropolation may easily introduce an error of vapor pressure of formic acid at -86°C by a factor of 2. Consequently, this error reflects on the calculation of sticking coefficient of formic acid.

After investigating the H_2, CO and CO_2 coverage

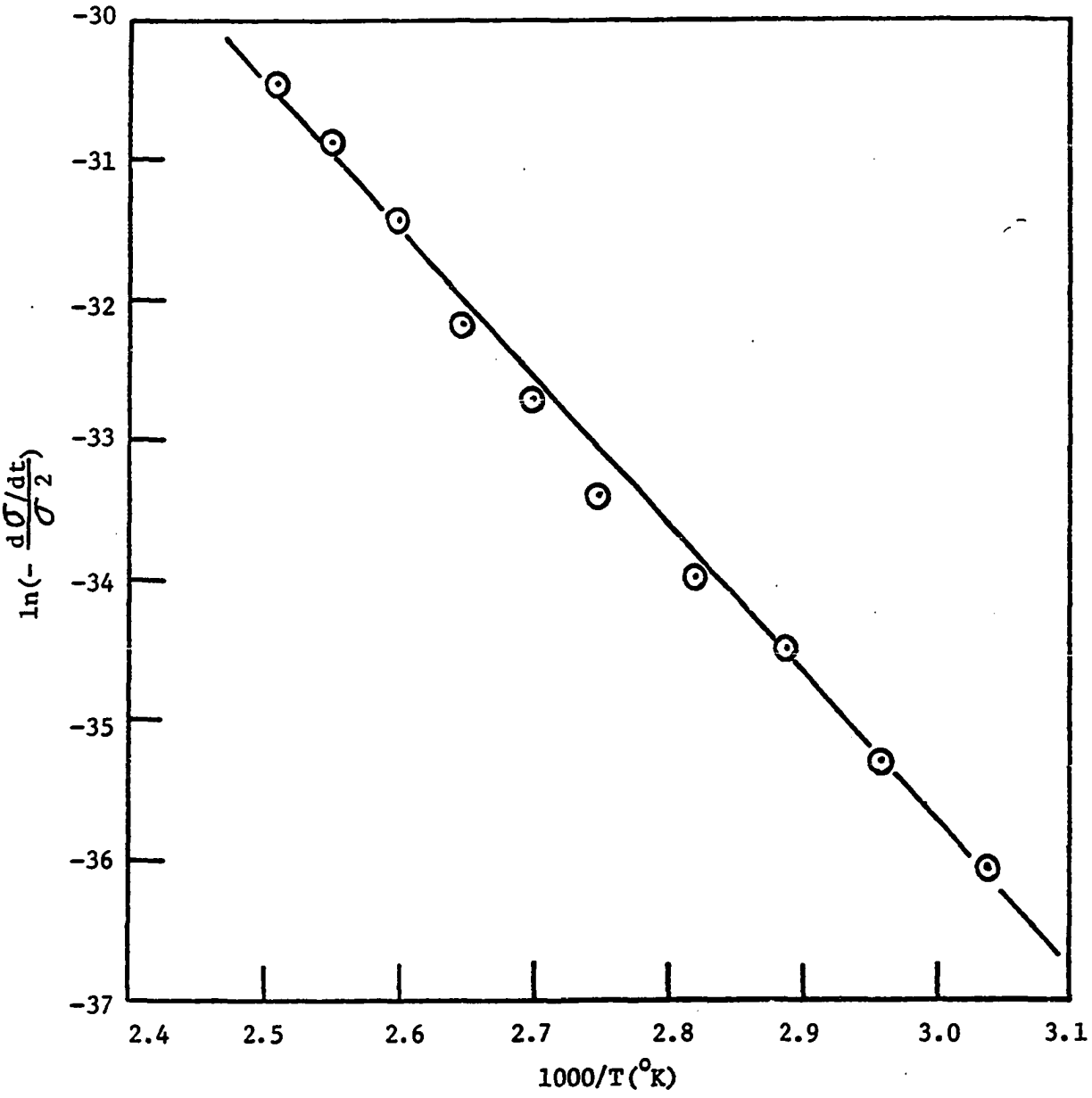

Figure 3-31 Logarithm of the ratio of desorption rate to square of coverage versus inverse temperature for carbon dioxide desorption after formic acid exposure.

versus HCOOH exposure curves, the coverage ratio of H_2:CO:CO_2 is 1:2:2 below 0.4 x 10^{15} molecules/cm^2 formic acid exposure. For formic acid exposure above 0.4 x 10^{15} molecules/cm^2 the ratio of H_2:CO:CO_2 is 1:1:1. These two ratios will be helpful in constructing a model for the decomposition of formic acid on clean Ni (100) surface in the next chapter.

After a cycle of saturated formic acid exposure and flash desorption, the Auger electron spectrum (as shown in Figure 3-32) was taken and indicated that oxygen has built up to a value of 1.27 x 10^{14} atoms/cm^2. This would indicate why the CO flash peak from HCOOH adsorption is so similar to that from pure CO_2 adsorption, since the oxygen also accumulates on the Ni surface after a sequence of pure CO_2 adsorptions and flash desorptions. Therefore, the CO flash peak observed after HCOOH adsorption is probably not directly associated with the decomposition of formic acid. This CO is more likely due to the dissociation of adsorbed CO_2 which is one of the major products of the decomposition of formic acid. Three other facts also lend support to this argument; (i) the CO peak temperature (433°K) from HCOOH adsorption is neither identical to the CO peak temperature (407°K) from pure CO adsorption nor identical to the same peak temperature (378°K) of both H_2 and CO_2 from HCOOH adsorption, (ii) the peak shape of CO from HCOOH adsorption is not similar to that from pure CO adsorption but is similar to that from pure CO_2 adsorption, and (iii) also the CO peak temperature (433°K) of HCOOH adsorption is identical to that of pure CO_2 adsorption.

From the discussion given above, it appears that the decomposition of formic acid on clean Ni (100) surface consists primarily of a dehydrogenation reaction and that the primary products are H_2 and CO_2, since the

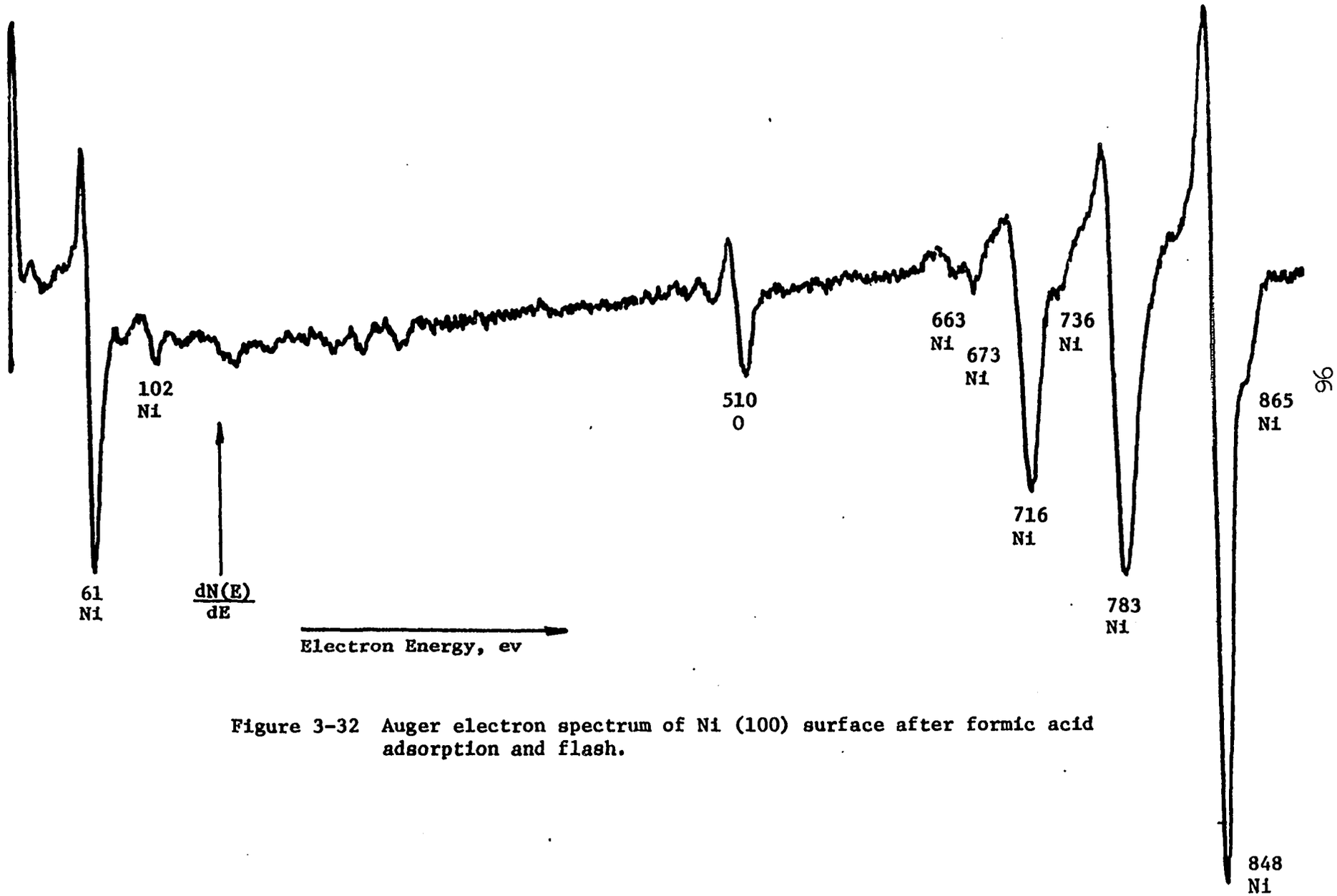

Figure 3-32 Auger electron spectrum of Ni (100) surface after formic acid adsorption and flash.

peak temperature of H_2 is identical to that of CO_2 for the adsorption of formic acid on Ni (100) surface. CO and oxygen are the dissociation products of CO_2 after the formic acid decomposition. In next chapter, a proposed model is presented to describe this interaction.

Recently, MaCarty, et al (38,39,40) reported results of decomposition of formic acid on clean Ni (110) surface by using flash desorption technique. Their results are given in Table 3-9.

They reported that the flash peak shapes of H_2 and CO_2 were extremly narrow. Therefore, they proposed an autocatalytic process with an unknown mechanism for the decomposition of HCOOH on Ni (110) surface to account for these narrow peaks. In the present study, this autocatalytic phenomena was not observed. Also, they observed the first order desorption reactions of H_2, CO and CO_2 following HCOOH adsorption on Ni (110) surface, which again is different from the observations of this study. As was mentioned previously, the desorption reactions of H_2 and CO_2 are second order and the desorption reaction of CO is first order, after HCOOH has been adsorbed on Ni (100) surface. This difference is most likely due to the difference in the crystal orientations used in the studies. They also observed two CO flash peaks whereas only a single CO flash peak was observed on the (100) plane. They proposed that the lower temperature CO peak ($373^{\circ}K$) is the cracking of CO_2 in their mass spectrometer. A low temperature CO peak due to the cracking of CO_2 was not observed in this study possibly because of the variation in the sensitivities and cracking patterns of different mass spectrometers. Futhermore, they reported that only one H_2 flash peak was observed. By contrast, two H_2 flash peak were detected on Ni (100). Their values of maximum coverage

Table 3-9

McCarty's Results of Decomposition of HCOOH on Ni (110)

Desorption	T_p(°K)	Order of reaction	E_{act} (Kcal/g-mole)	Maximum coverage (mole./cm^2)
H_2 from HCOOH adsorption	388	first	23.8	1.8×10^{14}
CO from HCOOH adsorption	438		26.7	1.8×10^{14}
	373	first	22.5	2.3×10^{13}
CO_2 from HCOOH adsorption	388	first	23.8	1.8×10^{14}

of H_2, CO and CO_2 are lower than those of this study although the ratio of the decomposition products at maximum coverage is same as that on the Ni (100) surface. These difference are undoubtedly due to the differences in the surface orientation of the nickel crystal although their results for the peak temperatures and desorption activation energies of the various reaction products from HCOOH adsorption are in good agreement with those of this study. Finally, they concluded that the decomposition of formic acid proceeds only through the dehydrogenation reaction and that a dissociation reaction of CO_2 is also involved. This conclusion is also consistent with results obtained on Ni (100).

CHAPTER IV

CONCLUSION AND RECOMMENDATION

4-1 Introduction

In the preceeding chapter, the results of the flash desorption spectra of the decomposition products (H_2, CO and CO_2) from formic acid adsorption have been presented. The spectra after the individual adsorption of H_2, CO and CO_2 on the clean Ni (100) surface have also been reported. These results are summarized in Table 4-1.

As mentioned previously, the decomposition of formic acid on clean Ni (100) surface is a dehydrogenation reaction which is accompanied by a dissociation reaction of CO_2. A proposed model for this process should be able to describe the reaction path and also to fit the stoichiometric relationship. From the observations of this study, the stoichiometric ratio of H_2, CO and CO_2 is 1:2:2 for low formic acid exposures ($\leq 0.4 \times 10^{15}$ molecules/cm^2). For a high formic acid exposure, this stoichiometric ratio becomes 1:1:1. Two possible models A and B primarily for high formic acid exposures, will be presented in Sections 4-2 and 4-3 respectively.

Before the presentation of these two models, the initial adsorption process of formic acid on Ni (100) surface is described since this process is identical for both models. The formic acid is first adsorbed on Ni (100) surface as a formate ion or radical and adsorbed hydrogen, i.e.,

Table 4-1

Results of Decomposition of HCOOH on Ni (100)

Desorption	$T_p(^oK)$	Order of reaction	(Kcal/g-mole)	Maximum coverage (mole./cm^2)
H_2 from H_2 adsorption	378	second	23.0	1.0×10^{14}
	460	-	-	1.1×10^{13}
CO from CO adsorption	407	first	25.1	7.7×10^{14}
CO from CO_2 adsorption	433	first	26.93	6.4×10^{14}
H_2 from HCOOH adsorption	378	second	23.5	3.7×10^{14}
	460	-	-	
CO from HCOOH adsorption	433	first	26.93	3.6×10^{14}
CO_2 from HCOOH adsorption	378	second	23.5	3.6×10^{14}

$$HCOOH \xrightarrow{+2^*} HCOO(ads) + H(ads). \qquad (4\text{-}1)$$

As more formic acid is admitted, hydrogen is released into gas phase:

$$HCOOH + H(ads) \longrightarrow HCOO(ads) + H_2\uparrow. \qquad (4\text{-}2)$$

This replacement of hydrogen by formic acid is consistent with the high rate of desorption of H_2 on Ni (100) surface and the relatively low heat of adsorption of H_2. Since this H_2 desorption occurs prior to the flash, it can not be detected by the mass spectrometer during flash. A few authors (1,4) have also proposed the reactions (4-1) and (4-2) suggested here.

4-2 Model A

The model presented in this section is only a general reaction path of decomposition of formate ion or radical on Ni (100) surface for high formic acid exposures. The reaction path for the low formic acid exposures will be treated as a special case in Section 4-5.

When the crystal is heated, two formate ions or radicals are decomposed into hydrogen and carbon dioxide. Also this hydrogen and part of the carbon dioxide are desorbed from the surface. Simultaneously, part of the CO_2 is dissociated into adsorbed CO and oxygen on the substrate. The desorption rate of H_2 and CO_2 reaches a maximum as temperature is raised up to 378°K. Above this temperature, the remaining adsorbed CO molecule begins to desorb into gas phase and the oxygen remains on the surface. The rate of CO desorption reaches a

maximum at 433°K. This instantneous process can be expressed on a temperature scale as

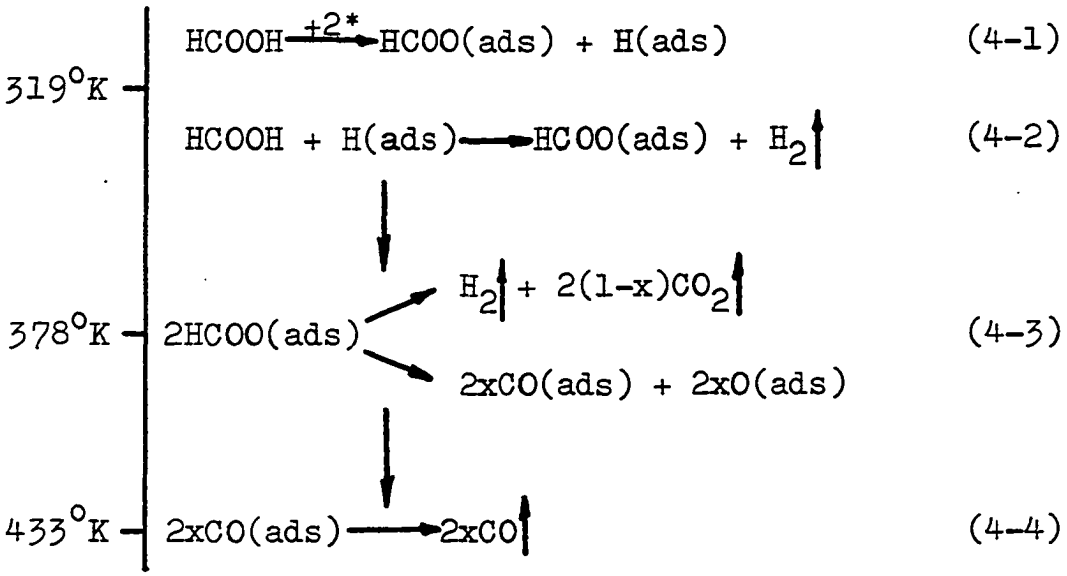

where x is the fraction of CO_2 dissociated into CO and oxygen. The stoichiometric relationship of products H_2, CO and CO_2 for this reaction path is 1:2(1-x):2x. From the observations of this study, this stoichiometric ratio is 1:1:1 for high HCOOH exposures. Therefore, the x in this model is 0.5 which means 50% of CO_2 is desorbed from the surface and 50% of CO_2 is dissociated to yield CO and oxygen after the formate ion or radical has decomposed. Then the above reaction can be rewritten as

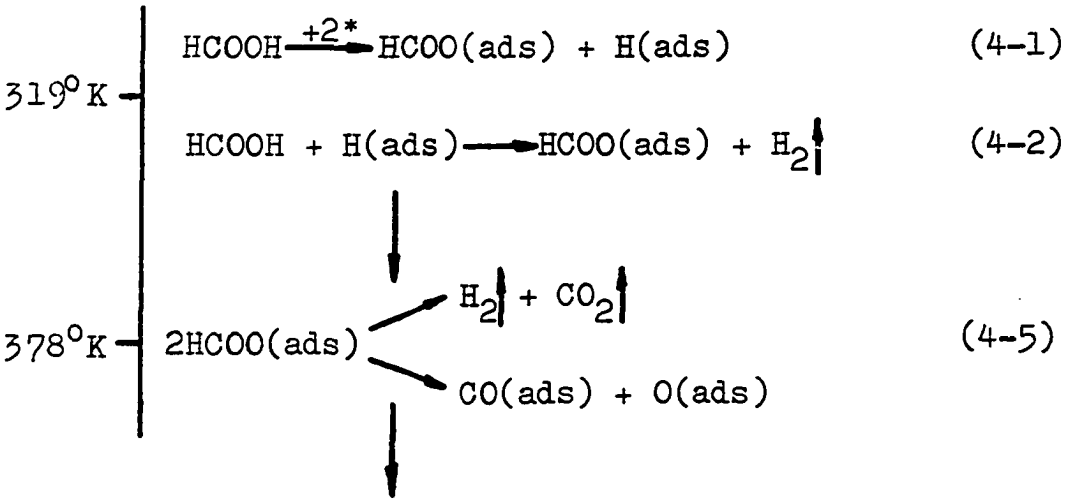

$$433^{\circ}K \left| \; CO(ads) \longrightarrow CO\uparrow . \right. \qquad (4\text{-}6)$$

The experimental results observed in this study which support this model will be discussed in Section 4-4.

4-3 Model B

Another possible model, which is quite different from model A is developed in this section. Again this model is only a general case for the decomposition of formic acid on Ni (100) surface for high formic acid exposures. The reaction path for low formic acid exposures will be discussed in Section 4-5.

After the formic acid is adsorbed on surface as formate ion or radical, it forms a complex between adsorbed hydrogen atom CO_2 without the dissociation of CO_2 on the surface. This adsorbed hydrogen of the complex on Ni (100) surface is probably bound weakly to the oxygen of the CO_2 which is also adsorbed on the substrate. Upon flashing, this adsorbed complex, CO_2-H, dissociates. Hydrogen is desorbed from surface and part of CO_2 is released with the hydrogen desorption into gas phase. The remaining CO_2 dissociates into adsorbed CO and oxygen. The desorption rate of H_2 and CO_2 reaches maximum at $378^{\circ}K$. As surface temperature increases from $378^{\circ}K$, the adsorbed CO molecule begins to desorb from surface while the oxygen is left on the substrate. The rate of CO desorption reaches maximum at a surface temperature of $433^{\circ}K$. This model can be expressed on a temperature scale as

$$\left| \begin{array}{ll} HCOOH \xrightarrow{\pm 2^{*}} HCOO(ads) + H(ads) & (4\text{-}1) \\ HCOOH + H(ads) \longrightarrow HCOO(ads) + H_2\uparrow & (4\text{-}2) \\ \downarrow & \end{array} \right.$$

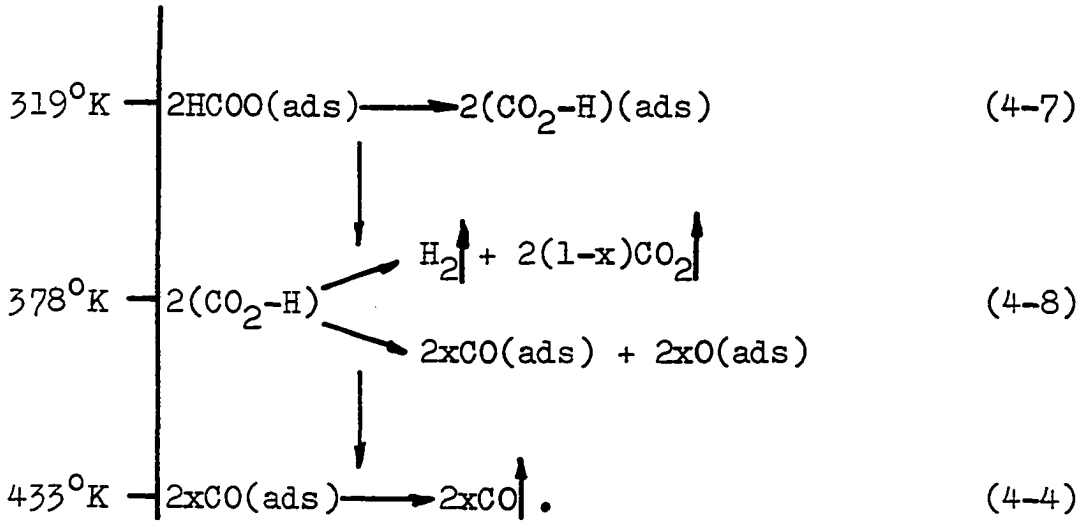

Again the x is the fraction of CO_2 dissociated into CO and oxygen. In the same manner as discussed in model A, the stoichiometric ratio of H_2, CO and CO_2 (1:1:1) gives x equal to 0.5. Then the above process can be rewritten as

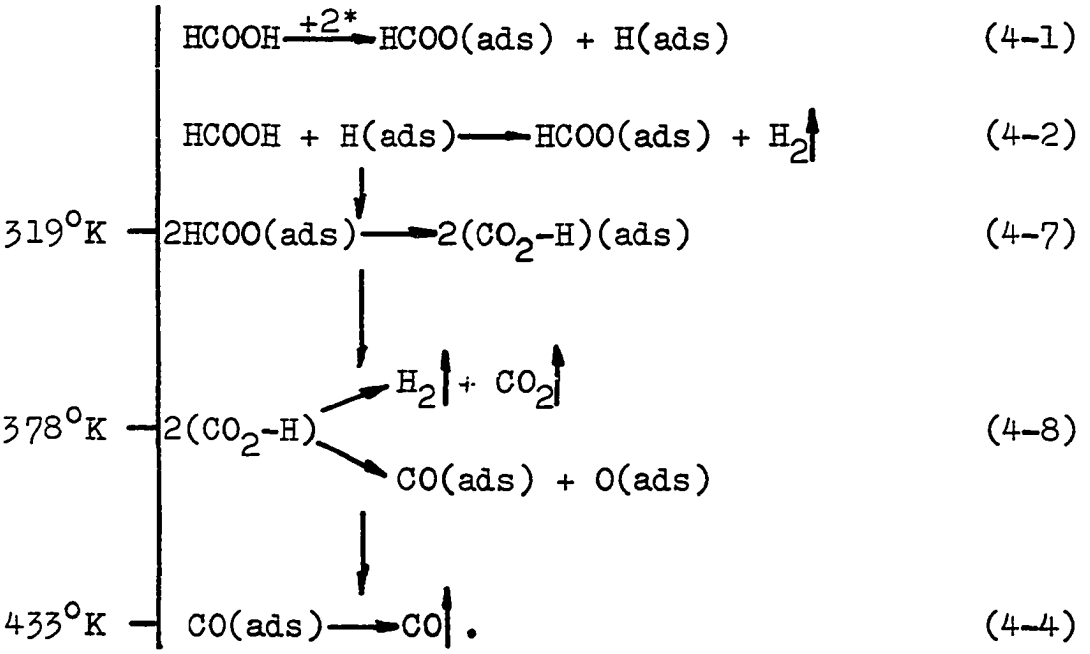

4-4 Experimental Support for Model A and Model B

Both models discussed above can explain the following results observed in this study; (i) stoichiometric

relationship of H_2, CO and CO_2 (1:1:1) for high HCOOH exposures, (ii) the second order desorption kinetics of H_2 and CO_2 and the overlapping H_2 and CO_2 flash peaks at same peak temperature, and (iii) the dissociation of CO_2 into CO and adsorbed oxygen and the first order desorption reaction of CO. It is difficult to determine which one of this two models best reflects the fate of the formic acid molecule after adsorption on the surface. However, the observation that the hydrogen α and β state peak temperatures from the pure hydrogen adsorption is identical to that from formic acid adsorption provides additional information for analysis of these two models.

In model A, H_2 and CO_2 are simultaneously and directly desorbed from the surface after the formate ion or radical decomposes during the flash. This accounts for the second order desorption kinetics of H_2 and CO_2 and also the overlapping H_2 and CO_2 flash peak at the same peak temperature. This hydrogen desorption after HCOOH adsorption is quite different from that of pure hydrogen adsorption. Therefore, it would be quite fortuitous that the hydrogen peak temperature from HCOOH adsorption is identical to that after hydrogen adsorption. Since identical hydrogen peak temperatures have been observed in this study for the HCOOH adsorption and H_2 adsorption, it is impossible to determine if this is coincidental or deterministic.

In model B, the hydrogen of the complex, CO_2-H, is adsorbed on the substrate and also forms a very weak bond to the oxygen of the adsorbed CO_2. Upon flashing, this weak bond between H and CO_2 is broken and the adsorbed hydrogen is desorbed from the surface. This hydrogen desorption process from HCOOH adsorption is similar to that of H_2 adsorption. Therefore, the hydrogen peak temperatures after both HCOOH adsorption

and H_2 adsorption should be identical. Since the weak bond between the CO_2 and H in the complex, CO_2-H, is broken simultaneously with H_2 desorption, the CO_2 is released into gas phase in the same manner as H_2. This explains the second order desorption kinetics of H_2 and CO_2 and also that the maximum desorption rates of H_2 and CO_2 occurring at the same temperature. Therefore, model B can explain the experimental results of this study more thoroughly than model A. This model B proposed a rather novel type of interaction between two adsorbed molecules. In particular it is proposed that although CO_2 will decompose into adsorbed CO and oxygen on a clean surface, in the presence of adsorbed hydrogen the adsorbed CO_2 molecule maintains its integrity. It should, however, be mentioned that Madey, et al (42), in an attempt to explain their isotopic exchange results for carbon monoxide, have proposed that adsorbed CO on polycrystalline tungsten forms an adsorbed dimer complex $(CO)_{2a}$. Clavenna and Schmidt (37) have also found evidence in their flash desorption studies of CO from W (100) that supports an adsorbed dimer.

4-5 Oxygen Effect on HCOOH Desorption

In preceeding sections of this chapter, two possible models of formic acid decomposition on Ni (100) surface for high HCOOH exposures have been proposed. In this section, the HCOOH decomposition on Ni (100) surface for low formic acid exposures is discussed. As mentioned before, the stoichiometric ratio of H_2, CO and CO_2 is 1:2:2 for low formic acid exposures ($\leq 0.4 \times 10^{15}$ molecules $/cm^2$). This apparent loss of hydrogen after HCOOH exposures will be attributed to the interaction of hydrogen and oxygen on the Ni (100) surface.

As described in Section 2-6, there is always a small

amount of oxygen (2.44% atomic percentage) on the Ni (100) surface after cleaning by heating and Ar ion bombardment. The amount of oxygen increases to a atomic percentage of 7.9% (1.27×10^{14} atoms/cm^2) after a saturated HCOOH exposure and flash. After flashing, the cystal was heated to a temperature 800°C in order to return the surfce to the pre HCOOH exposure condition. This suggests that there are probably at least two different adsorbed oxygen states on the Ni (100) surface.

As formic acid or hydrogen is adsorbed on the surface, it is proposed that part of hydrogen becomes adsorbed on the two different oxygen sites, i.e.,

$$H(ads) + O^*(ads) \longrightarrow O^*H(ads) \qquad (4\text{-}11)$$

$$H(ads) + O(ads) \longrightarrow OH(ads) \qquad (4\text{-}12)$$

where hydrogen is bound less strongly to O*. During the flash, the hydrogen bound to the lower oxygen atom is desorbed and the oxygen remains on the surface. This hydrogen desorption rate reaches a maximum at 460°K. This accounts for the hydrogen β state peak in the flash desorption spectra of hydrogen after formic acid exposure. The hydrogen bound to the high energy oxygen atom does not desorb from the substrate since the heating method for the flash can not raise surface temperature enough to desorb this hydrogen. The well-focused light beam heating method can only heat crystal to 625°K. At low formic acid exposure, approximately one half of the total amount of hydrogen atoms adsorbed are bound to the high energy oxygen atoms and do not desorb from surface. Then the stoichiometric ratio for H_2, CO and CO_2 is 1:2:2 for low formic acid exposures. At high formic acid exposure, the

amount of hydrogen bound to the high energy oxygen atoms becomes insignificant relative to the total hydrogen adsorbed on the surface. This proposal that hydrogen atoms are bound to oxygen atoms on Ni (100) is valid for both model A and model B.

If the number of oxygen atom left on the surface is calculated by mass balance for both models A and B, there should be 3.6×10^{14} atoms/cm^2. Calculating the number of oxygen atoms by using the Auger electron spectrum yielded a value of 1.27×10^{14} atoms/cm^2. This apparent inconsistency with the value from the flash desorption can be resolved by noting that the value is calculated by assuming that only one monolayer of Ni atoms are detected by Auger electron spectrometer. This assumption certainly is invalid and will introduce an error into the oxygen coverage calculation.

4-6 Comparison of Results between Ni (100) and Ni (110)

Recently, McCarty, et al (38,39,40) reported results for the decomposition of HCOOH on clean Ni (110) surface by using the flash desorption technique. Their results for adsorptions at room temperature are given in Table 4-2.

They observed a single hydrogen flash desorption peak for both hydrogen adsorption and HCOOH adsorption. The hydrogen flash peak exhibits second order desorption kinetics and occured at 369°K for hydrogen adsorption while the hydrogen flash peak is first order desorption kinetics and occured at 388°K after HCOOH adsorption. A single CO_2 flash peak at 388°K and a first order desorption reaction of CO_2 for HCOOH adsorption were also observed. Also, two CO flash peaks ocurred at 373°K and

Table 4-2

Results of Decomposition of HCOOH on Ni (110)

Desorption	$T_p(^oK)$	Order of reaction	E_{act} (Kcal/g-mole)	Maximum coverage (mole./cm^2)
H_2 from H_2 adsorption	369	second	22.3	2.0×10^{14}
CO from CO adsorption	438	first	26.7	4.4×10^{14}
CO from CO_2 adsorption	438	first	26.7	1.8×10^{14}
H_2 from HCOOH adsorption	388	first	23.8	1.8×10^{14}
CO from HCOOH adsorption	438	first	26.7	1.8×10^{14}
	373	first	22.5	2.3×10^{14}
CO_2 from HCOOH adsorption	388	first	23.8	1.8×10^{14}

438°K following HCOOH adsorption and first order desorption kinetics for these states were reported by them. The observation of a CO flash peak at 373°K indicates cracking of CO_2 in their mass spectrometer. They also observed extremly narrow flash peak shapes for H_2 and CO_2 after HCOOH adsorption. They proposed an autocatalytic process with an unknown mechanism for the decomposition of HCOOH on Ni (110) surface to account for these narrow peaks. Futhermore, they reported that temperature of the CO flash peak (438°K) after HCOOH adsorption was identical to that of the single CO flash peak after both CO and CO_2 adsorption. Finally, their maximum coverage ratio of the decomposition products of HCOOH, H_2, CO and CO_2 is 1:1:1. The coverage ratio of CO and CO_2 is 1:1 for their high HCOOH exposures and is less than 1:1 for low HCOOH exposures. In accordance with the discussion in Section 4-4, model A probably fits their observations since the identical peak temperature of H_2 and CO_2 flash peak (388°K) is not same as the peak temperature (369°K) after H_2 adsorption alone. Thus it is obvious that the elementary steps leading to H_2 desorption after the adsorption of HCOOH are different from those following H_2 adsorption. The desorption of H_2 after exposure to HCOOH is probably concurrent with the decomposition of the formate ion or radical on the Ni (110) surface.

In this study, two hydrogen flash peaks with peak temperatures of 378 and 460°K were observed for both H_2 adsorption and HCOOH adsorption. Both of the H_2 desorption steps for the low temperature peak are second order. A single second order CO_2 flash desorption peak after HCOOH adsorption with a peak temperature 378°K was obtained. The single first order CO flash desorption peak after HCOOH adsorption with peak temperature 433°K

is identical to that after CO_2 adsorption. Both these CO peak temperatures are different from that of a single first order CO flash desorption peak after CO adsorption The autocatalytical phenomena of decomposition of formic acid observed on Ni (100) was not found on Ni (100).

After comparing the results of this study to those of McCarty, et al, both observations indicate that the decomposition of formic acid on Ni (100) or Ni (110) surface is a dehydrogenation reaction and that a dissociation reaction of CO_2 is involved. The differences between these two studies are probably due to the different orientation of Ni crystal, different instrumentation used and the presence of residual oxygen on the "clean" Ni (100) surface.

4-7 Conclusion and Recommendation

In conclusion, the interaction of formic acid on clean Ni (100) surface is a dehydrogenation reaction with primary products of H_2 and CO_2 and also a dissociation reaction of CO_2 into CO and oxygen is accompanied. The desorptions of H_2 and CO_2 are second order kinetics with an activation energy of 23.5 Kcal/g-mole and the CO desorption is a first order reaction with an activation energy of 26.9 Kcal/g-mole.

In Sections 4-3 and 4-4, models A and B have been proposed for the decomposition of formic acid on Ni (100) surface. From the results of this study, it is difficult to verify which of these two models is the most appropriate for describing the interaction of formic acid on the Ni (100) surface. Perhaps, a study of the coadsorption of H_2 and CO_2 would resolve the conflict. An experimental program is recommended here to perform the coadsorption studies of H_2 and CO_2.

It is proposed that the most significant experiment would be the adsorption of CO_2 on a surface already containing a fraction of a monolayer of hydrogen. In model B, the concept of a surface complex between adsorbed CO_2 and hydrogen has been introduced. If such a complex exists, then the flash desorption spectra after the coadsorption of CO_2 and H_2 should be similar to the spectra after the adsorption of formic acid. In particular, one would expect to find a CO_2 desorption peak in contrast to the absence of this peak following CO_2 adsoprion on the clean surface. The absence of a CO_2 peak in the coadsorption experiment would tend to support model A. It has also been proposed that part of the β hydrogen peak is associated with hydrogen bound initially to oxygen on the surface. An analysis of the hydrogen flash desorption peak following the adsorption of hydrogen on a partially oxidized crystal surface would either lend support or disqualify this proposal. It is felt that these experiments are critical for a complete and detailed analysis of the decomposition of formic acid and the attendant evolution of the products of this reaction on the Ni (100) surface.

BIBLIOGRAPHY

1. Bond, G. S., "Catalysis by Metals," Academic Press, New York (1962).

2. Mars, P., Scholten, J. J. F., and Zwietering, P., Advan. Catal. 14, 35 (1963).

3. Giner, J., and Rissmann, E., J. Catal. 9, 115 (1967).

4. Sachtler, W. M. H., and Farhrenfort, J., Proc. 2nd international Congress on Catalysis Paris 1, 831 (1961).

5. Hriota, K., Kuwata, K., Otaki, T., and Ashi, S., proc. 2nd international Congress on Catalysis Paris 1, 809 (1961).

6. Inglis, H. S., and Taylor, D., Inorg. Phys. Theor. 2905; J. Chem. Soc. (A) (1969).

7. Fukuda, K., Nagashima, S., Noto, Y., Ouishi, T., and Tamaru, K., Trans. Faraday Soc. 64, 552 (1968).

8. Duell, M. J., and Robertson, A. J. B., Trans. Faraday Soc. 57, 1416 (1961).

9. Tamaru, K., Trans. Faraday Soc. 55, 824 (1959).

10. Auger, P., J. Phys. Radium 6, 205 (1925).

11. Chang, C. C., Surf. Sci. 25, 53 (1971).

12. Chang, C. C., in "Characterization of Solid Surface," edited by Kane, P. F., and Lanabee, G. R., Plenum Press, New York (1974).

13. Ehrlich, G., J. of Appl. Phys. 32, 4 (1961).

14. Redhead, P. A., Vacuum 12, 203 (1962).

15. Hasting, Hampton, Virginia.

16. Peavey, J. H., Ph.D. Dissertation, University of Wisconsin-Milwaukee, Milwaukee, Wisconsin (1972).

17. Varian Associates, Palo Alto, California.

18. "Kirk-Olhmer Encylopedia of Chemical Technology," Vol. 6, Interscience.

19. Mariner, T., and Bleakney, W., Phys. Rev. 72, 792 (1974).

20. Happ, G. P., and Stewart, D. W., J. of Am. Chem. Soc. 74, 4404 (1952).

21. "Catalog of Mass Spectrum Data," Amer. Pet. Inst. Res. Proj. 44, Nat. Bur. Stds, Washington, D. C., Serial No. 300.

22. Rapp, G. A., and Melton, C. E., J. of Am. Chem. Soc. 80, 3509 (1958).

23. Coolidge, A. S., J. of Chem. Soc. 52, 1974 (1930).

24. Lewin, G., "Fundamentals of Vacuum Science and Technology," MaGraw-Hill, New York (1965).

25. Lee, D. E., Master Thesis, The University of Oklahoma, Norman, Oklahoma (1973).

26. Horgan, A. M., and Dalins, F., J. Vac. Sci. Technol. 10, 523 (1973).

27. Lapujoulade, J., and Neil, K. S., Surf. Sci. 35, 288 (1973).

28. Gilbreath, W. P., and Wilson, D. E., J. Vac. Sci. Technol. 8, 45 (1971).

29. Lapujoulade, J., Suppl. Nuovo Cimento V, 433 (1967).

30. Horgan, A. M., and Dalins, F., Surf. Sci. 41, 624 (1974).

31. Park, R. L., and Farnsworth, H. E., J. Chem. Phys. 43, 2351 (1965).

32. Litchman, D., Krist, T. R., and McQuistan, P. B., Phys. Letters 20, 129 (1966).

33. Onchi, M., and Farnsworth, H. E., Phys. Letters 26A, 349 (1968).

34. Onchi, M., and Farnsworth, H. E., Surf. Sci. 11, 203 (1968).

35. Tracy, J. C., J. Chem. Phys. 56, 2736 (1972).

36. Klier, K., Zettlemoyer, A. C., and Lerdheiser, Jr., H., J. Chem. Phys. 52, 589 (1970).

37. Clavenna, L. R., and Schmidt, L. D., Surf. Sci. 33, 11 (1972).

38. McCarty, J. G., Falconer, J. L., and Madix, R. J., J. Catal. 30, 235 (1972).

39. Madix, R. J., Falconer, J. L., and McCarty, J. G., J. Catal. 31. 316 (1973)

40. Falconer, J. L., McCarty, J. G., and Madix, R. J., Surf. Sci. 42, 329 (1974).

41. Hayward, D. O., and Trapnell, B. M. W., "Chemisorption," Butterworths, London (1964).

42. Madey, T. E., Yates, Jr., J. T., and Stern, R. C., J. Chem. Phys. 42, 1372 (1965).

APPENDICES

APPENDIX A

EXPOSURE

As has been mentioned before, the pressure change of a particular gas is recorded versus time when this gas is leaked into the vacuum chamber. The area under this recorded curve is representative of the exposure of this gas to the crystal surface expressed as torr-sec, i.e.,

$$A_e = \int_o^t P dt \qquad \text{(A-1)}$$

where A_e = area under pressure-time curve or the exposure of this gas to the crystal surface (torr-sec)

P = pressure (torr)

t = time (sec).

The exposure (torr-sec) can be expressed as the number of molecules which have struck on unit surface area, by calculating the number of molecules incident on the unit surface area per second which is given by (24):

$$\frac{dN}{dt} = \frac{1}{4} n V_a \qquad \text{(A-2)}$$

where N = number of molecules incident on unit surface area (molecules/cm^2)

n = number of molecules in unit volume or molecules density (molecules/cm^3)

V_a = arithemetic average velocity of a molecule.

The arithemetic average velocity is

$$V_a = \left(\frac{8kT}{\pi m}\right)^{0.5} \qquad \text{(A-3)}$$

where k = Boltzman constant, 1.03×10^{-22} torr-liter/sec
T = temperature of gas (^{o}K)
m = mass of a molecule.

Then Equation (A-2) becomes

$$\frac{dN}{dt} = \frac{n}{4}\left(\frac{8kT}{\pi m}\right)^{0.5} \qquad \text{(A-4)}$$

For an ideal gas, the equation of state is

$$P = nkT \qquad \text{(A-5)}$$

Substituting Equation (A-5) into Equation (A-4), gives

$$\frac{dN}{dt} = (2\pi mkT)^{-0.5}P$$

$$= 3.5 \times 10^{22}(MT)^{-0.5}P \qquad \text{(A-6)}$$

where M is molecular weight of the gas.

In this study, the pressure, P, in Equation (A-6) is a function of time. After integrating both sides of Equations (A-6) and using (A-1) the exposure is given by

$$N = 3.25 \times 10^{22}(MT)^{-0.5}A_e \qquad \text{(A-7)}$$

After the area, A_e, under the pressure-time curve is measured by an integrator, Equation (A-7) is used to obtain the exposure of a particular gas to the surface with aunits of molecules/cm^2.

APPENDIX B

STICKING COEFFICIENT

At an ambient pressure, P, of a particulas gas, the number of this gas molecules colliding with a unit of a surface per second is equal to $P(2\pi mkT)^{-0.5}$. This has been shown in Appendix A, Equation (A-6). The sticking coefficient, s, is defined as the fraction of these collisions that result in adsorption. The rate of adsorption may be written as (42)

$$\frac{d\sigma}{dt} = sP(2\pi mkT)^{-0.5} \qquad \text{(B-1)}$$

where σ is the coverage of a particular gas on a specified surface. Referring to Equation (B-1) can be written as

$$\frac{d\sigma}{dN} = s. \qquad \text{(B-2)}$$

For most cases in this study, the coverage ,σ, can be expressed as a function of the exposure of a particular gas, N, by a polynomial equation, such as

$$\sigma = a_o + a_1 N + a_2 N^2 + \ldots \qquad \text{(B-3)}$$

wher a_o, a_1 and a_2 are constants. Therefore, the term $d\sigma/dN$ in Equation (B-2) can be obtained by the differentiation of Equation (B-3) with respect to N.

Generally, a plot of $d\sigma/dN$ versus the fractional coverage, Θ, gives a typical curve shown in Figure B-1.

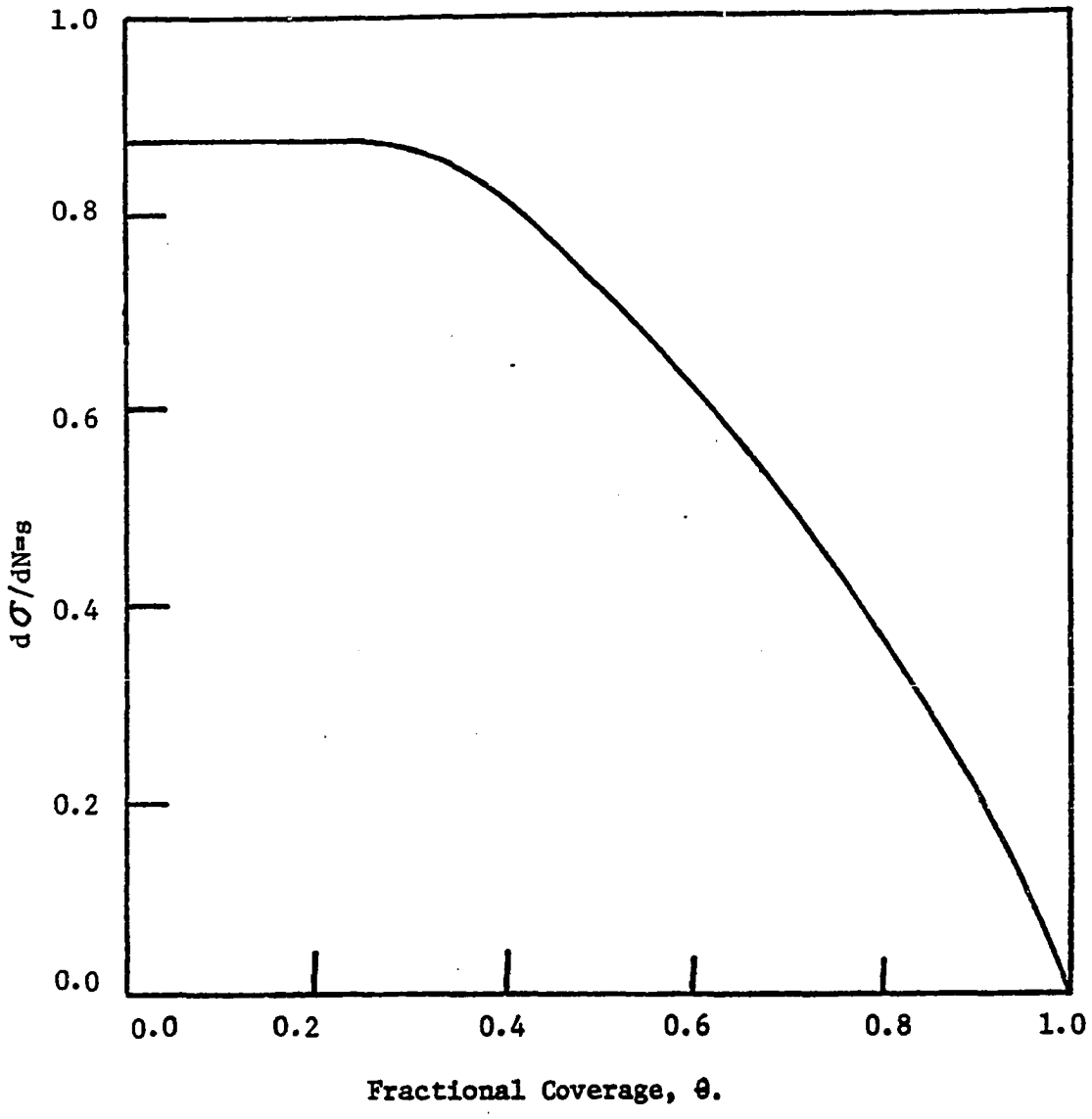

Figure B-1 Typical curve of $d\sigma/dN=s$ versus θ for sticking coefficient.

However, a plot of $d\sigma/dN$ versus θ of CO adsorption on Ni (100) surface, which is shown in Figure B-2 gives a stright line with aslope of -0.42. This suggests that a simple site occupation model of sticking coefficient is applicable. This model predicts that s should be proportional to the probability of an incident molecule finding a vacant site, i.e., $s \propto (1-\theta)$. For a simple site occupation model, the rate of adsorption is

$$\sigma_s \frac{d\theta}{dt} = (1-\theta)s^*P(2\pi mkT)^{-0.5} \qquad (B-4)$$

where σ_s is saturated coverage of a particular gas on a specified surface and s* is a modified sticking coefficient which would be independent of the surface coverage. Equation (B-4) can be rewritten as

$$\sigma_s \frac{d\theta}{(1-\theta)} = s^*(2\pi mkT)^{-0.5}Pdt. \qquad (B-5)$$

Referring to Equation (A-6), Equation (B-5) becomes

$$\sigma_s \frac{d\theta}{(1-\theta)} = s^*dN \qquad (B-6)$$

After integrating both sides, we obtain

$$-\ln(1-\theta) = s^*\frac{N}{\sigma_s} \qquad (B-7)$$

The sticking coefficient, s*, can be obtained as the slope of a straight line from the plot of $\ln(1-\theta)$ vs. N/σ_s. An alternative expression to Equation (B-4) is

$$\frac{d\sigma}{dN} = s^*(1-\theta) \qquad (B-8)$$

It is intresting to note that the relationship between

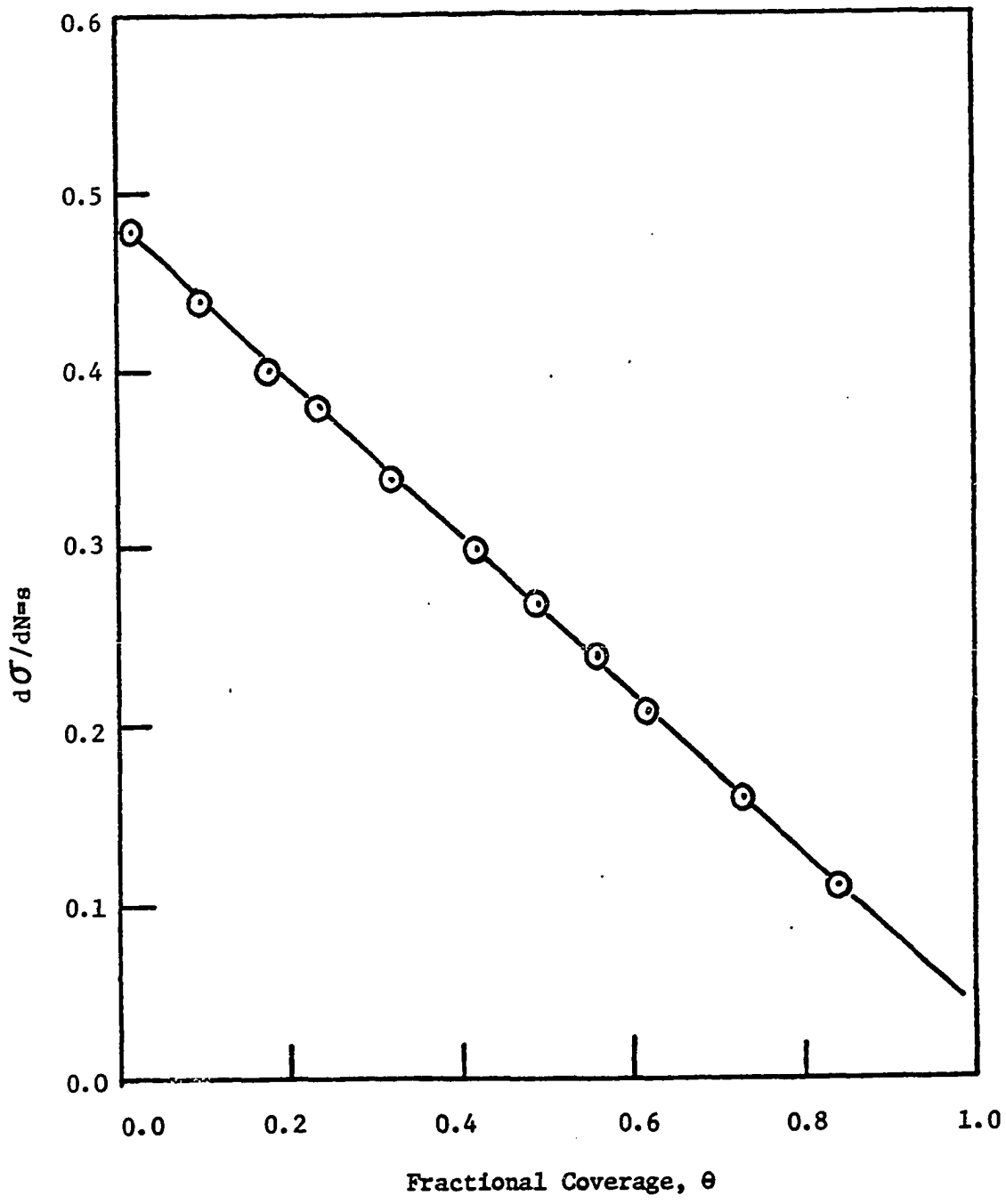

Figure B-2 Plot of $d\sigma/dN=s$ versus θ for sticking coefficient of carbon monoxide.

s in Equation (B-2) and s* in Equation (B-8) is $s=s^*(1-\theta)$ and $s \rightarrow s^*$ when $\theta \rightarrow 0$. Therefore, the simple site occupation model sticking coefficient is the limit of the sticking coefficient defined in Equation (B-1).

Another intresting fact has been observed in the CO desorption from CO_2 adsorbed on Ni (100) surface in this study. The plot of $d\sigma/dN$ versus θ (as shown in Figure B-3) indicates that the nature of this curve is between these curves shown in Figures B-1 and B-2. Therefore, both sticking coefficients, s and s*, for CO_2 adsorption have been calculated. The initial sticking coefficient, s, for CO_2 adsorption is 0.07. The sticking coefficient of simple site occupation model, s*, for CO_2 adsorption already has been reported in Section 3-3 as 0.1 ± 0.004.

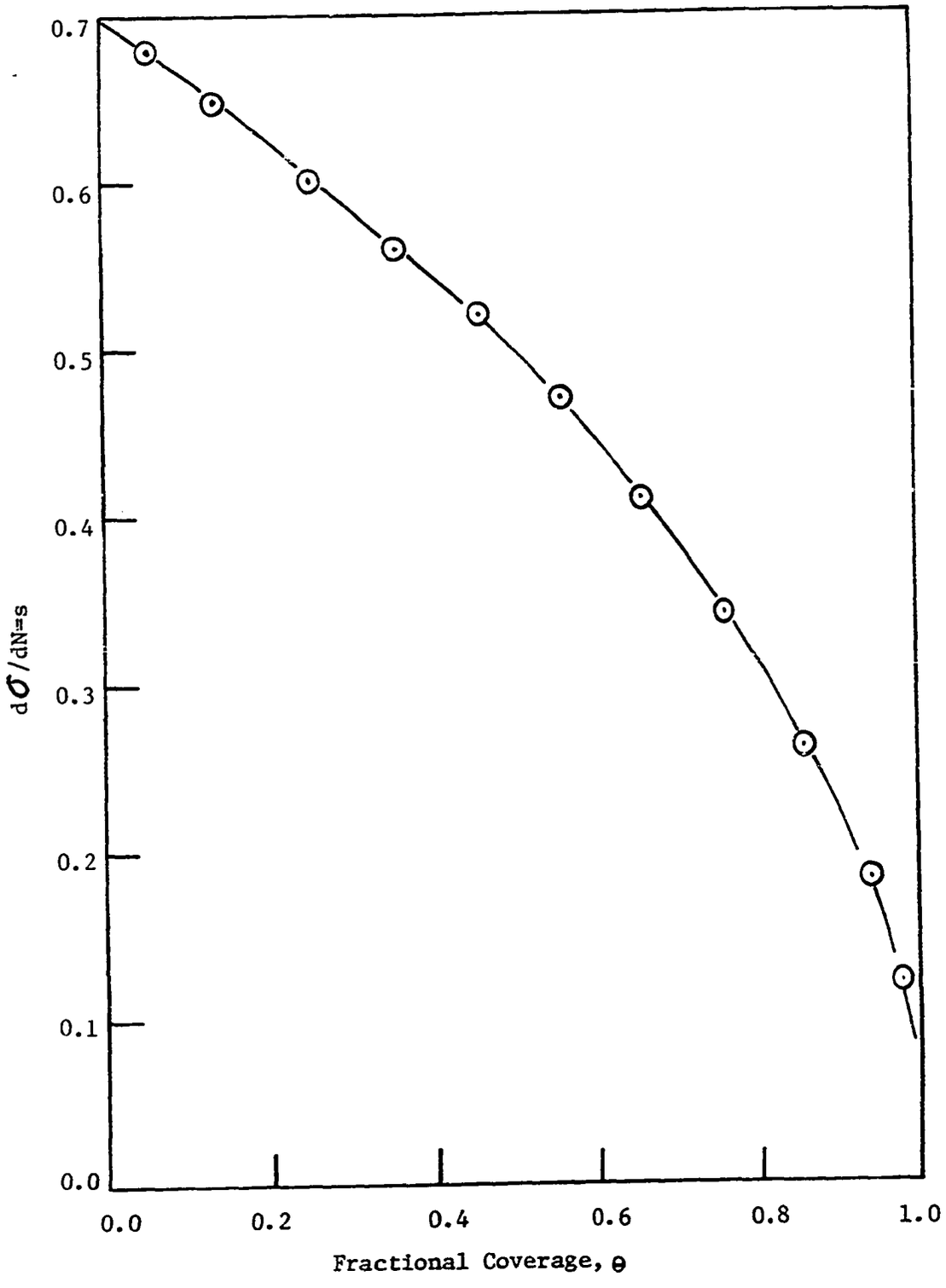

Figure B-3 Plot of $d\sigma/dN=s$ versus θ for sticking coefficient of carbon dioxide.